https://ntrs.nasa.gov/search.jsp?R=19870007548 2020-03-20T12:48:59+00:00Z

NASA Contractor Report 4037

Prediction of Vortex Shedding From Circular and Noncircular Bodies in Subsonic Flow

Michael R. Mendenhall
and Daniel J. Lesieutre

CONTRACT NAS1-17962
JANUARY 1987

NASA

NASA Contractor Report 4037

Prediction of Vortex Shedding From Circular and Noncircular Bodies in Subsonic Flow

Michael R. Mendenhall
and Daniel J. Lesieutre
Nielsen Engineering and Research, Inc.
Mountain View, California

Prepared for
Langley Research Center
under Contract NAS1-17962

National Aeronautics
and Space Administration

**Scientific and Technical
Information Branch**

1986

TABLE OF CONTENTS

PRECEDING PAGE BLANK NOT FILMED

TABLE OF CONTENTS (Concluded)

PREDICTION OF VORTEX SHEDDING FROM CIRCULAR AND NONCIRCULAR BODIES IN SUBSONIC FLOW

Michael R. Mendenhall
Daniel J. Lesieutre

Nielsen Engineering & Research, Inc.

SUMMARY

An engineering prediction method and associated computer code VTXCLD to predict nose vortex shedding from circular and noncircular bodies in subsonic flow at angles of attack and roll are presented. The axisymmetric body is represented by point sources and doublets, and noncircular cross sections are transformed to a circle by either analytical or numerical conformal transformations. The lee side vortex wake is modeled by discrete vortices in crossflow planes along the body; thus the three-dimensional steady flow problem is reduced to a two-dimensional, unsteady, separated flow problem for solution. Comparison of measured and predicted surface pressure distributions, flow field surveys, and aerodynamic characteristics are presented for bodies with circular and noncircular cross sectional shapes.

INTRODUCTION

Current missile applications requiring high aerodynamic performance can involve noncircular body shapes in subsonic flow at high angles of attack and nonzero roll angles. The angle of attack range may be sufficiently high to cause formation of body separation vortices, and the body vortex shedding characteristics are directly influenced by the body cross-sectional shape and the flow conditions. It is desirable to model the body vortex wake by means of a rational method capable of considering a variety of body shapes over a wide range of incidence angles and Mach numbers up to the critical speed. It is important that the separation vortex wake induced effects on the nonlinear aerodynamic characteristics of the body be handled properly with a method which correctly represents the physical characteristics of the flow field.

The phenomena of interest are the sheets of vorticity formed on the lee side of the body at high angles of attack. The vorticity is formed by boundary-layer fluid leaving the body surface from separation points on both sides of the body (Fig. 1). At moderate angles of incidence, the vorticity rolls up into a symmetrical vortex pair, but at higher angles, the vorticity becomes asymmetric as shown in the sketch in Figure 1(b). A method to predict these flow phenomena in the vicinity of circular and noncircular bodies in subsonic flow is described in References 1 and 2. The extension of the method to supersonic flow is described in Reference 3.

The purpose of this report is to describe an engineering prediction method and associated computer code developed to calculate the nonlinear aerodynamic characteristics and flow fields of noncircular bodies at high angles of attack at speeds up to the critical speed. The objectives of the method are to use a three-dimensional, attached flow, potential method to represent the body and a two-dimensional, incompressible, separated flow model to calculate the lee side vortex shedding from the body alone at angle of attack and angle of roll. The predicted pressure distribution on the body under the influence of the free stream and the separation vortex wake is used to calculate the aerodynamic loads on the body. Conformal mapping techniques are used to transform noncircular cross sections to a circle for calculation purposes.

The following sections of this report include a discussion of the approach to the problem and a description of the analysis and flow models required to carry out the calculation. The prediction method is evaluated through comparison of measured and predicted results on a variety of body shapes, including circular and elliptical cross sections. A user's manual for the computer code is also included. The manual consists of descriptions of input and output and of sample cases.

LIST OF SYMBOLS

a	semi-major or horizontal axis of elliptic cross section
A_ℓ	coefficients of conformal transformation, Eq. (8)
b	semi-minor or vertical axis of elliptic cross section
c_n	normal-force coefficient per unit length, Eq. (49)
c_y	side-force coefficient per unit length, Eq. (53)
C_A	axial-force coefficient, Eqs. (58) and (62)
C_ℓ	rolling-moment coefficient, Eq. (57)
C_m	pitching-moment coefficient, Eq. (51)
C_n	yawing-moment coefficient, Eq. (55)
C_p	pressure coefficient, Eq. (39)
C_{p_I}	incompressible pressure coefficient, Eq. (41)
C_y	side-force coefficient, Eq. (55)
C_N	normal-force coefficient, Eq. (50)
D	diameter of circular body, or equivalent diameter of noncircular body
G	complex velocity component, Eq. (28)

ℓ_{ref} reference length

L total number of Fourier coefficients used to describe transformation, Eq. (8); also model length

M_x rolling moment about the x-axis

M_y pitching moment about the y-axis

M_z yawing moment about the z-axis

M_∞ free-stream Mach number

p local static pressure

p_∞ free-stream static pressure

q_∞ free-stream dynamic pressure, $\frac{1}{2}\rho V_\infty^2$

Q source strength

r radial distance from a vortex to a field point

r' radial distance to a point on a noncircular body, Fig. 4

r_c vortex core radius, Eq. (59)

r_o radius of circle

Re_ξ Reynolds number based on boundary layer run length and minimum pressure conditions, $U_m\xi/\nu$

S reference area

u_e	surface velocity in crossflow plane
u_r	axial perturbation velocity
U	local velocity
v_R	radial perturbation velocity
v_θ	vortex induced velocity
v,w	velocity components in real plane
V_∞	free-stream velocity
W	complex potential, Eq. (26)
x,y,z	body coordinate system with origin at the nose: x positive aft along the model axis, y positive to starboard, and z positive up
x_m	axial location of center of moments
α	angle of attack
α_c	angle between free-stream velocity vector and body axis
β	angle of sideslip; also polar angle in σ-plane, Fig. 2; also $\sqrt{1-M_\infty^2}$
β'	local slope of body surface, Fig. 4
γ	ratio of specific heats

γ_r	exterior angles of body segment for numerical mapping, Eq. (6)
Γ	vortex strength
Δx	axial length increment
ζ	complex coordinate in an intermediate plane, Fig. 2(b)
η	vertical coordinate in an intermediate plane, Fig. 2(b)
θ	polar angle in ν- plane, Fig. 2(a)
ν	complex coordinate in circle plane, Fig. 2(a); also kinematic viscosity
ξ	run length, Eqs. (46) and (47); or lateral coordinate in an intermediate plane, Fig. 2(b)
ρ	free-stream density
σ	complex coordinate in real plane, Fig. 2(a)
τ, λ	lateral and vertical coordinates in circle plane, Fig. 2(a)
ϕ	roll angle
Φ	velocity potential in real plane
ψ	stream function in real plane

Subscripts and Superscripts

$(\bar{\ })$	conjugate of complex quantity
$(\ )_m$	vortex m
$(\ )_{cp}$	center of pressure
$(\ )'$	incompressible quantity; or surface values in Fig. 4

GENERAL APPROACH

Bodies at high angles of attack exhibit distributed vorticity fields on their lee side due to boundary-layer fluid leaving the body surface at separation lines. One approach for modeling these distributed vorticity fields has involved the use of clouds of discrete potential vortices. Underlying the basic approach is the analogy between two-dimensional unsteady flow past a body and the steady three-dimensional flow past an inclined body. In fact, the three-dimensional steady flow problem is reduced to the two-dimensional unsteady separated flow problem for solution. Linear theory for the attached flow model and slender body theory to represent the interactions of the vortices are combined to produce a nonlinear prediction method. The details of the application of this approach to the prediction of subsonic flow about circular and noncircular bodies are presented in References 1 and 2. Other investigators have used this approach to successfully model the subsonic flow phenomena in the vicinity of circular cross section bodies (Refs. 4 and 5). The purpose of this report is to document in detail the subsonic analysis of References 1 and 2 and to describe the code VTXCLD assembled to accomplish the subsonic vortex shedding calculations.

The calculation procedure is carried out in the following manner. The axisymmetric body is represented by discrete point sources and doublets, and the strength of the individual singularities is determined to satisfy a flow tangency condition on the body in a nonseparated uniform flow at angle of incidence and roll. Compressibility effects on the body are included by a Gothert transformation which keeps the cross section shape unchanged but stretches the axial body coordinate. Starting at a crossflow plane near the body nose, the pressure distribution on the body is computed using the full compressible Bernoulli equation. The boundary layer in the crossflow plane is examined for separation using modified versions of Stratford's separation criteria. The Stratford separation criteria are based on two-dimensional incompressible flow. At the predicted separation points, incompressible vortices with their strength determined by the vorticity transport in the boundary layer are shed into the flow field. The trajectories of these free vortices between this crossflow plane and the next plane downstream are calculated by integration of the equations of motion of each vortex, including the influence of the free stream, the body, and other vortices. The pressure and trajectory calculations are carried out by mapping the noncircular cross section shape to a circle using either analytical or numerical conformal transformations. The vortex induced velocity contribution to the body tangency boundary condition includes image vortices in the circle plane. At the next downstream crossflow plane, new vortices are shed, adding to the vortex cloud representing the wake on the lee side of the body. This procedure is carried out in a stepwise fashion over the entire length of the body. The details of the individual methods combined into the prediction method are described in the following section.

METHODS OF ANALYSIS

The development of an engineering method to predict the pressure distributions on arbitrary missile bodies in subsonic flow at high angles of incidence requires the joining of several individual prediction methods. In this section, the individual methods are described briefly, and the section concludes with a description of the complete calculation procedure.

Conformal Mapping

The crossflow plane approach applied to arbitrary missile bodies results in a noncircular cross section shape in the presence of a uniform crossflow velocity and free vortices in each plane normal to the body axis. The procedure used to handle the noncircular shapes is to determine a conformal transformation for mapping every point on or outside the arbitrary body to a corresponding point on or outside a circular body. The two-dimensional potential flow solution around a circular shape in the presence of a uniform flow and external vortices is well known and has been documented numerous places in the literature (Refs. 6 and 7). Thus, the procedure is to obtain the potential solution for the circular body and transform it to the noncircular body. Conformal transformations used are of two distinct types, analytical and numerical.

Analytic transformation.- For very simple shapes like an ellipse [Fig. 2(a)], the transformation to the circle can be carried out analytically as described in Reference 7. For example,

$$\sigma = \nu + \frac{a^2 - b^2}{4\nu} \tag{1}$$

where

$$\sigma = y + iz \tag{2}$$

in the real plane, and

$$\nu = \tau + i\lambda \tag{3}$$

in the circle plane. The derivative of the transformation is

$$\frac{d\sigma}{d\nu} = 1 - \left[\frac{a^2 - b^2}{4\nu^2}\right] \tag{4}$$

which is required for the velocity transformation discussed later.

Numerical transformation.- For complex noncircular shapes, the transformation cannot be carried out analytically and a numerical transformation is required. The numerical transformation chosen is described in detail in Reference 8, and a brief summary of the conformal mapping procedure follows.

The sequence of events in the numerical mapping is shown in Figure 2(b). The arbitrary cross section shape of the body in the σ-plane is required to have a vertical plane of symmetry. The transformation of interest will map the region on and outside the body in the σ-plane to the region on and outside a circle in the ν-plane. The first step is a rotation to the ζ-plane so that the cross section is symmetric about the real axis. Thus,

$$\zeta = i\sigma$$

$$= \xi + i\eta \tag{5}$$

A mapping that transforms the outside of the body in the ζ-plane to the outside of the unit circle is

$$\zeta = \int \frac{1}{\nu^2} \prod_{r=1}^{m} (\nu - \nu_r)^{\frac{\gamma_r}{\pi}} \, d\nu \tag{6}$$

where γ_r are the exterior angles of the m segments of the body cross section. In Equation (6), Π denotes a product series. For a closed body

$$\sum_{r=1}^{m} \gamma_r = 2\pi \tag{7}$$

The final transformation has the form

$$\sigma = -i\left[\nu + \sum_{\ell=1}^{L} \frac{r_o^{\ell+1} A_\ell}{\nu^\ell}\right] \qquad (8)$$

where the A_ℓ coefficients are obtained through an iterative scheme described in Reference 8 and r_o is the radius of the equivalent circle in the ν-plane. The derivative of the transformation is

$$\frac{d\sigma}{d\nu} = -i\left[1 - \sum_{\ell=1}^{L} \frac{r_o^{\ell+1} \ell A_\ell}{\nu^{\ell+1}}\right] \qquad (9)$$

which is required for the velocity calculations described in a later section.

The above numerical mapping procedure has been applied to a wide range of general cross section shapes with good success.

Body Model

A three-dimensional representation of the missile volume is needed for purposes of predicting the absolute pressure coefficient on the surface (Ref. 2). Since the model must be a computationally efficient means of representing both circular and noncircular bodies in compressible flow up to the critical speed, a method using discrete singularities on the body axis is described in this section. As described in Reference 3, a panel method can be used to represent the missile surface; however, increased computational requirements make the present approach more desirable for an engineering prediction method.

Circular bodies.- The volume of an axisymmetric body is well represented by a series of point sources and sinks distributed on the axis. A number of models in varying degrees of complexity are available for this task; for example, see References 9-12. For use in VTXCLD, a discrete source model from the latter reference was selected for its accuracy, economy, and reliabilty.

Given a series of K point sources (sinks) distributed on the missile axis, the induced axial and radial velocities at a point (x,r) are

$$\frac{u_r}{V_\infty \cos\alpha_c} = \sum_{k=1}^{k} \frac{Q'_k\left[\frac{x}{L} - \frac{x_k}{L}\right]}{\left[\left[\frac{x}{L} - \frac{x_k}{L}\right]^2 + \left[\frac{r}{L}\right]^2\right]^{3/2}} \tag{10}$$

$$\frac{v_R}{V_\infty \cos\alpha_c} = \sum_{k=1}^{K} \frac{Q'_k\left[\frac{r}{L}\right]}{\left[\left[\frac{x}{L} - \frac{x_k}{L}\right]^2 + \left[\frac{r}{L}\right]^2\right]^{3/2}} \tag{11}$$

where

$$Q'_k = \frac{Q_k}{4\pi L^2 V_\infty \cos\alpha_c} \tag{12}$$

is the dimensionless source strength. Q'_k and x_k are the source strength and axial locations, respectively, of the k-th source. The body surface slope at the j-th body point obtained from Equations (10) and (11) is

$$\left.\frac{dr}{dx}\right|_j = \frac{\dfrac{v_{R_j}}{V_\infty \cos\alpha_c}}{1 + \dfrac{u_{r_j}}{V_\infty \cos\alpha_c}} \qquad \text{for } j=1,\ldots,(N-3) \tag{13}$$

Equation (13) produces a set of K-3 linear equations in the unknown source strengths. For a closed body, imposing the condition of the sum of the source strengths to be zero gives the relation

$$\sum_{k=1}^{K} Q'_k = 0 \tag{14}$$

The remaining two conditions are the imposition of stagnation points at the nose and tail of the body. These conditions from Equation (10) are

$$\sum_{k=1}^{K} \frac{Q'_k}{\left[\frac{x_k}{L}\right]^2} = 1 \tag{15}$$

$$\sum_{k=1}^{K} \frac{Q'_k}{\left[1 - \frac{x_k}{L}\right]^2} = -1 \tag{16}$$

Given the source positions on the missile axis, Equations (13) through (16) comprise the total set of equations to solve for the source strengths. The predicted hull shape from the stream function is

$$\psi' = \frac{1}{2}\left[\frac{r}{L}\right]^2 - \sum_{k=1}^{K} Q'_k \left\{1 + \frac{\left[\frac{x}{L} - \frac{x_k}{L}\right]}{\left[\left[\frac{x}{L} - \frac{x_k}{L}\right]^2 + \left[\frac{r}{L}\right]^2\right]^{1/2}}\right\} = 0 \tag{17}$$

which must be solved by iteration.

The above method has proved successful in modeling a variety of axisymmetric missile bodies; however, some care is required because of the ill-conditioned matrix. Best results are obtained if the discrete sources are spaced at intervals of 60% of the local radius and if the surface slope description of the body is smooth without discontinuities. Boundary conditions are satisfied at points midway between the source locations. The prediction of an approriate source distribution is an automated part of VTXCLD, and the user must only specify missile geometry.

Noncircular bodies.- An appropriate body model for missiles with noncircular cross sections is a surface panel method similar to that described in Reference 3; however, the use of a panel model adds significantly to the cost of each computation. For this reason an alternate approach was selected for use with noncircular bodies.

The noncircular body is replaced with an equivalent axisymmetric body having the same cross sectional area distribution as the actual body. There are approximations involved with this model since the induced u-velocity due to noncircular effects are neglected; however, for bodies that do not deviate greatly from circular, the approximations are acceptable. Some guidelines are included with the user's instructions to illustrate possible problem areas and the magnitude of the approximation associated with the model.

Compressibility effects.- The selection of a compressibility correction scheme must take into consideration the configurations of interest and the calculation procedure. For example, vortex shedding and tracking is very dependent on cross sectional shape, and numerical transformations add significantly to computation time; therefore, it is advantageous that the compressibility transformation used have no effect on the cross sectional shape. With this guideline and based on similar experiences and requirements (Ref. 12), a transformation which modifies only the axial coordinate is needed. The Gothert Rule, described in Reference 13 and others, is the choice for the compressibility transformation. A brief description of the method included in VTXCLD follows.

The transformation from the compressible (x,y,z) coordinate system to the incompressible (x',y',z') system is

$$x' = x/\beta$$

$$y' = y$$

$$z' = z \tag{18}$$

where

$$\beta = \sqrt{1-M_{\infty}^2} \tag{19}$$

As a result of Equation (18), the body slope and angle of attack become

$$\frac{dr'}{dx'} = \beta \frac{dr}{dx} \tag{20}$$

$$\alpha' = \beta\alpha \tag{21}$$

and the velocity fields are related by

$$u = u'/\beta^2$$

$$v = v'/\beta$$

$$w = w'/\beta \tag{22}$$

The vortex shedding scheme in VTXCLD requires that the compressibility correction be applied in a manner slightly different from the usual. At the initiation of the calculation, the actual missile body is transformed to the incompressible shape by the above stretching procedure, and the source distribution is obtained as described above. The modified incompressible flow conditions are used to calculate the velocity field associated with the body. This velocity field is transformed back to the compressible domain so that it is available for use in vortex tracking and compressible pressure coefficient calculations. The compressible pressure coefficient is used to locate separation and define the shed vorticity. Since the compressibility transformation has no direct effect on the cross sectional shape or the discrete wake vortices, the separation and vortex tracking calculations take place in the compressible domain. No compressibility effects are considered for the vortex induced velocities.

Vortex Shedding Model

The body vortex shedding model described in this section is nearly the same as the subsonic model presented in Reference 2; therefore, only the differences between the two models will be discussed in detail.

Equations of motion.- The equations of motion of a shed nose vortex in the presence of other free vortices in the vicinity of a body in a uniform stream follow. In the circle (ν) plane, the position of a vortex, Γ_m, is

$$\nu_{m_\Gamma} = \tau_m + i\lambda_m \tag{23}$$

and an image of Γ_m is located at

$$\nu_{m_{-\Gamma}} = \frac{r_o^2}{\bar{\nu}_m} \tag{24}$$

to satisfy the flow tangency condition on the body surface. In the real plane, the position of the vortex Γ_m is

$$\sigma_{m_\Gamma} = y_m + iz_m \tag{25}$$

The complex potential in the real plane is

$$W(\sigma) = \Phi - i\psi \tag{26}$$

and the corresponding velocity at Γ_m is

$$v_m - iw_m = \frac{dW_m(\sigma)}{d\sigma} = \frac{d}{d\nu}\,[W_m(\sigma)]\,\frac{d\nu}{d\sigma}\bigg|_{\substack{\sigma=\sigma_m \\ \nu=\nu_m}} \tag{27}$$

The complex potential of Γ_m is not included in Equation (27) to avoid the singularity at that point. The derivative of the transformation is obtained from Equations (4) or (9).

The total velocity at Γ_m in the crossflow plane is written as

$$\frac{v_m - iw_m}{V_\infty} = G_\alpha + G_\beta + G_n + G_m + G_T + G_r \tag{28}$$

where each term in Equation (28) represents a specific velocity component in the σ-plane. The first term represents the uniform flow due to angle of attack

$$G_\alpha = -i\sin\alpha\left[1 + \left[\frac{r_o}{\nu_m}\right]^2\right]\frac{d\nu}{d\sigma}\bigg|_{\sigma=\sigma_m} \tag{29}$$

The second term represents the uniform flow due to angle of yaw.

$$G_\beta = -\sin\beta \left[1 - \left[\frac{r_o}{\nu_m}\right]^2 \right] \left.\frac{d\nu}{d\sigma}\right|_{\sigma=\sigma_m} \tag{30}$$

In compressible flow, the velocity components from Equations (29) and (30) used in the surface pressure calculations include effects of the compressibility transformation described in a previous section.

The next term represents the influence of all vortices and their images, with the exception of Γ_m.

$$G_n = i \sum_{n=1}^{N} \frac{\Gamma_n}{2\pi r_o V_\infty} \left[\frac{1}{(\nu_m/r_o)-(r_o/\bar{\nu}_n)} - \frac{1}{(\nu_m/r_o)-(\nu_n/r_o)} \right] \Bigg|_{n\neq m} \left.\frac{d\nu}{d\sigma}\right|_{\sigma=\sigma_m} \tag{31}$$

The next term is due to the image of Γ_m.

$$G_m = i \frac{\Gamma_m}{2\pi r_o V_\infty} \left[\frac{1}{(\nu_m/r_o)-(r_o/\bar{\nu}_m)} \right] \left.\frac{d\nu}{d\sigma}\right|_{\sigma=\sigma_m} \tag{32}$$

The fifth term in Equation (28) represents the potential of Γ_m in the σ-plane and is written as

$$G_T = -i \frac{\Gamma_m}{2\pi V_\infty} \left[\frac{1}{2}\right] \frac{d}{d\nu} \left[\frac{d\nu}{d\sigma}\right]_{\sigma=\sigma_m} \tag{33}$$

The last term in Equation (28) represents the velocity components induced by the body source singularities representing the volume effects.

$$G_r = \frac{v_r - iw_r}{V_\infty} \qquad (34)$$

where v_r and w_r are components of v_R from Equation (11).

Since the body source singularities are three-dimensional, they contribute an induced axial velocity, u_r, given by Equation (10). Compressibility effects are included through the stretching of the axial coordinate and subsequent transformation of the induced velocity components.

The differential equations of motion for Γ_m are

$$\frac{d\bar{\sigma}_m}{dx} = \frac{v_m - iw_m}{V_\infty \cos\alpha_c + u_r} \qquad (35)$$

where

$$\bar{\sigma}_m = y_m - iz_m \qquad (36)$$

Therefore, the two equations which must be integrated along the body length to determine the trajectory of Γ_m are

$$\frac{dy_m}{dx} = \frac{v_m}{V_\infty \cos\alpha_c + u_r} \qquad (37)$$

and

$$\frac{dz_m}{dx} = \frac{w_m}{V_\infty \cos\alpha_c + u_r} \qquad (38)$$

There are a pair of equations like (37) and (38) for each vortex in the field. As new vortices are shed, the total number of equations to solve increases by two for each added vortex. These differential equations are solved numerically using a method which automatically adjusts the step size to provide the specified accuracy.

Surface pressure distribution.- The surface pressure distribution on the body is required to calculate the forces on the body and the separation points. The surface pressure coefficient is determined from the Bernoulli equation in the form

$$C_p = \frac{2}{\gamma M_\infty^2}\left\{\left[1 + \frac{\gamma-1}{2} M_\infty^2 (C_{p_I})\right]^{\frac{\gamma}{\gamma-1}} - 1\right\} \tag{39}$$

where

$$C_p = \frac{p - p_\infty}{\frac{1}{2}\rho V_\infty^2} \tag{40}$$

and

$$C_{p_I} = 1 - \left[\frac{U}{V_\infty}\right]^2 - \frac{2\cos\alpha_c}{V_\infty}\frac{d\phi}{dx} \tag{41}$$

where U is the total velocity (including V_∞) at a point on the body.

The last term in Equation (41) represents the axial velocity missing from the two-dimensional singularities in the flow model. In this case, the shed vortices and the doublet part of Equations (29) and (30) are the only singularities contributing to this term. The complex potential of these two-dimensional singularities is

$$\begin{aligned} W(\nu) &= \phi + i\psi \\ &= \sum_{n+1}^{N} \frac{\Gamma_n}{2\pi}\left[-i\,\ln(\nu - \nu_n) + i\,\ln\left(\nu - \frac{r_o^2}{\bar{\nu}_n}\right)\right] \\ &\quad + i\,\frac{r_o^2}{\nu} V_\infty \sin\alpha - \frac{r_o^2}{\nu} V_\infty \sin\beta \end{aligned} \tag{42}$$

The "unsteady" term in Equation (41), evaluated on the body surface, is

$$\frac{d\phi}{dx} = \text{Real} \left. \frac{dW(\nu)}{dx} \right|_{r=r_o} \tag{43}$$

Equation (43) becomes

$$\frac{d\phi}{dx} = \sum_{n=1}^{N} \frac{\Gamma_n}{2\pi} \left\{ - \left[\frac{(\tau - \tau_n) \frac{d\lambda_n}{dx} - (\lambda - \lambda_n) \frac{d\tau_n}{dx}}{(\tau - \tau_n)^2 + (\lambda - \lambda_n)^2} \right] \right.$$

$$- \left[\frac{(\tau r_n^2 - \tau_n r_o^2) \left[2\lambda\tau_n \frac{d\tau_n}{dx} + 2\lambda\lambda_n \frac{d\lambda_n}{dx} - r_o^2 \frac{d\lambda_n}{dx} - 2r_o\lambda_n \frac{dr_o}{dx} \right]}{(\tau r_n^2 - \tau_n r_o^2)^2 + (\lambda r_n^2 - \lambda_n r_o^2)^2} \right]$$

$$\left. + \left[\frac{(\lambda r_n^2 - \lambda_n r_o^2) \left[2\tau\lambda_n \frac{d\lambda_n}{dx} + 2\tau\tau_n \frac{d\tau_n}{dx} - r_o^2 \frac{d\tau_n}{dx} - 2r_o\tau_n \frac{dr_o}{dx} \right]}{(\tau r_n^2 - \tau_n r_o^2)^2 + (\lambda r_n^2 - \lambda_n r_o^2)^2} \right] \right\}$$

$$+ \frac{2V_\infty}{r_o} \frac{dr_o}{dx} (\lambda \sin\alpha - \tau \sin\beta) \tag{44}$$

where

$$r_n^2 = \tau_n^2 + \lambda_n^2 \tag{45}$$

Separated wake.- The separated wake on the lee side of the body is made up of a large number of discrete vortices, each vortex originating from one of two possible locations at each time step in the calculation. The major portion of the lee side vortex wake has its origin at the primary separation points on each side of the body. The remainder of the wake originates from the secondary separation points located in the reverse flow region on the lee side of the body. Both of these points are illustrated in the sketch of a typical crossflow plane of an elliptic cross section body shown in Figure 3. The mechanics of the calculation of the individual vortices follows.

As described in References 1 and 2, the pressure distribution for the primary flow in the crossflow plane is referenced to the conditions at the minimum pressure point, and a virtual origin for the beginning of the boundary layer is calculated. The adverse pressure distribution downstream of the minimum pressure point is considered with either Stratford's laminar (Ref. 14) or turbulent (Ref. 15) separation criterion to determine whether or not separation has occurred. These criteria, based on two-dimensional, incompressible, flat plate data, are adjusted for three-dimensional crossflow effects in Reference 2. The laminar separation criterion states that the laminar boundary layer separates when

$$C_p^{1/2} \left[\xi \frac{dC_p}{d\xi} \right] \approx 0.087 \sin\alpha_c \tag{46}$$

In a turbulent boundary layer, separation occurs when

$$C_p \left[\xi \frac{dC_p}{d\xi} \right]^{1/2} (Re_\xi x\ 10^{-6})^{-0.1} \approx 0.35 \sin\alpha_c \tag{47}$$

The $\sin\alpha_c$ in Equations (46) and (47) is the three-dimensional modification.

If the criteria indicate a separation point, the vorticity flux across the boundary layer at separation is shed into a single point vortex whose strength is

$$\frac{\Gamma}{V_\infty} = \frac{u_e^2}{2V_\infty^2} \frac{\Delta x}{\cos \alpha_c} \delta \tag{48}$$

assuming no slip at the wall. δ is the vortex reduction factor described below.

The initial position of the shed vortex is determined such that the surface velocity in the crossflow plane at the separation point is exactly canceled by the shed vortex and its image. When this criterion results in a vortex initial position that is too near to the body surface, certain numerical problems can cause difficulty in calculating the trajectory of this vortex. If the initial position of the vortex is nearer than five percent of the body radius from the surface, the vortex is generally placed five percent of the equivalent body radius from the surface. This position represents the approximate thickness of the boundary layer.

The calculation of secondary separation is carried out in the same manner as described above for primary separation. It is necessary that a reverse flow region exist on the lee side of the body and that a second minimum pressure point be found in this region. Surface flow visualization of secondary separation regions on bodies at high angles of attack in subsonic flow are shown in Reference 16. For purposes of this analysis, the reverse flow is assumed to be laminar from the lee side stagnation point to the secondary separation point, and Stratford's laminar criterion is used to locate secondary separation. Laminar separation in the reverse flow region is expected because of the low velocities on this portion of the body. The vortex released into the flow at the secondary separation point has the opposite sign of the primary vortex and is generally weaker in strength.

Transition.- In general, the primary separation on a missile is either laminar or turbulent, depending on the Reynolds number of the flow; however, as noted in Reference 17, there is an angle of attack and Reynolds number range over which the character of the separation is transitional. Flow visualization of the transition phenomenon on missile shapes is available in References 16 and 18. Body vortex shedding technology is not developed to the level that prediction of the beginning of transition nor the length of the transition is practical. Correlation of the limited amount of data available has permitted the authors to define approximately the limits of transition. The results of the correlation indicate that the separation switches from laminar to turbulent when the Reynolds number based on the length from the nose times the sine of the angle of incidence is approximately 7×10^4. The length of the transition region is about one body diameter. More analysis is required to verify the correlation, and the authors recommend that transition effects be included with great care.

Reduction factor.- The empirical vortex reduction factor, δ, in Equation (48) is widely used in discrete vortex methods to provide better agreement between measured and predicted vorticity strength in the wake. Various investigators (e.g., Refs. 2, 4, and 19) recommend a value in the range $0.6 < \delta < 1.0$ for subsonic flow with 0.6 being the more common value. Based on the experience of the authors, the proper value of δ can vary with the geometry and flow conditions. For example, $\delta = 0.6$ is an appropriate value for an ogive-cylinder missile in subsonic flow, but $\delta = 1.0$ is a better value for a boattail body in subsonic flow. Unless otherwise noted, $\delta = 0.6$ is used for all predicted results presented in this report.

Forces and moments.- The forces and moments on the body are computed by integration of the pressure distribution around the body. At a specified station on the body, the normal-force coefficient on a Δx length of the body is

$$c_n = \frac{\left[\frac{\Delta n}{\Delta x}\right]}{q_\infty D} = \frac{1}{D} \int_0^{2\pi} C_p r' \cos\beta' \, d\beta \tag{49}$$

where r' is the distance from the axis of the body to the body surface and β' is the local slope of the body in the crossflow plane. This is illustrated in the sketch in Figure 4. For circular bodies, $r' = r_o$ and $\beta' = \beta$. The total normal force coefficient on the body is

$$C_N = \frac{N}{q_\infty S} = \frac{D}{S} \int_0^L c_n dx \tag{50}$$

and the pitching-moment coefficient is

$$C_m = \frac{M_y}{q_\infty S \ell_{ref}} = \frac{D}{S} \int_0^L c_n \left[\frac{x_m - x}{\ell_{ref}}\right] dx \tag{51}$$

The center of pressure of the normal force is

$$\frac{x_{cp_n}}{\ell_{ref}} = \frac{x_m}{\ell_{ref}} - \frac{C_m}{C_N} \tag{52}$$

Similarly, the side-force coefficient on a Δx length of the body is

$$c_y = \frac{\left[\frac{\Delta s}{\Delta x}\right]}{q_\infty D} = -\frac{1}{D} \int_0^{2\pi} C_p r' \sin\beta' \, d\beta \tag{53}$$

The total side-force coefficient on the body is

$$C_y = \frac{F_y}{q_\infty S} = \frac{D}{S} \int_0^L c_y dx \tag{54}$$

and the yawing-moment coefficient is

$$C_n = \frac{M_z}{q_\infty S \ell_{ref}} = -\frac{D}{S} \int_0^L c_y \left[\frac{x_m - x}{\ell_{ref}}\right] dx \tag{55}$$

The center of pressure of the side force is

$$\frac{x_{cp_y}}{\ell_{ref}} = \frac{C_n}{C_y} + \frac{x_m}{\ell_{ref}} \tag{56}$$

A noncircular body at an arbitrary roll angle may experience a rolling moment caused by the nonsymmetry of the loading around the body. The total rolling moment on the body is calculated by summing the moments of the individual components of normal force and side force around each cross section and integrating over the body length. Using Equations (4) and (5), the rolling moment coefficient is calculated as

$$C_\ell = \frac{M_x}{q_\infty S \ell_{ref}}$$

$$= \frac{1}{S\ell_{ref}} \int_o^L \left[\int_o^{2\pi} (yC_p r' \cos\beta' - zC_p r' \sin\beta') d\beta \right] dx \tag{57}$$

Though the primary purpose of the vortex shedding method is not to predict drag or axial force on the missile, a procedure to estimate both pressure drag (excluding base drag) and skin friction is included. The pressure contribution to the axial-force coefficient is

$$C_{A_p} = \frac{1}{S} \int_o^L \int_o^{2\pi} C_p \frac{dr'}{dx} d\beta \; dx \tag{58}$$

The local skin-friction coefficient, based on the assumption of a 1/7th power law velocity profile in the boundary layer, is

$$C_f = .0592 \left(\frac{V_\infty x}{\nu} \right)^{-.2} \tag{59}$$

which produces a drag coefficient due to friction

$$C_{D_f} = \frac{2\pi}{S} \int_o^L r_o \, C_f \; dx \tag{60}$$

At high angles of incidence, streamlines around the body are inclined at approximately

$$\alpha_s = \tan^{-1} (2 \tan \alpha_c) \quad (61)$$

therefore, the axial component of the friction drag is

$$C_{A_f} = C_{D_f} \cos \alpha_s \quad (62)$$

The total axial-force coefficient is the sum of Equations (58) and (62).

Vortex core. - The diffusion core model (Ref. 2) for the point-vortex induced velocities removes the singularity at the vortex origin and effectively reduces the velocities near the vortex. The tangential velocity induced by a single point vortex is written as

$$\frac{v_\theta}{\Gamma} = \frac{1}{2\pi r} \left[1 - \exp \left[\frac{r^2 V_\infty}{4 x \nu} \right] \right] \quad (63)$$

where r is the distance from the vortex to the field point and x is a measure of the age of the vortex. The induced velocity from this core model is illustrated in the following sketch.

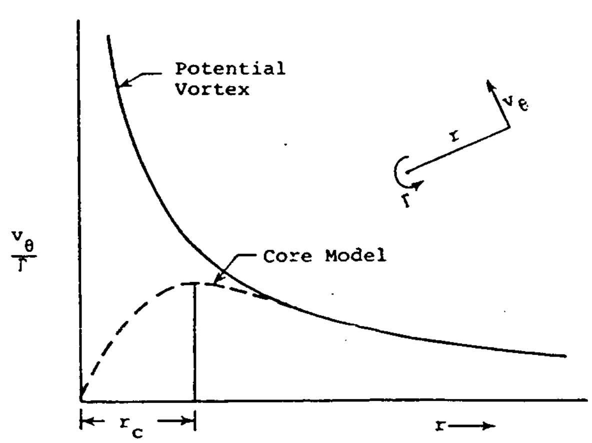

Sketch - Vortex Induced Velocity

The vortex core model represented by Equation (63) has received considerable attention in the context of body vortex induced effects, and it has a number of shortcomings. Since the exponential term is a function of r, the flow medium (ν), and the age of the vortex (x), the core is constantly changing size as the vortex moves through the field. Under certain conditions, the core radius, denoted as r_c in the sketch, can become very small and the induced velocity becomes unrealistically large. In an attempt to further modify the core model to keep the induced velocities within physically realistic limits, the following modification was made in Reference 3. The location of the maximum induced velocity, r_c in the sketch, is fixed at a specific radius to be selected by the user. Given a core radius, the vortex induced velocity is

$$\frac{v_\theta}{\Gamma} = \frac{1}{2\pi r}\left[1 - \exp - \left[1.256 \frac{r^2}{r_c^2}\right]\right] \qquad (64)$$

The core model described by Equation (64) is included in the version of the code described in this report, and in a later section, guidelines for the selection of an appropriate core radius are presented. Results indicate that this simple core model provides adequate smoothing for the necessary velocity calculations.

Other investigations of discrete vortex models must use a core model of some type. Although there are many different core models, all serve the same purpose as those described above, and nearly all are directed at eliminating the singularity and reducing the maximum induced velocity. The code VTXCLD described in this report is easily modified to incorporate another core model if the user desires to do so.

Asymmetry.- An axisymmetric missile at large angles of attack in subsonic flow will exhibit asymmetries in the vortex field and associated induced side force. The vortex cloud approach described herein will predict no asymmetry at any angle of attack on a missile with a vertical plane of symmetry unless the solution is perturbed. Every investigator (e.g., Refs. 2, 5, and 19) has a favorite means of introducing a perturbation to the solution, and no good argument can be made for one over another. Unfortunately, the size and type of perturbation has an effect on the final solution; therefore, some empircal information is required to calibrate the perturbation for a particular geometry and flow condition.

In Reference 2 and in VTXCLD, the perturbation is introduced by a small modification of the predicted symmetric separation points on either side of the missile at the first few integration steps near the nose. The solution is then allowed to develop on its own. Some results for various magnitude perturbations are presented in Reference 2 and this report.

PROGRAM VTXCLD

Program VTXCLD is a rational flow model which predicts the nonlinear forces and moments acting on slender circular and noncircular bodies at high angles of attack in steady subsonic flow conditions. The nonlinear effects are obtained by modeling the lee side separation vorticity with discrete vortices in the crossflow planes. The code has application as an engineering prediction method for use in preliminary design and analysis studies of missiles at high angles of incidence, and as such, it is important that the code be simple and economical to use and require a minimum of empirical information. However, it is equally important that the code adequately represent the important nonlinear flow phenomena and simulate the major physical features of the flow field.

The following sections are a user's manual for program VTXCLD. These sections include descriptions of the program, the calculation procedure, input preparation, sample input and output cases which illustrate various program features, and program limitations.

General Description

This section provides a general description of program VTXCLD and its various subroutines. The code is written in modular form so that as improvements in flow models become available or as other modifications are required they are easy to incorporate. The flow of the calculation is described in this report and detailed comments are provided throughout the code to assist the user in understanding the order of calculation.

The computer code consists of the program VTXCLD and 39 subroutines. The overall flow map of the program is shown in Figure 5 where the general relationship between the subroutines and external references can be seen. Communication between the program modules is handled primarily by named common blocks. A cross reference table for the calling relationship between the program subroutines is shown in Figure 6. A similar table for the named common blocks is shown in Figure 7.

The program is written in standard FORTRAN. Execution on a VAX 11/750 can vary from 10 seconds to more than 45 minutes depending on various factors such as the geometry, the integration interval (DX), the number of shed vortices, the use of flow symmetry, and the flow conditions.

Subroutine Description

This section briefly describes the main program VTXCLD and its various subroutines.

VTXCLD — This is the main program for calculating the forces and moments on a slender body in a steady flow condition including the nonlinear effects of lee side separation vorticity.

AMAP — Transforms a specified point in the circle plane to its corresponding point in the body plane.

ASUM — Calculates velocity term due to transformation for noncircular bodies.

BMAP — Sets up a table of points on the actual body corresponding to specified points on the circle.

BODY — Organizes the flow through VTXCLD. It organizes calls to predict vortex shedding, to calculate surface velocities and pressures, and to calculate the overall forces and moments on the body.

CMAP — Transforms a specified point in the body plane to its corresponding point in the circle plane.

COMBIN — Combines vortices which are separated by a distance less than or equal to "RGAM". (The resulting vortex strength is the sum of the individual strengths and its location is the centroid of the combined vortices).

CONFOR	Calculates the coefficients of the numerical conformal mapping function. Transforms the region outside of a polygonal shape with a vertical plane of symmetry to the region outside of a circle.
CPPOT	Calculates a potential pressure distribution at a given x station (the effects of separation vortices are not present in the C_p calculation). This is used in determining a turbulent separation point for the transition region.
DFEQKM	Obtains vortex paths between stations x and x to Dx using a Kutta-Merson integration scheme.
DPHIDT	Calculates the two-dimensional unsteady pressure term for use in the unsteady Bernoulli equation.
DZDNU	Calculates the differential of the transform of a polygonal shape to a circle.
F	Calculates the derivatives of the vortex equations of motion which are used in conjunction with DFEQKM to obtain the vortex paths.
FDPSDR	Calculates the axial velocity due to a three-dimensional source distribution.
FORCEP	Calculates the forces and moments on the body by an integration of the surface pressure distribution.
FPSI	Calculates the body shape represented by a three-dimensional source distribution.
FPVEL	Calculates the velocity at specified field points.

INPT	Reads in and prints out the body geometry, the flow conditions, various program options, and restart quantities.
INVERS	Solves simultaneous equations, Ax = B.
PLOT	Creates a line printer plot of the body and its vortex wake at any given x station. It is composed of the following subroutines: PLOTV, PLOTA2, PLOTA5, PLOTA6, PLOTA7, and PLOTA8.
RDRDX	Calculates r and dr/dx at a given x station.
RDRDXI	Initializes the calculation of r and dr/dx for subroutine RDRDX.
SEPRAT	Predicts the position in the crossflow plane where separation occurs based on the Stratford criteria for laminar and turbulent flows.
SHAPE	Determines the body geometric parameters from a table look-up of input data.
SKIN	Estimates the axial skin friction force on the body.
SORDIS	Calculates the source distribution representing an axisymmetric body of revolution given the body shape and slope at each x station.
SORVEL	Calculates perturbation velocities due to a three-dimensional source distribution. Used by subroutine SORDIS in calculation of the source distribution.

SRCVEL Calculates perturbation velocities due to a three-dimensional source distribution.

SUM Analytical mapping of an elliptical cross section.

TRANSN Calculates the body separation points in the transition region.

VCENTR Calculates the centroid of each vortex field.

VLOCTY Calculates the velocity components in the cross flow plane at a specified field point.

VTABLE Sets up the arrays of free vorticity for two cases: (1) The vorticity in the working array GAM is distributed into the individual arrays GAMP, GAMM, GAMR, GAMA, or (2) the vorticity in the individual arrays GAMP, GAMM, GAMR, GAMA is distributed into the working array, GAM, in the proper order.

Z Calculates the transformation of a polygonal shape to a circle of radius RZ.

Program Limitations and Suggestions

Program VTXCLD predicts the aerodynamic forces acting on slender bodies alone at high angles of attack, with some limitations. Certain of the limitations that follow are basically rules-of-thumb for the use of the program which have been determined through program verification and experience with the code.

Mach number.- The major limitation in the program is the Mach number or compressibility correction. The compressibility correction added to VTXCLD is based on small perturbation theory which restricts the body to be slender, the angle of attack to be small, and the Mach number to be approximately 0.8 or less. The slender body restriction is not a new restriction as this assumption is inherent in the crossflow analogy used by VTXCLD to predict lee side vorticity. These restrictions result from the assumptions made for small perturbation theory, and any cases outside these restrictions should be viewed with caution; however, VTXCLD has been applied to blunt nose shapes such as spheroids or ellipsoids with good success. Typical missile shapes with slender noses pose no problems to the method.

Source distribution.- The following suggestions should be observed when using the source distribution calculation in VTXCLD. The source distribution in VTXCLD places three-dimensional point sources on the axis of the body (or equivalent body in a noncircular case). For subsonic Mach numbers it is necessary to close the body to calculate a smooth source distribution. Generally, the body can be closed at its base by including a smooth boattail, and a successful technique for most cases is to close the model with its nose. The source distribution does not handle rapid changes or discontinuities in body slope well.

The source distribution calculation often has a problem with short pointed noses as well. Short blunted noses seem to cause no difficulty because they resemble Rankine bodies, a single point source in a uniform stream. Sharp pointed noses often cause an oscillation in the source strength on the afterbody resulting in an oscillation in the velocities and thus an oscillation in the axial pressure distribution. This has been observed with a two-caliber ogive nose but was not apparent for a 2.5-caliber ogive. The oscillations were minor in their effect on the total calculation and result, but the user should be aware of their possibility.

Incidence angle.- The well-known and little-understood phenomenon of wake asymmetry at large incidence angles ($\alpha_c > 30°$) is available as an option in VTXCLD. As described in a previous section, the naturally symmetric nature of the vortex shedding analysis must be perturbed to produce an asymmetric solution; however, the asymmetric capability within VTXCLD has been demonstrated and will be described in the RESULTS section. The user must be aware of the limitations associated with this portion of the code in order to apply appropriate judgement in the evaluations of the results. Based on the author's experience with asymmetry, care must be taken in the choice of the perturbation parameter and its effect on the results. This is to serve as a warning, and the user should be aware that this portion of the code is in need of additional development.

Transition.- The transition capability included in the code is also in an early stage of development. The character of the vortex wake, whether originating from laminar or turbulent separation points, has an important effect on the predicted nonlinear aerodynamics characteristics. As previously discussed, additional development is needed to better understand the origin and length of the transition regions. The user is cautioned to be very careful in the interpretation of predicted results in flow regimes which may be in a transition region as defined by Lamont in Reference 17.

Secondary separation.- The capability to predict secondary separation or separation in the reverse flow region on the lee side of the body is included in VTXCLD. As discussed in a later section, there are certain flow conditions in which secondary separation has an important role; for example, asymmetric shedding at large incidence angles. Numerical problems associated with tracking the secondary vorticity have been observed, and some additional effort is required to make secondary separation a useful option. Therefore, it is recommended that this option be treated as a research feature and not used for production calculations.

Error Messages and Stops

The code VTXCLD has numerous internal error messages. These messages are generally explicit and are described below. There are several execution terminations at numbered stops within the program. These are described in the table below with some suggestions to correct the problem.

The error message "CONVERGENCE NOT OBTAINED IN INTEGRATION" is printed out when the trajectory calculation does not converge within the specified tolerance, E5. Also printed out is the axial station, XI, and the integration interval, H. This error results in a STOP 40 which is discussed in the table to follow.

In the calculation of the source distribution it is possible to get the message "MATRIX IS SINGULAR." This occurs when one of the pivot elements in the influence matrix is zero. This error results in a STOP 300.

The other major error messages are found in the numerical conformal mapping routine CONFOR. The message "***ERROR IN THE SUM OF EXTERIOR ANGLES***" is printed if the routine has difficulty calculating appropriate body angles within a specified tolerance. Another message "***COEFFICIENT AN(1) = _____ GREATER THAN +- 0.0001 AFTER _____ ITERATIONS OUT OF _____" is printed on the rare occasions when the mapping procedure is having difficulty converging on a solution. These messages are informational and do not result in a program STOP. However, the user is advised to check the transformed shape carefully with the actual shape before using the results.

Termination Message	Description
STOP 1	This is the normal stopping condition. Program VTXCLD
STOP 40	The vortex trajectory integration has failed to converge at an axial station. This problem is usually caused by: (1) two or more vortices in close proximity rotating about one another so rapidly that the integration subroutine cannot converge on a solution, or (2) a vortex is too near the body surface. These situations are often dependent on specific flow conditions and the body shape. The following steps should be tried to resolve the problem. Increase the integration tolerance E5, or increase the size of the combination parameter RGAM so that it is greater than the distance between the troublesome vortices. It often helps to increase the integration interval DX and restart the calculation procedure from a previous station. Subroutine BODY
STOP 41	The vortex trajectory calculation has resulted in a vortex inside the body. This is a rare but serious problem which indicates a major problem with the solution. Subroutine BODY
STOP 44	The total number of shed vortices exceeds 200. To correct this combine some vortices and restart the calculation, or increase the integration interval, DX, so that fewer vortices are shed. Subroutine BODY

STOP 45	The maximum number of positive or negative primary separation vortices exceeds 70. Use the same remedy as for STOP 44. Subroutine BODY
STOP 46	The maximum number of positive or negative secondary (reverse flow) separation vortices exceeds 30. Use the same remedy as for STOP 44 but only combine like vortices. If one of the above steps does not work, the reverse flow calculation can be turned off by setting NSEPR = 0. Subroutine BODY
STOP 201 STOP 202	There is an error in the vortex tables in subroutine VTABLE. Check the input values of NBLSEP, NSEPR, NVP, NVM, NVA, NVR, and RGAM in Items 1 through 6.
STOP 300	There is a singular influence matrix in the solution for the three-dimensional source distribution. Check the input geometry for errors. Subroutine INVERS
STOP 301	The maximum number of iterations is exceeded in the source calculation. Check the input geometry. This problem can occur if the body has a long slender nose followed by a cylindrical section and then a long slender tail. If this is the case, one solution is to close the body off with a blunter and/or shorter tail. Subroutine SORDIS

Input Description

This section describes the input data and format required by program VTXCLD. The input formats are shown in Figure 8, and the definitions of the individual variables are provided in the following paragraphs. Note that some length parameters in the input list are dimensional variables; therefore, special care must be taken that all lengths and areas are input in a consistent set of units.

The remainder of this section includes a description of each of the input variables and indices required for the use of program VTXCLD. The order follows that shown in Figure 8 where the input format for each item and the location of each variable on each card is presented. Data input in I-format are right justified in the fields, and data input in F-format may be placed anywhere in the field and must include a decimal point.

Item 1 is a single card containing 15 integer flags. These flags are right justified in a five column field and are used to specify several options available in VTXCLD.

Item	Variable	Description
1 (15I5)	NCIR	Cross section flag, determines the type of body cross section. = 0, circular body = 1, elliptical body = 2, arbitrary body
	NCF	Mapping flag, specifies whether the required mapping is input or calculated. (NCIR = 2) = 0, calculate mapping

	= 2,	input mapping
ISYM	Vortex shedding symmetry flag.	
	= 0,	symmetric shedding
	= 1,	nonsymmetric shedding
NBLSEP	Separation flag.	
	= 0,	no separation
	= 1,	laminar separation
	= 2,	turbulent separation
NSEPR	Reverse flow separation flag.	
	= 0,	no reverse flow separation (preferred)
	= 1,	reverse flow separation
NDFUS	Vortex core model flag.	
	= 0,	potential vortex model
	= 1,	diffuse vortex model (preferred)
NDPHI	Two-dimensional unsteady pressure term flag.	
	= 0,	omit $\partial\phi/\partial t$ term in C_p equation
	= 1,	include $\partial\phi/\partial t$ term (preferred)
INP	Nose force flag.	
	= 0,	estimate nose forces ahead of the first axial station (preferred)
	= 1,	zero nose forces ahead of the first axial station

NXFV	Number of x stations at which the flow field is calculated and/or special output is generated. (0 < NXFV < 8)
NFV	Number of field points for flow field calculation. (0 < NFV < 200)
NVP	Number of +Γ vortices on +y side of body for a restart calculation. (0 < NVP < 70)
NVR	Number of reverse flow vortices on +y side of body for a restart calculation. (0 < NVR < 30)
NVM	Number of −Γ vortices on −y side of body for a restart calculation. (0 < NVM < 70)
NVA	Number of reverse flow vortices on −y side of body for a restart calculation. (0 < NVA < 30)
NASYM	Asymmetric vortex shedding flag. = 0, no asymmetry = 1, forced asymmetry

Item 2 is a single card containing 10 integer flags/parameters. These values are used to specify several options available in VTXCLD.

Item	Variable	Description
2 (10I5)	NHEAD	Number of title cards in Item 3. (NHEAD > 0)
	NPRNTP	Pressure distribution print flag. = 0, pressure distribution output only at special output stations (NXFV > 0) = 1, pressure distribution output at each x station
	NPRNTS	Vortex separation print flag. = 0, no separation output = 1, separation point summary (pre ferred) = 2, detailed separation calculation (for diagnostic purposes only)
	NPRNTV	Vortex field summary output flag. = 0, vortex field is output at special output stations only (NXFV > 0) = 1, vortex field is output at every x station
	NPLOTV	Vortex field printer-plot flag. = 0, no plots = 1, plot full cross section, constant scale = 2, plot half cross section, constant scale

= 3, plot full cross section, variable scale

NPLOTA	Additional output flag. = 0, no additional output = 1, additional output only at special x station (NXFV > 0) = 2, additional output at each station
NTH	Numerical conformal mapping angle flag. = 0, calculate circle θ's for mapping at 5° increments (preferred) = 1, input θ's
NCORE	Vortex core radius flag. = 0, maximum allowable local vortex core size is .05*SD = 1, no upper limit on the local vortex core size, the vortex core size is given by: RCORE*D
NSKIN	Axial skin friction estimation flag. = 0, no skin friction estimation = 1, axial skin friction estimated
NCOMP	Compressibility correction flag. = 0, incompressible calculation = 1, compressibility correction applied (Mach number must be input in Item 6)

Item 3 is a set of NHEAD title/summary cards which are printed at the top of the first output page. They are reproduced in the output just as they are input.

Item	Variable	Description
3 (20A4)	TITLES	NHEAD title/summary cards to be output on first page.

Item 4 is a single card containing reference information needed to form the aerodynamic coefficients.

Item	Variable	Description
4 (5F10.5)	REFS	Reference area, S_{ref}. REFS > 0.
	REFL	Reference length, ℓ_{ref}. REFL > 0.
	XM	Axial position of the moment center, measured from the body nose.
	SL	Body length, L.
	SD	Maximum body diameter, D.

Item 5 is a single card containing the flow conditions.

Item	Variable	Description
5 (3F10.5)	ALPHAC	Angle of incidence (degrees). $(0° < \alpha_c < 90°)$
	PHI	Angle of roll, ϕ, (degrees).

	RE	Reynolds number based on maximum body diameter, SD, and V_∞.($V_\infty D/\nu$)

Omit Item 6 if NCOMP = 0.

Item 6 is a single card which contains the freestream Mach number M_∞. This item is included only if NCOMP in Item 2 is nonzero.

Item	Variable	Description
6 (F10.5)	MACH	Freestream Mach number.

Item 7 is a single card which specifies the axial extent of the run, the transition region, and parameters associated with the vortex wake.

Item	Variable	Description
7 (8F10.5)	XI	Initial x station, XI > 0, dimensional quantity. (Note: XI > DX/2)
	XF	Final x station, XF > XI, dimensional quantity.
	DX	x increment for vortex shedding calculation. Typical value, DX ≈ D/2.
	XTR1	Beginning of transition region, dimensional quantity.
	XTR2	End of transition region, dimensional quantity.

EMKF	Minimum distance of shed vortex starting position from the body surface. = 1.0, shed vortices located according to stagnation point criterion > 1.0, minimum radii position of shed vortices. Typical value, EMKF = 1.05
RGAM	Vortex combination factor. = 0.0, vortices are not combined (preferred) > 0.0, radial distance within which vortices are combined
VRF	Vortex reduction factor, δ_1 to account for observed decreases in vortex strength. = 0.6, for bodies with bases = 1.0, for closed bodies

Item 8 is a single card containing the integration tolerance, asymmetry perturbation information, alternate separation criteria, and the core radius.

Item	Variable	Description
8 (8F10.5)	E5	Error tolerance for the vortex trajectory calculation. Typical range, E5 = 0.01 to 0.05 or larger if appropriate.

XTABL	Location at which a table of points on the body and on the circle are printed. = 0.0, no table of points is printed (preferred) > 0.0, table of points for all x < XTABL
XASYMI	Initial x station for asymmetric perturbation.
XASYMF	Final x station for asymmetric perturbation.
DBETA	Angular displacement of separation points for asymmetry perturbation.
SEPL	Stratford laminar criterion. = 0.0, program uses SEPL = .087 (preferred) > 0.0, program uses input value
SEPT	Stratford turbulent criterion. = 0.0, program uses SEPT = .350 (preferred) > 0.0, program uses input value
RCORE	Ratio of the local core radius to the local body diameter. Default value is .025. Maximum allowable value is $.025*D/r_o$.

Item 9 is a single card containing two flags for the source distribution. The source distribution may be input (NSOR > 0), calculated from the body geometry (NSOR = -1), or omitted from the solution (NSOR = 0). If the Mach number is not equal to zero (NCOMP > 0) then a different source distribution is required for each Mach number.

Item	Variable	Description
9 (2I5)	NSOR	Source distribution flag. = -1, calculate the source distribution from the input geometry input = 0, no sources (not recommended) > 0, number of sources to be input
	NPRT	Source distribution print flag. = 0, output source locations and strengths = 1, above output plus input and source geometry comparison = 2, above output plus source-induced surface velocities

Omit Items 10 and 11 if NSOR < 0.

Items 10 and 11 contain the nondimensional source locations and nondimensional source strengths, respectively.

Item	Variable	Description
10 (6E12.5)	XSRC	Nondimensional source locations, x/L. (NSOR values, 6 per card)

Item	Variable	Description
11 (6E12.5)	QS	Nondimensional source strengths, $Q/4\pi L^2 V_\infty \cos\alpha_c$.

Items 12 through 15 contain the body geometry information. This information must be included for all bodies whether in circular or noncircular.

Item	Variable	Description
12 (I5)	NXR	Number of entries in the body geometry table. ($1 < NXR < 101$)

Item	Variable	Description
13 (8F10.5)	XR	Nondimensional axial stations in the geometry table, x/L. (NXR values, 8 per card)

Item	Variable	Description
14 (8F10.5)	R	Nondimensional body radius at the NXR x/L-stations, r_o/L (NXR values, 8 per card). For an ellipse, $r_o = (a + b)/2$. For arbitrary bodies, r_o is equivalent radius.

Item	Variable	Description
15 (8F10.5)	DR	Body slope at the NXR x/L stations dr_o/dx. (NXR values, 8 per card)

Omit Items 16 and 17 if NCIR $\neq$ 1.

Items 16 and 17 contain the nondimensional horizontal and vertical half axis lengths if the cross sections are elliptical, NCIR = 1.

Item	Variable	Description
16 (8F10.5)	AE	Nondimensional horizontal half axis length of the elliptical cross section at the NXR x/L-stations, a/L. (NXR values, 8 per card)

Item	Variable	Description
17 (8F10.5)	BE	Nondimensional vertical half axis length of the elliptical cross section at the NXR x/L-stations, b/L. (NXR values, 8 per card)

Omit Items 18 through 29 if NCIR $\neq$ 2.

Items 18 through 29 are used to specify a body of arbitrary cross section shape. This body should also be polygonal in shape (i.e., negative interior angle can cause problems in the numerical conformal mapping procedure).

Omit Item 18 if NTH = 0.

Item	Variable	Description
18 (8F10.5)	TH	Special table of circle angles for arbitrary body mapping, (i = 1, 73), or to be used only if the density of points on the cross section needs adjusting to improve the resolution of pressure distribution. Not recommended under normal conditions.

Item	Variable	Description
19 (2I5)	MNFC	Number of mapping coefficients for the arbitrary body. (MNFC < 100)
	MXFC	Number of axial stations at which the arbitrary body is specified. (1 < MXFC < 10). For a similar shape at all cross sections, MXFC=1.

Item	Variable	Description
20 (8F10.5)	XFC	x stations at which the arbitrary body is specified. (MXFC values, 8 per card). For a similar cross section body, MXFC=1, XFC(1) < XI.

Omit Items 21 through 23 if NCF > 0.

Items 21 through 23 are repeated for each of the MXFC axial stations when the transformation coefficients are to be calculated (NFC = 0).

Item	Variable	Description
21 (I5)	NR	Number of points describing the arbitrary body cross section ($2 < NR < 30$). (Note: NR must be the same for all x stations.)

Item	Variable	Description
22 (6E12.5)	XRC	Horizontal coordinates of the arbitrary body cross section. (NR values, 6 per card). The convention for ordering the coordinates from bottom to top in a counter-clockwise fashion is observed, Figure 9. Right/left body symmetry is required.
23 (6E12.6)	YRC	Vertical coordinates of the arbitrary body cross section. (NR values, 6 per card). See Figure 9.

Omit Items 24 through 29 if NCF = 0.

Items 24 through 29 are repeated for each of the MXFC axial stations if the numerical transformations are available from a previous calculation. The only purpose for providing the option to input the mapping parameters is to eliminate the need to recompute the numerical mapping in subsequent runs and save computation time.

Item	Variable	Description
24 (2F10.5)	ZZC	Mapping offset distance.
	RZC	Equivalent radius of transformed cross section.

Item	Variable	Description
25 (I5)	NR	Number of points describing the arbitrary body cross section (NR $\leq$ 30). (Note: NR must be the same for all x stations.)

Item	Variable	Description
26 (6E12.5)	XRC	Horizontal coordinates of the arbitrary body cross section. (NR values, 6 per card). See Figure 9 and convention for Item 22.

Item	Variable	Description
27 (6E12.5)	YRC	Vertical coordinates of the arbitrary cross section. (NR values, 6 per card). See Figure 9.

Item	Variable	Description
28 (6E12.5)	THC	Circle angles θ, of body points. (NR values, 6 per card)

Item	Variable	Description
29 (6E12.5)	AFC	Mapping coefficients. (MNFC values, 6 per card)

Omit Items 30 and 31 if NXFV = 0.

Item 30 is a single card containing the x stations at which additional output is printed and/or calculated if NXFV > 0.

Item	Variable	Description
30 (8F10.5)	XFV	x stations at which additional output is printed or calculated. (NXFV values, 8 values maximum)

Omit Item 31 if NFV = 0.

Item 31 is a set of NFV cards which contains the coordinates of the field points where the velocity components are to be calculated at each of the axial stations in Item 30.

Item	Variable	Description
31 (2F10.5)	YFV,ZFV	y and z coordinates of the field points for the velocity field calculation. (NFV cards, maximum of 200)

It is important that all points lie outside the body surface at all axial stations.

Omit Items 32 through 37 if NVP + NVR + NVM + NVA = 0

Items 32 through 36 provide information needed to restart the calculation procedure. It is not necessary to input all four types of vorticity in a restart calculation.

Item 32 is a single card containing the nose force and moment coefficients at the restart point; that is, X = XI. These values may be set equal to zero, but the resulting forces and moments from the current calculation will be in error.

Item	Variable	Description
32 (5F10.5)	CN	Normal-force coefficient
	CY	Side-force coefficient
	CA	Axial pressure force coefficient
	CDI	Axial skin friction force coefficient
	CM	Pitching-moment coefficient
	CR	Yawing-moment coefficient
	CSL	Rolling-moment coefficient

Item 33 is a set of NVP cards which specify a cloud of positive primary body separation vorticity, usually on the right side of the body. The variable XSHEDP associated with each vortex is used only to identify individual vortices and permit the user to follow individual vortices during the calculation.

Omit Items 33 if NVP = 0.

Item	Variable	Description
33 (4F10.5)	GAMP	+y primary vorticity, Γ/V_∞.
	YGP	Horizontal coordinate, y, of vortex.
	ZGP	Vertical coordinate, z, of vortex.
	XSHEDP	Origin of the vortex.

Item 34 is a set of NVR cards which specify a cloud of reverse flow (secondary) body separation vorticity. This array is a convenient way to put an arbitrary cloud of additional vorticity which is to be maintained separately from the other body vorticity in the field.

Omit Item 34 if NVR = 0.

Item	Variable	Description
34 (4F10.5)	GAMR	+y reverse flow vorticity, Γ/V_∞.
	YGR	Horizontal coordinate, y, of vortex.
	ZGR	Vertical coordinate, z, of vortex.

XSHEDR	Origin of the vortex.

Item 35 is a set of NVM cards which specify a cloud of negative primary body separation vorticity, usually on the left side of the body. In the case of a symmetric flow field (ISYM=0), this block of vorticity is automatically defined as the mirror image of the positive vorticity input in Item 33.

Omit Item 35 if ISYM = 0 or NVM = 0.

Item	Variable	Description
35 (4F10.5)	GAMM	-y primary vorticity, Γ/V_∞.
	YGM	Horizontal coordinate, y, of vortex.
	ZGR	Vertical coordinate, z, of vortex.
	XSHEDR	Origin of the vortex.

Item 36 is a set of NVA cards which specify a cloud of reverse flow (secondary) body separation vorticity. This block of vorticity is analogous to Item 34, and it is omitted if NVA = 0 or if ISYM = 0. As with the previous item, this block of vorticity is automatically defined as the mirror image of the negative vorticity input as Item 34 if symmetry is required by ISYM = 0.

Omit Item 36 if ISYM = 0 or NVA = 0.

Item	Variable	Description
36 (4F10.5)	GAMA	-y reverse flow vorticity, Γ/V_∞.
	YGA	Horizontal coordinate, y, of vortex.

	ZGA	Vertical coordinate, z, of vortex.
	ZSHEDA	Origin of the vortex.

Item 37 contains the pressure distribution at the initial x station for a restart calculation. If a symmetric case is being considered, ISYM=0, only half of the pressure distribution is needed.

Item	Variable	Description
37 (3F10.5)	YBO	y body coordinate.
	ZBO	z body coordinate.
	CPO	pressure coefficients at (YBO, ZBO).

This concludes the input deck for a single run of VTXCLD. The code is not set up to stack input for multiple cases because of the sometimes long and generally unpredictable run times.

Input Preparation

In this section, some additional information is provided to assist the user in the preparation of input for certain selected problems. The previous section on the input description must be used to understand the individual variables which go into VTXCLD, and this section will permit the user to select the appropriate input to get optimum results from the code.

Numerical mapping.- The specification of the appropriate numerical mapping parameters (Items 18 through 29) depends on the shape of the cross section. In the interest of optimum computation time, the fewest possible terms in the transformation series (MNFC in Item 19) should be used which will produce an adequate mapping. Each different shape should be checked by the user to determine the proper number of coefficients. For example, a simple cross section which is similar to a circle may require as few as 10 coefficients. Others may require as many as 20 coefficients for an excellent mapping. If a large number of calculations are to be made for a noncircular shape, it is worthwhile for the user to try different numbers of coefficients in an effort to find an optimum number. Not only should the shapes be compared carefully, the unseparated flow pressure coefficients should be compared to evaluate the quality of the mapping.

The numerical mapping now included in VTXCLD has been used for a variety of cross section shapes, and very few problems have been observed. One general problem area is bodies with concave sides. The mapping procedure has difficulty converging on a set of coefficients. Usually the body shape can be modified slightly, to give the concave region a flat or slightly convex shape, and the mapping converges easily. This small change in the shape probably has very little effect on the predicted pressure distribution. This is an example of the type of problem to which the user should be alert.

<u>Integration interval</u>.- Choice of the appropriate integration interval (DX in Item 7) depends to a large extent on the type of results of interest. If the user is interested in detailed nose loads and separation on the nose, where the radius is changing rapidly, the internal should be smaller than the recommended D/2. On very long bodies, the recommended interval is usually adequate for accurate predictions.

<u>Vortex core</u>.- The core size specification is referenced to the local body diameter (RCORE in Item 8). The default value is

0.025, and this value is adequate for most cases. The larger the core radius specified, the more the vortex effects are reduced. To eliminate the possibility of negating the vortex effect entirely, a maximum vortex core of .05 times the maximum body diameter is built into the code. Except in unusual situations, the default value is recommended, and this is the value used in the comparisons with data shown in a later section.

Sample Cases

In this section, nine sample input cases are described to illustrate the various program options available in VTXCLD. The purpose is to point out the available features and options and to provide a range of sample inputs which will help users prepare input for specific cases. Table I provides a summary of the sample input cases to assist the user in finding an appropriate example.

Sample Case 1, Figure 10(a), is a test run based on the 3-caliber ogive-cylinder body in Reference 20. This run will also be used as the sample output case in the next section. It is recommended that this case be run initially to provide a check with the results presented in a following section. The input for the first sample case is described in detail, and for the following cases, only the major differences are discussed.

Input Item 1 indicates that the case consists of a body with a circular cross section, NCIR = 0, and a symmetric vortex wake, ISYM = 0. The separation criteria is laminar, NBLSEP = 1, and a diffuse vortex core model is to be used, NDFUS = 1. NDPHI = 1 indicates that the two-dimensional unsteady pressure term is included in pressure calculation. NXFV = 7 and NFV = 0 are included to denote special output to be printed for seven axial stations which are specified in Item 30. If NFV > 0, the flow field will be calculated at the 7 axial stations in addition to any special output.

Input Item 2 indicates there will be four title cards input in Item 3. NPRNTP = 0 specifies the pressure distribution be output at the seven special x stations specified by NXFV, and NPRNTS = 1 causes a summary of the separation points to be output at all x stations. The flag NPRNTV = 0 results in a summary of the vortex field at the seven axial stations specified. NPLOTV = 3 and NPLOTA = 1 specifies that a line printer plot of the vortex field is created at the seven special x stations if separation has occurred. NSKIN = 1 will result in an estimation of the skin friction on the body, and NCOMP = 0 specifies an incompressible calculation.

Input Item 3 is a set of four title/summary cards which are printed at the top of the first output page.

Input Item 4 contains the reference information for the run. The reference area, REFS, is the maximum cross sectional area, the reference length, REFL, is the maximum diameter, and the moment center, XM, is located at the end of the ogive nose. The length of the body, SL, is 50.478 inches, and the maximum body diameter, SD, is 4.7 inches.

Item 5 contains the flow conditions. The angle of attack, ALPHAC is 15 degrees and the Reynolds number, RE, is 440000. There is no roll angle for this case, PHI = 0.0.

Item 7 specifies run parameters. The calculation procedure begins at x station, XI, 2.35 and continues to station, XF, 47.0 in DX increments of 2.35 or one body radius. Separation vortices are initially placed a minimum 1.05 radii, EMKF, from the axis of the missile. The vortex reduction factor, VRF, is set to 0.6 as recommended for bodies which do not close themselves.

The only major item of interest in input Item 8 is the tolerance for the vortex trajectory calculation, E5. This is set to 0.05, a typical value. Some additional comments on this tolerance are contained in the previous section on Error Messages and Stops.

Input Item 9 contains the flags for the source distribution calculation. NSOR = -1 specifies the source distribution is unknown and is to be calculated by VTXCLD. NPRT = 2 provides for additional output regarding the source distribution. This output includes a comparison of the input geometry and the geometry calculated from the source distribution which provides a good means of checking the calculated source distribution. Also printed are the surface velocities calculated by the source distribution.

Input Item 12 contains NXR, the number of entries in the body geometry table. Items 13, 14, and 15 are the axial stations, XR, the corresponding body radii, R, and the body slopes, DR, respectively. The axial stations and the radii are nondimensionalized with respect to the body length, SL.

The final input for this case is Item 30 which identifies XFV, the seven axial stations where special output is printed.

The following sample case inputs are discussed only briefly with some elaboration of the parameters of special interest.

Sample Case 2, Figure 10(b), is the same as Sample Case 1 except the source distribution is input and the angle of attack is changed. NSOR = 61 in Item 9 indicates that there are 61 source locations, XSRC, and strengths, QS, input via Items 10 and 11, respectively. The locations and strengths were obtained from the results of Sample Case 1. The angle of attack, ALPHAC, in Item 5 is changed to 20 degrees.

Sample Case 3, Figure 10(c), is a body with 2:1 elliptical cross section. This model is described in Reference 21. The elliptical cross section is handled by an analytical conformal mapping, NCIR = 1 in Item 1, and the other inputs required for the ellipse are the half-axis lengths, AE and BE, input in Items 16 and 17.

Sample Case 4, Figure 10(d), is a body of square cross section with rounded corners from Reference 22. A compressible Mach number is specified. For this cross section, a numerical conformal mapping must be used, NCIR = 2 in Item 1. NCF = 0 in Item 1 indicates that the mapping coefficients are to be calculated. The desired number of mapping coefficients, MNFC, is set to 20 in Items 19. Item 19 also specifies the number of axial stations at which the body is defined, MXFC = 1. MXFC = 1 is used because all of the axial stations are similar in shape; therefore, it is necessary to calculate mapping coefficients only at a single station. If the cross sections along the body are not similar, mapping coefficients must be calculated at a number of different sections. Item 20 is the axial station, XFC, at which the mapping coefficients are calculated. In Item 21, NR = 25 is the number of points describing the body cross section and Items 22 and 23 contain the horizontal and vertical coordinates of the cross section, respectively.

Compressibility is included by setting the compressibility flag, NCOMP, to 1 in Item 1. The freestream Mach number is defined in Item 6, MACH = 0.5.

Sample Case 5, Figure 10(e), illustrates the required input for an axisymmetric body at nonzero Mach number. This case is Sample Case 1 with a compressibility correction. NCOMP in Item 2 is set to 1, and the Mach number, MACH, is set to 0.8 in Item 6. The source distribution is calculated because it changes with Mach number.

Sample Case 6, Figure 10(f), illustrates the specification of a transition region. The beginning and end of the transition region are specified in Item 7. The beginning, XTR1 = 7.05, and the end, XTR2 = 11.75, define the region over which the separation criteria changes from laminar to turbulent.

Sample Case 7, Figure 10(g), illustrates the required input for a case in which an asymmetric wake occurs. In order to obtain an asymmetric vortex wake, the flags ISYM and NASYM in Item 1 are set to 1. The required symmetric perturbation is specified in Item 8 where the initial x station for the perturbation, XASYMI = 0.0, and the final station, XASYMF = 5.145, are defined. The angular displacement of the separation points, DBETA, is 2.0 degrees over the entire region. In Item 2, NPRNTP and NPRNTV have been set to 1. This will cause the pressure distribution and vortex wake to be printed at each x station.

The velocity field is calculated at 57 (NFV) field points at seven axial stations, NXFV. These inputs are defined in Item 1. The seven axial stations where the velocity field is desired are specified in Item 30, and the 57 field points where the velocities are calculated are included in Item 31.

Sample Case 8, Figure 10(h), is a lobe body from Reference 23 shown to illustrate another arbitrary cross section body. The noncircular input has similar format to the rounded square body of Sample Case 4, and the only difference is in the body cross section specification in Items 22 and 23. No source distribution is input or calculated for this case; therefore, this situation approximates a two-dimensional example in which the axial coordinate represents time.

Sample Case 9, Figure 10(i), is an example of a restart calculation for Sample Case 2. The case is restarted from XI =

21.15 and continued to XF = 47.0. Additional input required for this case are the overall loadings in Item 32, the vortex locations and strengths in Items 33 and 35, and the pressure distribution in Item 37. This case is included to illustrate the means to restart a calculation which did not finish or one in which the vortex field was adjusted to include additional vortices from a forward lifting surface.

Output Description

A typical output file from VTXCLD is described in this section. In general, the output quantities from VTXCLD are labeled and each page is headed with approximate descriptive information. The output from Sample Case 1, Figure 10(a), requires 52 pages, and it will be described briefly page by page. Representative pages are shown in Figure 11.

The first output page contains the title/summary cards, the reference quantities, the flow conditions, the initial run conditions, and the run flags. Page 1 is simply an echo of the input parameters. Also contained on this page are the force and moment definitions. Pages 2 and 3 echo the input body geometry, XR, R, and DR. The dimensional X and R values are also printed.

Pages 4 through 10 contain information from the three-dimensional source distribution calculation. Page 4 is a summary of the source placement and the body geometry at these locations. Page 5 shows the source locations and strengths, and pages 6 and 7 are a comparison of the input geometry shape, R/L(INPT), and the shape calculated from the source distribution R/L(S.D.). This comparison is indicative of the quality of the source distribution. A second indication of difficulties with the source distribution will show up in the number of iterations required to find the proper shape, M-INDEX. If this number is less than four or five, the chances are good the source distribution is a good representation of the body. If this number is large, examine the input and predicted shapes carefully for problems. Pages 8 and 9 are the surface velocities calculated by the source distribution, and they should be examined to ensure that no exceedingly large velocities occur, another indication of a problem with the body model. Small oscillations in the velocities on the cylindrical portion of a body are to be expected.

Page 10 contains a summary of source locations and strengths, and the values on this page are in the correct format for input into VTXCLD for additional cases using the same geometry. See Sample Case 2 for an example. Also contained on page 10 are the x stations at which special output is printed.

Page 11 starts the output from the analysis part of the code. The first numeric line on page 11 contains the axial locations, the local radius, the body slope, and the transition Reynolds number, RETR. Since axial station x = 2.35 is a special output station specified in Item 30, the pressure distribution is printed. The predicted results on pages 11 and 12 are a summary of the velocities and pressures on the circumference at this particular x station. The coordinates are dimensional, and the velocities are made dimensionless by the freestream velocity. The pressure coefficient is followed by the unsteady term, $d\phi/dt$.

Following the pressure distribution is a summary of the section loadings and the overall loadings up to the current section. CN(X), CY(X), and CA(X) are the normal-, side-, and axial-force coefficients per unit length, respectively. CN, CY, and CA are the overall normal-, side-, and axial-force coefficients from the nose to the current x station, respectively. CM, CR, and CSL are the pitching-, yawing-, and rolling-moment coefficients, respectively. XCPN and XCPY are the x locations of the centers of pressures for the normal and side forces, respectively.

The next line of output is the estimation of the axial skin friction coefficient followed by the total axial force coefficient made up of the pressure force and the skin friction force.

The final block of information on page 12 contains a summary of the pressure distribution and the separation points at x station 2.35. It is noted here that no separation occurs at this station.

Output pages 13 and 14 have the same format as pages 11 and 12 so they will not be discussed in detail. The x station is 4.7, a special output station, so the pressure distribution is again output. The last two lines of page 14 indicate that separation occurs at this axial station. The last block of information contains the intitial locations and strengths of the separated vortices.

Page 15 shows the force and moment summary and separation information for x = 7.05. This format is the same as the previous stations; however, the pressure distribution is not output at this station because x = 7.05 is not a special output station.

Axial station 9.4 is again a special output station. Page 16 is a summary of the vortex wake at this station after the trajectories of the individual vortices have been calculated. Each individual vortex in the field is described in terms of its location in the real plane (Y, Z) and the transformed circle plane (YC, ZC). The last block of information is the centroid of vorticity on each side of the body. This includes all the vorticity, including that in the feeding sheet; therefore, the numerical centroid location may be lower than expected because of the effect of the vortices in the feeding sheet.

Page 17 has the same format as page 11 described previously. Page 18 is a line printer plot of the cross section and the vortex wake. Page 19 is a summary of the separation points at x = 9.4, as was described for page 12.

The remainder of the output pages, except the final three, repeat the formats described previously. A typical output station has a force and moment and separation summary like page 15. Special output stations have a wake summary, pressure distribution output, line printer plot, and separation summary like pages 16 - 19.

The last three pages of the output shown in Figure 11(t), (u) and (v) give a summary of the total loadings, the vortex wake, and the pressure distribution. Page 50 contains a line printer plot of the vortex wake at the final x station and a summary of the total loads on the body. Page 51 is a summary of the vortex wake in tabular form. This information can be used for a restart of the calculation. Page 52 is a summary of the pressure distribution at the last x station; needed for a restart calculation.

RESULTS

For purposes of evaluating the accuracy and range of applicability of the subsonic vortex shedding model and associated computer code VTXCLD, comparisons of measured and predicted aerodynamic characteristics are presented. Results for both circular and noncircular bodies are shown for a wide range of flow conditions including flow asymmetry and compressibility effects. Since the major objective is the validation of the prediction method, not all predicted results are in good agreement with experiment to illustrate to the user where problems may occur during general use of the code. Typical results from the prediction method follow.

Circular Bodies

The prediction method was applied to an ogive-cylinder model (Ref. 20) in subsonic flow over a range of angles of attack to evaluate the pressure prediction ability of the code. The configuration has a three-caliber ogive nose and a 7.7-caliber cylindrical afterbody. Circumferential pressure distributions at a number of axial stations are available for a range of flow conditions.

As shown in Sample Case 1, the model is represented by 61 point sources and sinks on the axis, and the ogive nose is used to close the model at the base. Because of the low Reynolds numbers of the experiment, laminar separation is used for all predictions for this model. Comparisons of measured and predicted normal force distributions at α = 10, 15, and 20 degrees are presented in Figure 12. The predicted results with vortex wake effects included are in good agreement with experiment for the angles shown. The significant influence of the lee side vorticity is illustrated for α = 10 and 20 degrees where the potential flow or slender body theory results without vortex induced effects are shown as a dashed curve. Note that the vortex effects are small on the nose at α = 10 degrees and they begin to grow as the vortex increases in strength toward the end of the afterbody. At α = 20 degrees, the vortex effects are important on the nose, and they become a dominant effect on the cylindrical portion of the model.

Details of the predicted characteristics are shown in Figure 13 where comparisons of measured and predicted pressure distributions for α = 15 and 20 degrees are presented. The predicted results including vortex induced effects are represented by the solid curves and those without vortex effects are shown as dashed curves. At α = 15 degrees in Figure 13(a), the vortex effects do not become significant until approximately 4.5 diameters from the nose. Some of the roughness in the rational flow model results is caused by individual vortices moving too near the body surface during the trajectory calculation. The vortex core model does tend to smooth the vortex induced effects, but there can still be a large local effect. These local irregularities have a minimal effect on the integrated loads.

The higher angle results shown in Figure 13(b) exhibit much larger vortex induced effects because the separation vortices are stronger and occur earlier on the body. The fact that there are more vortices with greater individual strength causes the local irregularities to be greater. This minor problem could be corrected to some extent by decreasing the axial interval (DX) of separation. The individual strengths of the vortices would decrease, but there would be more vortices forming the cloud. Smoother pressure distributions may result at the expense of additional computation costs.

The predicted vortex cloud on the ogive cylinder model at α = 15 degrees is shown in Figure 14. As observed above, the cloud does not become significant until approximately 4.5 diameters from the nose even though separation begins at one diameter from the nose.

The total normal-force coefficient is shown in Figure 15 where both potential-flow and rational-flow model results are compared with experiment. As noted in the pressure coefficient comparisons, the vortex induced effects become significant at α = 10 degrees and grow with increasing angle. At low angles the predicted results are in good agreement with the low Reynolds number measurements, but at high angles, the theory is in better agreement with the high Reynolds number results. This phenomenon is not completely understood at this time, and further evaluation with other experimental measurements is recommended.

The effects of compressibility on the measured and predicted normal force distributions are shown in Figure 16 for α = 15 degrees. Predicted compressibility effects exhibit the correct trend, but they are less than those measured on the nose. The overshoot at the shoulder of the model is not predicted.

Measured and predicted pressure distributions are presented in Figure 17. The increment in pressure coefficient due to compressibility effects appears to be in reasonable agreement with experiment, although there is some disagreement in the lower pressure regions near $\beta > 60$ degrees on the nose. This obviously accounts for the problem with normal force discussed above. The decreasing effect of compressibility along the cylindrical portion of the body is in good agreement with experiment.

The above comparisons indicate the compressibility correction included in the prediction method and code represents the measured effects; however, further verification is needed. The limited experimental data available are not sufficient to define the Mach number and angle of attack limits of the code.

Additional comparisons of measured and predicted pressure distributions on other axisymmetric bodies are presented for further verification. For these comparisons, the 2.0- and 3.5-caliber ogive-cylinder models tested by Lamont (Refs. 17 and 24) over a wide range of angles of attack and Reynolds numbers are used. Only experimental data at moderate angles of attack are considered to guarantee flow symmetry.

In Figure 18, measured and predicted circumferential pressure distributions on the 3.5-caliber ogive-cylinder model at α = 20 degrees are compared. The predictions are shown with (solid curve) and without (dashed curve) vortex induced effects included. As in the previous results, the separation-vortex effects improve the shape of the pressure distribution curves, particularly on the lee side; however, there is a general lack of agreement between the experiment and theory. There appears to be a uniform shift between the measured and predicted pressure coefficients, even on the windward side of the model where vortex induced effects should be negligible.

In Figure 19, similar comparisons are shown for the 2.0-caliber ogive-cylinder model at α = 30 degrees. Because of the higher angle of attack, vortex induced effects are larger than before, but the character of the comparisons is nearly the same; that is, on the cylindrical portion of the model, the experiment and theory disagree by a constant increment in pressure. There are other areas of disagreement as it appears that the predicted vortex effects are often stronger than exhibited by the experiment.

In an effort to better understand the use of the vortex cloud prediction method and in an attempt to resolve the differences discussed above, the following is presented for discussion purposes. Since the windward meridian should have minimal vortex induced effects at moderate angles of attack, a comparison of experiment and theory along this meridian should be a measure of the accuracy of the linear or attached-flow part of the theory. In Figure 20, a number of experimental results for various ogive-cylinder models at α = 20 degrees are compared with a single predicted result. The ogive noses vary from 1.5 to 3.5 diameters in length (Refs. 17, 20, 24, and 25), but the pressure on the cylinder aft of the nose should be nearly independent of the nose shape. The predicted pressures are for the 3.5-caliber ogive of Lamont and the 3-caliber ogive of Tinling and Allen. It is observed that the theoretical results are in agreement with the experiments of References 20 and 25 and in disagreement with the experiments of References 17 and 24. The authors have no explanation for these discrepancies.

At higher angles of attack, the separation vorticity becomes asymmetric and causes both an induced normal force and side force. As discussed in a previous section, an asymmetric solution develops only after the solution is perturbed, and the final result is somewhat dependent on the perturbation. Some preliminary results are presented to illustrate an asymmetric result.

Detailed flow field measurements and pressure distributions on a 3.0-caliber ogive-cylinder model at α = 45 degrees are available in Reference 26. Based on earlier experience with asymmetric solutions (Ref. 2), the perturbation region was limited to the first diameter of length of the nose, and the magnitude of the perturbation was varied to find an appropriate solution. In Reference 2, the position of the shed vorticity was used as the criterion to evaluate the perturbation; however, in the present solution, a more appropriate criterion is the frequency of variation of the predicted side-force distribution. In Figure 21, the measured and predicted normal-force and side-force distributions are shown. Two different perturbations, $\Delta\beta$ = 1 and 2 degrees, are shown, and even though the magnitude of the predicted side force is less than that measured, the frequency of the side force matches best when $\Delta\beta$ = 2 degrees. This is the perturbation used for all the predicted results to follow. The predicted normal force is below the level of the measured normal force by a small amount, but the side force is considerably less than that measured. It is apparent that the vortex induced effects are too weak for this case.

Measured and predicted circumferential pressure distributions at three axial stations are shown in Figure 22. Since the flow is asymmetric, the full circumference is shown in these comparisons. The major areas of disagreement are generally for $80° < \beta < 160°$ and $200° < \beta < 270°$; although at the aft station where the error in side force is greatest, the disagreement is concentrated in the region 80° < β < 160° which causes the maximum effect on predicted side force. The explanation of this problem is best accomplished by a discussion of the separation wake using the following figures.

The predicted vortex cloud at x/D = 4.7 is shown in Figure 23 where an obvious asymmetry has developed. At this station, the cloud on the left side of the body has nearly broken away from its feeding sheet and formed a free vortex. Reverse flow vorticity is not included in the predicted results because of numerical difficulties with this particular case. The pressure distribution on the lee side and the reverse flow velocity field induced by the primary vortex field permits the calculation of secondary separation and the shedding of secondary vorticity. When these phenomena were included in the calculation, the effects of the additional vorticity were lost when the primary vorticity pulled the secondary vortices into the main cloud and effectively eliminated their local effect on the pressure distribution. The need for the secondary vorticity is illustrated in the following figures.

The measured velocity field at the same axial station is shown in Figure 24(a) where the individual flow vectors are shown. The predicted velocity vectors in the same general region of the lee side flow field are shown in Figure 24(b). Both measured and predicted flow fields are similar in magnitude and flow directions except in the reverse flow region near the surface of the body. It is obvious in Figure 24(a) that a secondary vortex field exists in the region of interest, 120° < β < 170°. The difficulties with the predicted secondary separation vorticity were not resolved in the current investigation.

The success of the previous flow field comparisons stimulated another set of comparisons to be sure the previous results were not fortuitous nor accidental. Experimental flow field velocity components on the lee side of a 3.5-caliber ogive-cylinder model at α = 22.4 and 37.5 degrees are available in Reference 27. At the lower angle of attack, α = 22.4 degrees, the symmetric flow field is shown in Figure 25 for three different positions in and near the vortex cloud. The location of the experimental results and the predicted vortex cloud are shown in the sketches in the figure. In each case the predicted downwash velocity distribution is in very good agreement with the experimental results. The observed roughness when the predictions are carried out through the center of the cloud is caused by the influence of a discrete vortex too near the calculated point.

At α = 37.5 degrees, the flow asymmetry was developed with a $\Delta\beta$ = 2 degrees perturbation in accordance with the previous asymmetric results. The velocity field comparisons are shown in Figure 26, and the location of the results and the asymmetric vortex field is illustrated in the sketches. As above, the agreement is very good. The roughness of the predictions is again caused by the near proximity of several discrete vortices as seen in the sketches.

Noncircular Bodies

The noncircular body options in VTXCLD have been tested for a number of different cross section shapes, both elliptic and arbitrary, to verify the transformation procedures. Unfortunately, only a limited quantity of experimental data are available for comparison purposes. A series of elliptic bodies and one square body with rounded corners are examined to illustrate the capabilities of the code.

Measured normal-force coefficients on a series of elliptic cross section bodies at high angles of attack are available in Reference 21. The cross section shapes are 1.5, 2, and 3.5:1 ellipses with equal areas, and each model has a 3-caliber ogive nose and 7-caliber cylindrical afterbody. Measured and predicted normal-force coefficients are shown in Figure 27. Agreement between experiment and theory is very good for $\alpha < 20$ degrees for all models, and the error at larger angles of attack appears to be nearly the same for the three cross sections. As expected, the nonlinear effects become more evident as the ratio of major to minor axes increases.

The predicted vortex cloud patterns at the end of the body for each of the three cross sections are shown in Figure 28. The dimensionless strength of the vorticity on the positive side of each body is also shown in the figure.

Though pressure measurements are not available, it is interesting to observe the change in pressure distribution along the elliptic bodies as the vortex strength increases. In Figure 29, the predicted pressure distributions around the 2:1 elliptic body at $\alpha = 20$ degrees for three axial stations are shown. The solid curves from the rational flow model are compared with the potential flow distributions, and it appears that the major nonlinear effects are an increase in the minimum pressure at the side of the body and lower pressure on the lee side of the body.

The prediction method was next applied to a square body with rounded corners at $\alpha = 20$ degrees and $M_\infty = 0.5$ from Reference 22. The model has a 3-caliber nose followed by a 10-caliber cylindrical afterbody. The measured and predicted normal-force coefficients for the body at $\phi = 0$ and 45 degrees roll angles are compared in Figure 30(a) and (b), respectively. At $\phi = 0°$, the predicted normal force is greater than the measured value. It is interesting that the measured results show very little effect of corner radius; that is, the smallest radius tested behaves like a circular cross section at subsonic Mach numbers.

Measured and predicted results on the same body rolled 45 degrees are shown in Figure 30(b). The agreement is very good for the three Mach numbers 0.5, 0.7, and 0.8. In the rolled condition, the effect of corner radius is significant on the measured normal force. This phenomena may be explained by looking at the vortex shedding results.

In Figure 31, the predicted vortex wake on the square body with rounded corners is shown for ϕ = 0 and 45 degrees. At ϕ = 0, separation can occur at either the upper or lower corner, and it may occur at both locations simultaneously if the lower portion of the flow reattaches on the flat side. The prediction method cannot handle multiple separation or reattachment; therefore, it is not surprising that the normal-force coefficients in Figure 30(a) are in poor agreement. When the model is rolled 45 degrees, there is only one adverse pressure region near the corner on the side, and a single separation location is indicated. The prediction method appears to have little problem with this situation. The vortex strengths shown on each figure indicate that the vortex wake from the ϕ = 45 degrees flow condition is slightly stronger than that corresponding to the unrolled condition.

CONCLUSIONS

An engineering prediction method based on a rational flow modeling technique and the associated code VTXCLD to predict the vortex shedding from circular and noncircular bodies in subsonic flow at angles of attack and roll are described. Comparisons of measured and predicted aerodynamic characteristics and flow field quantities are used to verify the flow model and prediction method for a variety of configurations under a wide range of flow conditions. The method has proved successful in representing the principal features of the complex flow field on the lee side of missiles at moderate angles of attack; therefore, it has application as an engineering or preliminary design technique directed at the prediction of nonlinear aerodynamic characteristics resulting from high angle of attack flows.

The prediction method described herein has further application as one component of a larger prediction method for complete configurations consisting of an arbitrary body and multiple fins. The ability to model the correct flow field in the vicinity of the body leads to the capability to calculate body separation wake induced interference effects on fins and other control surfaces. The vortex shedding analysis and prediction techniques are also applicable for use in other codes; for example, the methods developed in this investigation can be transferred to higher order codes such as panel codes. This was demonstrated in the supersonic vortex shedding work reported in Reference 3.

Finally, the prediction method presented in this report must be considered as preliminary. Even though verification of the method by comparisons with experiment has demonstrated some success, there are configurations and flow conditions which must be approached with caution. For this reason, several recommendations for improvements to the method are suggested in the following section.

RECOMMENDATIONS

In the course of development and verification of the code VTXCLD, several specific areas requiring additional work were identified. Since the additional effort was beyond the scope of the present investigation, they are noted below as recommendations for future work.

The first and most important recommendation is for a thorough testing and further verification of VTXCLD. The code should be applied to a variety of configurations and flow conditions for which experimental results are available for comparison purposes. This should better define the operational limits of the method. The major difficulty will be the lack of useful experimental results on noncircular bodies.

As noted in the text, use of the code at high angles of incidence for asymmetric vortex wake calculations presents a problem regarding the required perturbation necessary to develop asymmetric solutions. It is recommended that the code be applied to a number of asymmetric cases for which experimental data are available in an effort to correlate the magnitude and location of the perturbation in light of comparisons with data. This is the only method which will permit the code to be used with confidence for asymmetric flow conditions.

A similar problem exists with the transition option included in the code. Some effort should be expended to better understand the effects of changing the character of separation from laminar to turbulent. As before, correlation of predicted results with experiment may provide the necessary rules for using transition with confidence.

The numerical difficulty associated with secondary separation discussed in a previous section needs further investigation. A minor modification may correct the problem, but some additional effort is required to understand the source of the problem.

The prediction method may have additional uses which have not been explored. For example, the code has vortex shedding technology built into it which can be transferred to three-dimensional panel codes. The code also has potential use in providing separation line and vortex wake information for starting solutions for higher order prediction methods.

Nielsen Engineering & Research, Inc.
Mountain View, CA 94043-2287
November 1985

REFERENCES

1. Spangler, S. B. and Mendenhall, M. R.: Further Studies of Aerodynamic Loads at Spin Entry. Report ONR-CR212-225-3, U.S. Navy, June 30, 1977.

2. Mendenhall, M. R., Spangler, S. B., and Perkins, S. C., Jr.: Vortex Shedding from Circular and Noncircular Bodies at High Angles of Attack. AIAA Paper 79-0026, January 1979.

3. Mendenhall, M. R. and Perkins, S. C., Jr.: Prediction of Vortex Shedding From Circular and Noncircular Bodies in Supersonic Flow. NASA CR-3754, January 1984.

4. Marshall, F. J. and Deffenbaugh, F. D.: Separated Flow Over Bodies of Revolution Using an Unsteady Discrete-Vorticity Cross Wake. NASA CR-2414, June 1974.

5. Deffenbaugh, F. D. and Koerner, W. G.: Asymmetric Wake Development and Associated Side Force on Missiles at High Angles of Attack. AIAA Paper 76-364, July 1976.

6. Mendenhall, M. R. and Nielsen, J. N.: Effect of Symmetrical Vortex Shedding on the Longitudinal Aerodynamic Characteristics of Wing-Body-Tail Combinations. NASA CR-2473, January 1975.

7. Nielsen, J. N.: Missile Aerodynamics. McGraw-Hill Book Co., Inc., 1960.

8. Skulsky, R. S.: A Conformal Mapping Method to Predict Low-Speed Aerodynamic Characteristics of Arbitrary Slender Re-Entry Shapes. J. of Spacecraft, Vol. 3, No. 2., February 1966, pp. 247-253.

9. Wolfe, W. P. and Oberkampf, W. L.: A Design Method for the Flow Field and Drag of Bodies of Revolution in Incompressible Flow. AIAA Paper 82-1359, August 1982.

10. Janikowsky, L. C. and Sarpkaya, T.: Optimized Discrete-Singularity Representation of Axisymmetric Bodies. AIAA Paper 85-0284, January 1985.

11. Christopher, P. A. T.: The Generation of Axi-Symmetric Bodies in Incompressible Flow by Means of Distributions of Complex Sources. Cranfield Report CoA 8304, March 1983.

12. Goodwin, F. K., Nielsen, J. N., and Dillenius, M. F. E.: A Method for Predicting Three-Degree-of-Freedom Store Separation Trajectories at Speeds up to the Critical Speed. AFFDL-TR-71-81, July 1971.

13. Shapiro, A. H.: The Dynamics and Thermodynamics of Compressible Fluid Flow. The Ronald Press Co., New York, 1953.

14. Cebeci, T., Mosinskis, G. J., and Smith, A. M. O.: Calculation of Viscous Drag and Turbulent Boundary-Layer Separation on Two-Dimensional and Axisymmetric Bodies in Incompressible Flow. McDonnell Douglas Rept. MDC JO 973-01 (Contract N00014-70-C-0099), November 1970.

15. Stratford, B. S.: The Prediction of Separation of the Turbulent Boundary Layer. J. of Fluid Mech., Vol. 5, 1959, pp. 1-16.

16. Keener, E.: Oil-Flow Separation Patterns on an Ogive Forebody. NASA TM-81314, October 1981.

17. Lamont, P. J.: Pressure Measurements on an Ogive-Cylinder at High Angles of Attack with Laminar, Transitional, or Turbulent Separation. AIAA Paper 80-1556, August 1980.

18. Meier, H. U. and Kreplin, H. P.: Experimental Investigation of the Transition and Separation Phenomena on a Body of Revolution, 2nd. Symposium on Turbulent Shear Flows, Imperial College, London, July 1979.

19. Sarpkaya, T.: An Inviscid Model of Two-Dimensional Vortex Shedding for Transient and Asymptotically Steady Separated Flow Over a Cylinder. AIAA Paper 79-0281, January 1979.

20. Tinling, B. E. and Allen, C.Q.: An Investigation of the Normal-Force and Vortex-Wake Characteristics of an Ogive-Cylinder Body at Subsonic Speeds, NASA TN D-1297, April 1962.

21. Schindel, L. H. and Chamberlain, T. E.: Vortex Separation on Slender Bodies of Elliptic Cross Section. MIT Aerophysics Laboratory Technical Report 138, (Contract N600/19/-65138), August 1967.

22. Schneider, W.: Experimental Investigation of Bodies with Non-Circular Cross Section in Compressible Flow. AGARD-CPP-336, Trondheim, Norway, September 1982.

23. Townsend, J. C., Howell, D. T., Collins, I. K., and Hayes, C.: Surface Pressure Data on a Series of Analytic Forebodies at Mach Numbers From 1.70 to 4.50 and Combined Angles of Attack and Sideslip. NASA TM-80062, June 1979.

24. Lamont, P. J.: The Complex Asymmetric Flow Over a 3.5D Ogive Nose and Cylindrical Afterbody at High Angles of Attack. AIAA Paper 82-0053, January 1982.

25. Hartmann, K.: Über den Einfluss der Reynoldszahl auf die Normalkräfte schlanker Flugkörperumpfe. DFVLR-AVA 25176A20, October 14, 1976.

26. Yanta, W. J., Wardlaw, A. B., and Sternklar, D.: Vortex Asymmetry Development on a Tangent Ogive. NSWC TR 82-394, October 1982.

27. Fidler, J. E., Schwind, R. G., and Nielsen, J. N.: An Investigation of Slender-Body Wake Vortices. NEAR TR 108, (Contract DAAHO1-75-C-0008), Feb. 1976.

TABLE I. SAMPLE CASES FOR PROGRAM VTXCLD

Sample Case	Ref.	Body Cross Section	M_∞	α_C	ϕ	General Comments	Execution Time VAX 11/750
1	20	Circular	0.00	15°	0°	Circular ogive-cylinder with flow symmetry and laminar separation. 3-D source distribution representing the body volume is calculated. Detailed output at selected x stations.	88 sec.
2	20	Circular	0.0	20°	0°	Sample as Sample Case 1 except the source distribution is input. The angle of attack has been changed to 20°.	84 sec.
3	21	2:1 Ellipse	0.0	15°	0°	Elliptic ogive-cylinder, analytical conformal mapping case.	101 sec.
4	22	Rounded Square	0.5	20°	0°	Rounded square ogive-cylinder, numerical conformal mapping case. Compressibility correction for M_∞.	1775 sec.
5	20	Circular	0.8	15°	0°	Same as Sample Case 1 except M_∞=.8, compressibility correction.	95 sec.
6		Circular	0.0	20°	0°	Same as Sample Case 2 except a transition region is specified from x = 7.05 to 11.75.	106 sec.
7	27	Circular	0.0	45°	0°	Circular ogive-cylinder at α = 45° with asymmetric vortex shedding. An asymmetric perturbation of 2° is specified for $0 < x < 5.145$.	1395 sec.
8		Lobe	0.0	15°	0°	Lobe cylinder with no volume effects (no 3-D sources), numerical conformal mapping.	69 sec.
9		Circular	0.0	15°	0°	Restart of Sample Case 1 from x station 21.15.	N/A

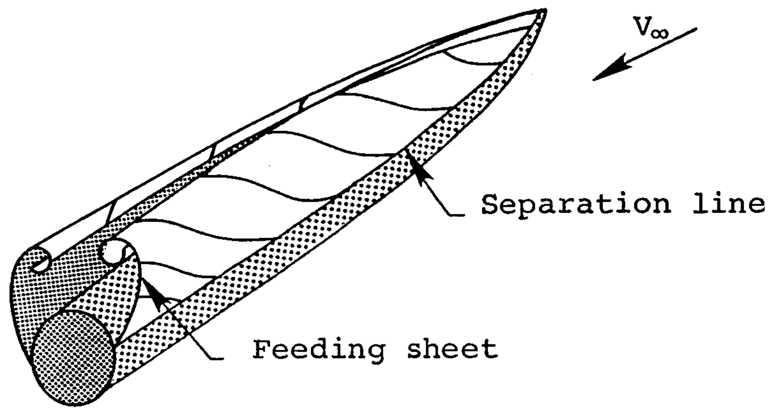

(a) Symmetric separation.

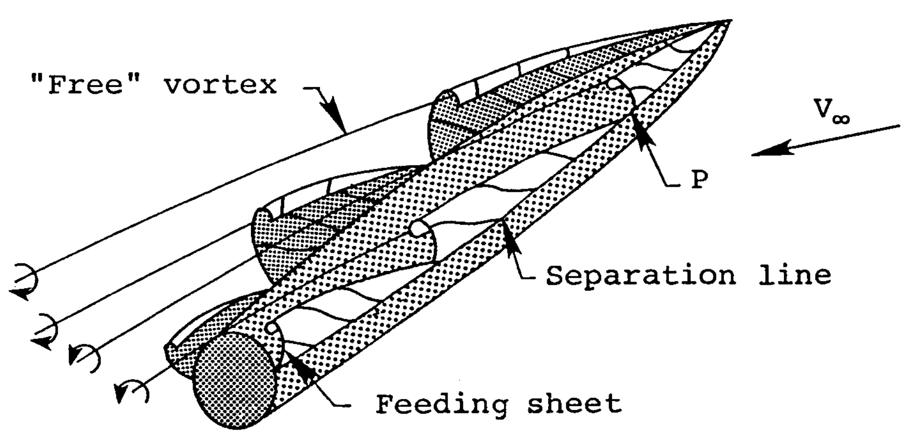

(b) Asymmetric separation.

Figure 1.- Lee side vortex formation on an inclined body.

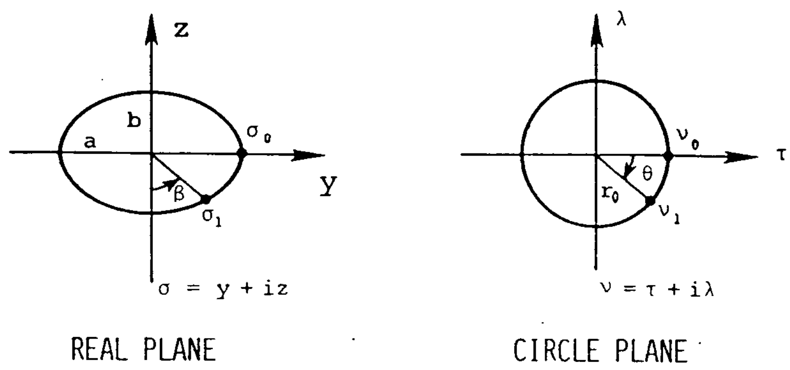

(a) Analytical transformation procedure

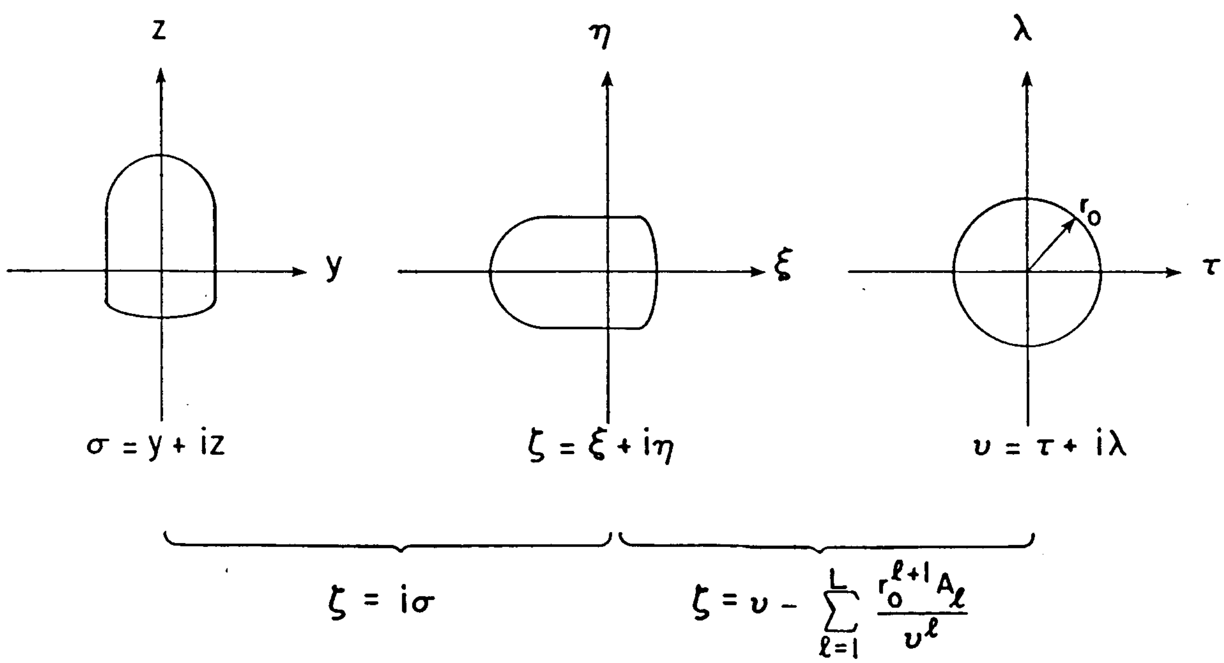

(b) Numerical transformation procedure

Figure 2.- Conformal mapping nomenclature.

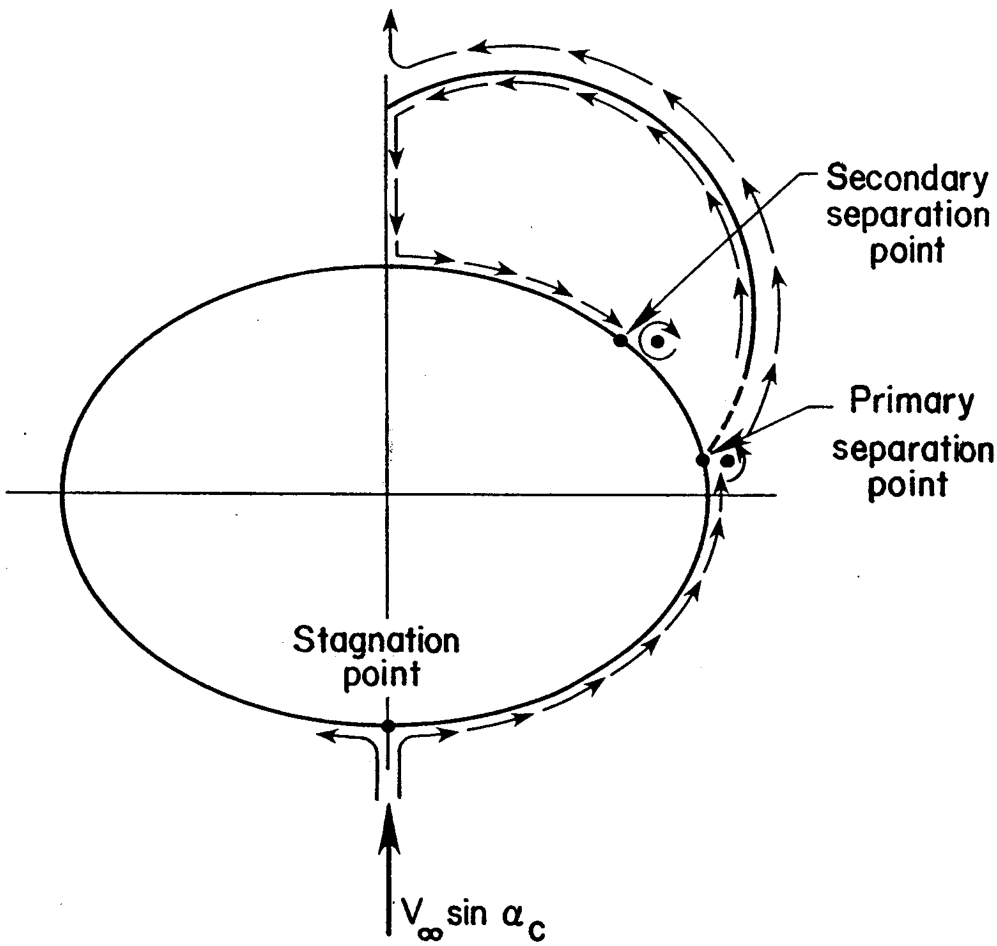

Figure 3. - Sketch of crossflow plane separation points.

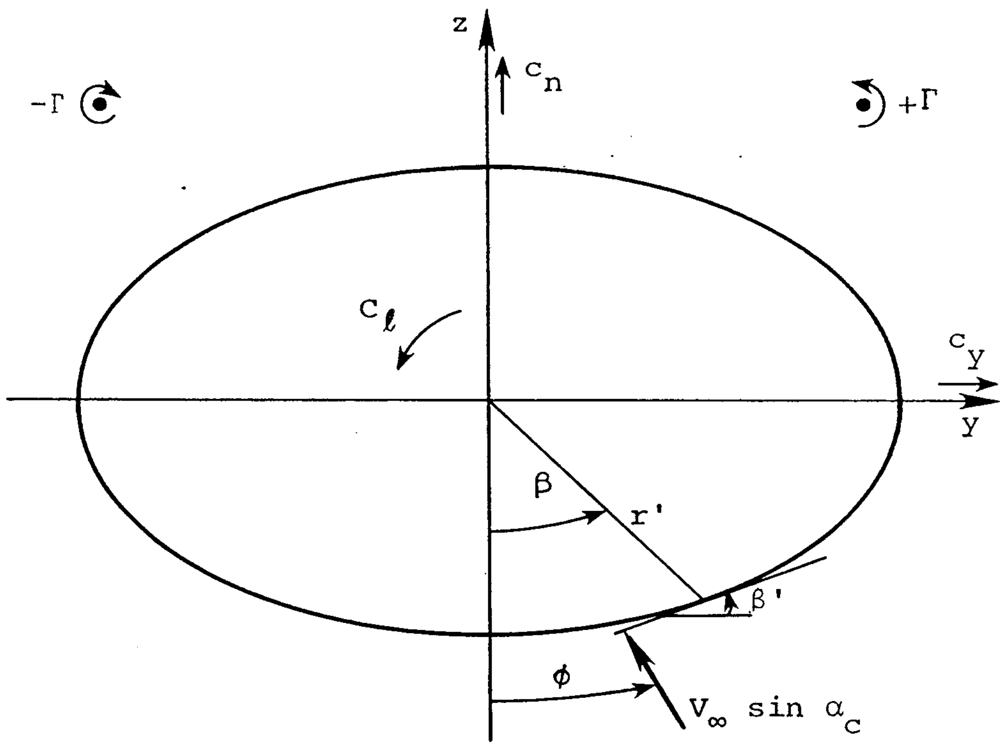

Figure 4. - Body crossflow plane nomenclature.

FLOW CHART OF PROGRAM - VTXCLD

```
PROGRAM
VTXCLD

  |--INPT      ----SORDIS  ----RDRDXI
  |            |            |--RDRDX
  |            |            |--INVERS
  |            |            |--FPSI
  |            |            |--FDPSDR
  |            |            |--SORVEL
  |            |--CONFOR   ----Z
  |--BODY      ----F       ----SHAPE
  |            |            |--BMAP     ----AMAP    ----Z
  |            |            |--CMAP     ----DZDNU
  |            |            |            |--Z
  |            |            |--SRCVEL
  |            |            |--VLOCTY   ----SUM     ----DZDNU
  |            |                         |--ASUM
  |            |--SHAPE
  |            |--BMAP     ----AMAP    ----Z
  |            |--CMAP     ----DZDNU
  |            |            |--Z
  |            |--SRCVEL
  |            |--VLOCTY   ----SUM     ----DZDNU
  |            |            |--ASUM
  |            |--DPHIDT
  |            |--SKIN
  |            |--FORCEP
  |            |--PLOTV    ----PLOTA2  ----PLOTA8  ----PLOTA6
  |            |                        |           |--PLOTA5
  |            |                        |--PLOTA7
  |            |--FPVEL    ----CMAP    ----DZDNU
  |            |            |           |--Z
  |            |            |--SRCVEL
  |            |            |--VLOCTY  ----SUM     ----DZDNU
  |            |                        |--ASUM
  |            |--SEPRAT
  |            |--CPPOT    ----SRCVEL
  |            |            |--SUM     ----DZDNU
  |            |--TRANSN
  |            |--VTABLE
  |            |--DFEQKM   ----F       ----SHAPE
  |            |                        |--BMAP    ----AMAP    ----Z
  |            |                        |--CMAP    ----DZDNU
  |            |                        |           |--Z
  |            |                        |--SRCVEL
  |            |                        |--VLOCTY  ----SUM     ----DZDNU
  |            |                                    |--ASUM
  |            |--VCENTR
  |            |--COMBIN
  |--PLOTV     ----PLOTA2  ----PLOTA8  ----PLOTA6
                            |           |--PLOTA5
                            |--PLOTA7

PROGRAM
  END
```

Figure 5.- Subroutine calling sequence for program VTXCLD.

CROSS REFERENCE MAP PAGE = 1

SUBROUTINE NAME / EXTERNAL REFERENCES	AMAP	ASUM	BMAP	BODY	CMAP	COMBIN	CONFOR	CPPOT	DFEQKM	DPHIDT	DZDNU	F	FDPSDR	FORCEP	FPSI	FPVEL	INPT	INVERS	PLOTA2	PLOTA5	PLOTA6	PLOTA7	PLOTA8	PLOTV	RDRDX	RDRDXI	SEPRAT	SHAPE	SKIN	SORDIS	SORVEL	SRVEL	SUM	TRANSN	VCENTR	VLOCTY	VTABLE	VTXCLD	Z
AMAP			X																																				
ASUM																																				X			
BMAP				X								X																											
BODY																																						X	
CMAP				X								X				X																							
COMBIN				X																																			
CONFOR																	X																						
CPPOT				X																																			
DFEQKM				X																																			
DPHIDT				X																																			
DZDNU					X																												X						
F				X					X																														
FDPSDR																														X									
FORCEP				X																																			
FPSI																														X									
FPVEL				X																																			
INPT																																						X	
INVERS																														X									
PLOTA2																								X															
PLOTA5																							X																
PLOTA6																							X																
PLOTA7																			X																				
PLOTA8																			X																				
PLOTV				X																																		X	
RDRDX																														X									
RDRDXI																														X									
SEPRAT				X																																			
SHAPE				X								X																											
SKIN				X																																			
SORDIS																	X																						

(a) Page 1

Figure 6.- Subroutine cross reference list for program VTXCLD.

CROSS REFERENCE MAP PAGE = 2

SUBROUTINE NAME / EXTERNAL REFERENCES	AMAP	ASUM	BMAP	BODY	CMAP	COMBIN	CONFOR	CPPOT	DFEQKM	DPHIDT	DZDNU	F	FDPSDR	FORCEP	FPSI	FPVEL	INPT	INVERS	PLOTA2	PLOTA5
SORVEL																				
SRCVEL				X				X				X				X				
SUM								X												
TRANSN				X																
VCENTR				X																
VLOCTY				X								X				X				
VTABLE				X																
Z	X				X		X													

SUBROUTINE NAME / EXTERNAL REFERENCES	PLOTA6	PLOTA7	PLOTA8	PLOTV	RDRDX	RDRDXI	SEPRAT	SHAPE	SKIN	SORDIS	SORVEL	SRCVEL	SUM	TRANSN	VCENTR	VLOCTY	VTABLE	VTXCLD	Z
SORVEL										X									
SRCVEL																			
SUM																X			
TRANSN																			
VCENTR																			
VLOCTY																			
VTABLE																			
Z																			

(b) Page 2

Figure 6.- Concluded

CROSS REFERENCE MAP PAGE = 1

SUBROUTINE NAME / COMMON BLOCKS	AMAP	ASUM	BMAP	BODY	CMAP	COMBIN	CONFOR	CPPOT	DFEQKM	DPHIDT	DZDNU	F	FDPSDR	FORCEP	FPSI	FPVEL	INPT	INVERS	PLOTA2	PLOTA5
$BLANK	X			X			X			X						X				
BLREV				X													X			
BLSEP				X													X			
BLTRAN				X													X			
BPLTA1																			X	
BPLTA2																			X	
BSCALE																			X	
CBODY				X										X			X			
CFLAG				X				X									X			
CFLT				X													X			
CNTROD				X						X										
CONF					X		X										X			
CONST	X		X	X	X		X	X		X		X		X		X	X			
COP				X													X			
CPPOT				X				X												
DYDX				X						X										
DZDX				X						X										
FLOW				X				X		X							X			
FRICT				X													X			
LOADP				X										X			X			
MACH				X				X		X							X			
MAP1	X	X	X	X	X		X	X			X	X		X		X	X			
MAP2			X	X				X						X			X			
MAPB	X		X	X	X							X				X				
MAPC	X		X	X	X							X				X				
MAPN	X	X	X		X		X				X						X			
MAPNTH			X														X			
MAPP	X				X		X				X						X			
MAPX				X								X								
MINPRT									X											

SUBROUTINE NAME / COMMON BLOCKS	PLOTA6	PLOTA7	PLOTA8	PLOTV	RDRDX	RDRDXI	SEPRAT	SHAPE	SKIN	SORDIS	SORVEL	SRCVEL	SUM	TRANSN	VCENTR	VLOCTY	VTABLE	VTXCLD	Z
$BLANK																X			
BLREV							X												
BLSEP							X							X					
BLTRAN														X					
BPLTA1		X	X																
BPLTA2																			
BSCALE			X	X															
CBODY																			
CFLAG																		X	
CFLT																			
CNTROD															X				
CONF								X											
CONST																X		X	
COP														X				X	
CPPOT																			
DYDX																			
DZDX																			
FLOW									X			X				X		X	
FRICT									X									X	
LOADP									X									X	
MACH										X		X				X			
MAP1							X	X					X			X		X	X
MAP2				X			X		X					X				X	
MAPB																			
MAPC																			
MAPN								X											X
MAPNTH																			
MAPP								X											X
MAPX																			
MINPRT																			

(a) Page 1

Figure 7.- Common block cross reference list for program VTXCLD.

CROSS REFERENCE MAP PAGE = 2

SUBROUTINE NAME / COMMON BLOCKS	AMAP	ASMU	BMAP	BODY	CMAP	COMBIN	CONFOR	CPPOT	DFEQKM	DPHIDT	DZDNU	F	FDPSDR	FORCEP	FPSI	FPVEL	INPT	INVERS	PLOTA2	PLOTA5	PLOTA6	PLOTA7	PLOTA8	PLOTV	RDRDX	RDRDXI	SEPARAT	SHAPE	SKIN	SORDIS	SORVEL	SRCVEL	SUMA	TRANSN	VCENTR	VLOCTY	VTABLE	VTXCLD	Z
PHI				X				X		X						X																				X			
PRESS				X										X													X							X				X	
PRINTF																													X										
PROLD														X			X																						
RATIO														X			X												X										
RDRDXC																									X	X				X									
RE				X													X												X										
REF				X										X			X							X			X		X							X			
RZZZ																	X											X											
SHPE				X										X			X								X	X		X	X	X									
SOURCE				X									X		X		X													X	X	X							
SYMTRY				X				X				X					X										X											X	
VCORE																	X																			X			
VEL				X				X		X		X				X	X																			X			
VFPTS				X												X	X																						
VORTEX				X		X				X		X					X							X											X	X	X	X	
VTXTBL				X		X				X							X							X											X		X	X	
ZFLOW																	X										X												

(b) Page 2

Figure 7.- Concluded

ITEM

(1)

NCIR	NCF	ISYM	NBLSEP	NSEPR	NDFUS	NDPHI	INP	NXFV	NFV	NVP	NVR	NVM	NVA	NASYM
5	10	15	20	25	30	35	40	45	50	55	60	65	70	75

(2)

NHEAD	NPRNTP	NPRNTS	NPRNTV	NPLOTV	NPLOTA	NTH	NCORE	NSKIN	NCOMP
5	10	15	20	25	30	35	40	45	50

(3)

TITLE (NHEAD cards)
80

(4)

REFS	REFL	XM	SL	SD
10	20	30	40	50

(5)

ALPHAC	PHI	RE
10	20	30

(6)*

MACH
10

(7)

XI	XF	DX	XTR1	XTR2	EMKF	RGAM	VRF
10	20	30	40	50	60	70	80

(8)

E5	XTABL	XASYMI	XASYMF	DBETA	SEPL	SEPT	RCORE
10	20	30	40	50	60	70	80

* Omit item (6) if NCOMP ≤ 0

(a) Page 1

Figure 8.- Input forms for Program VTXCLD.

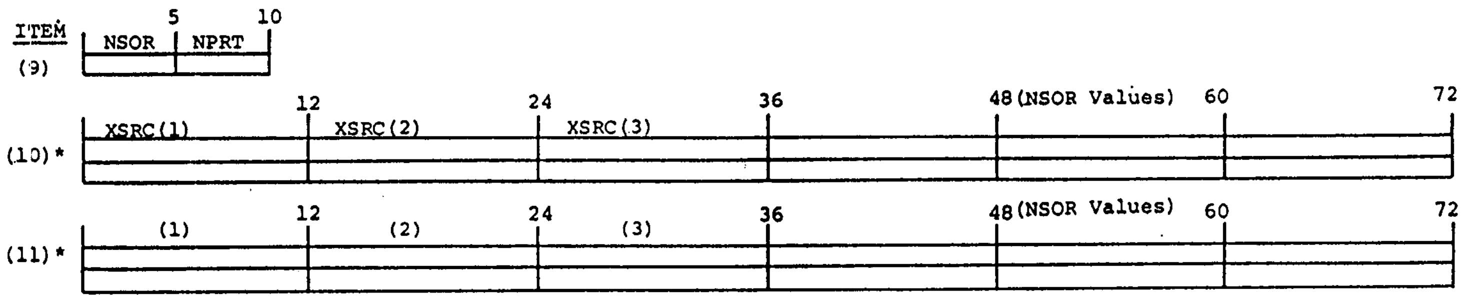

* Omit items (10) and (11) if NSOR $\leq$ 0

(b) Page 2

Figure 8.- Continued.

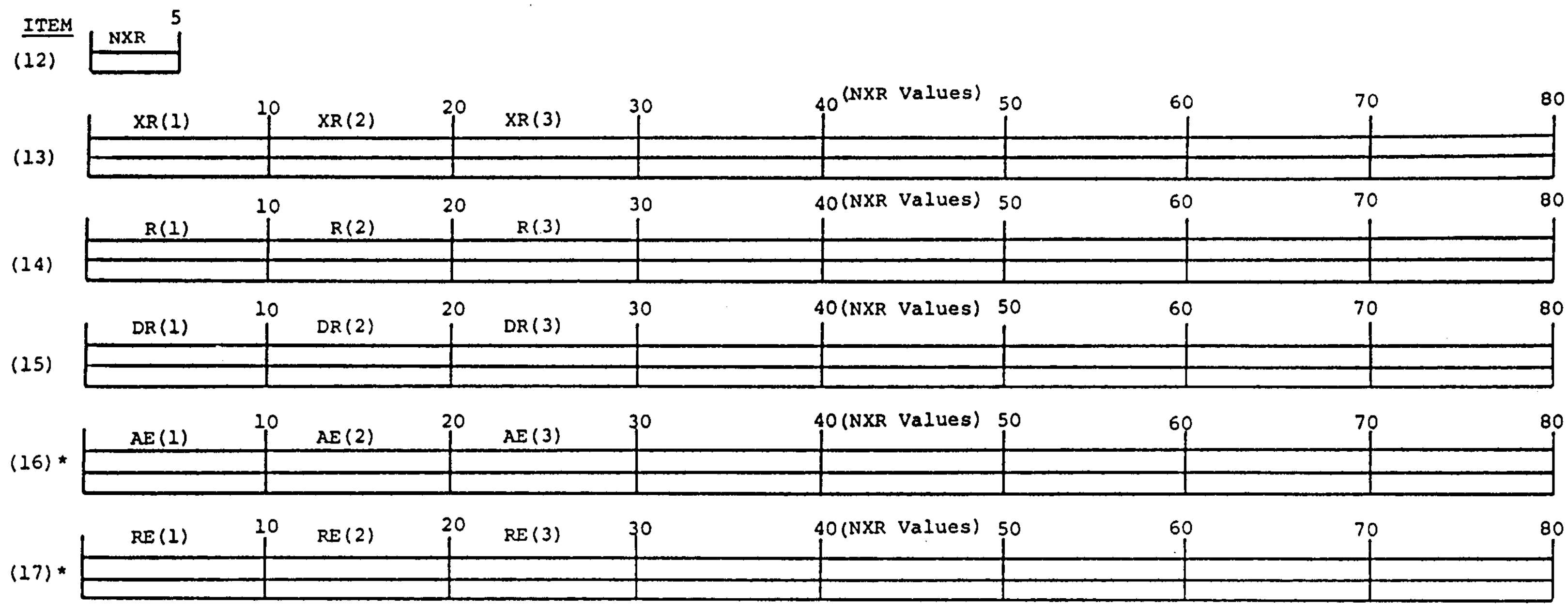

* Omit items (16) and (17) if NCIR ≠ 1

(c) Page 3

Figure 8.- Continued.

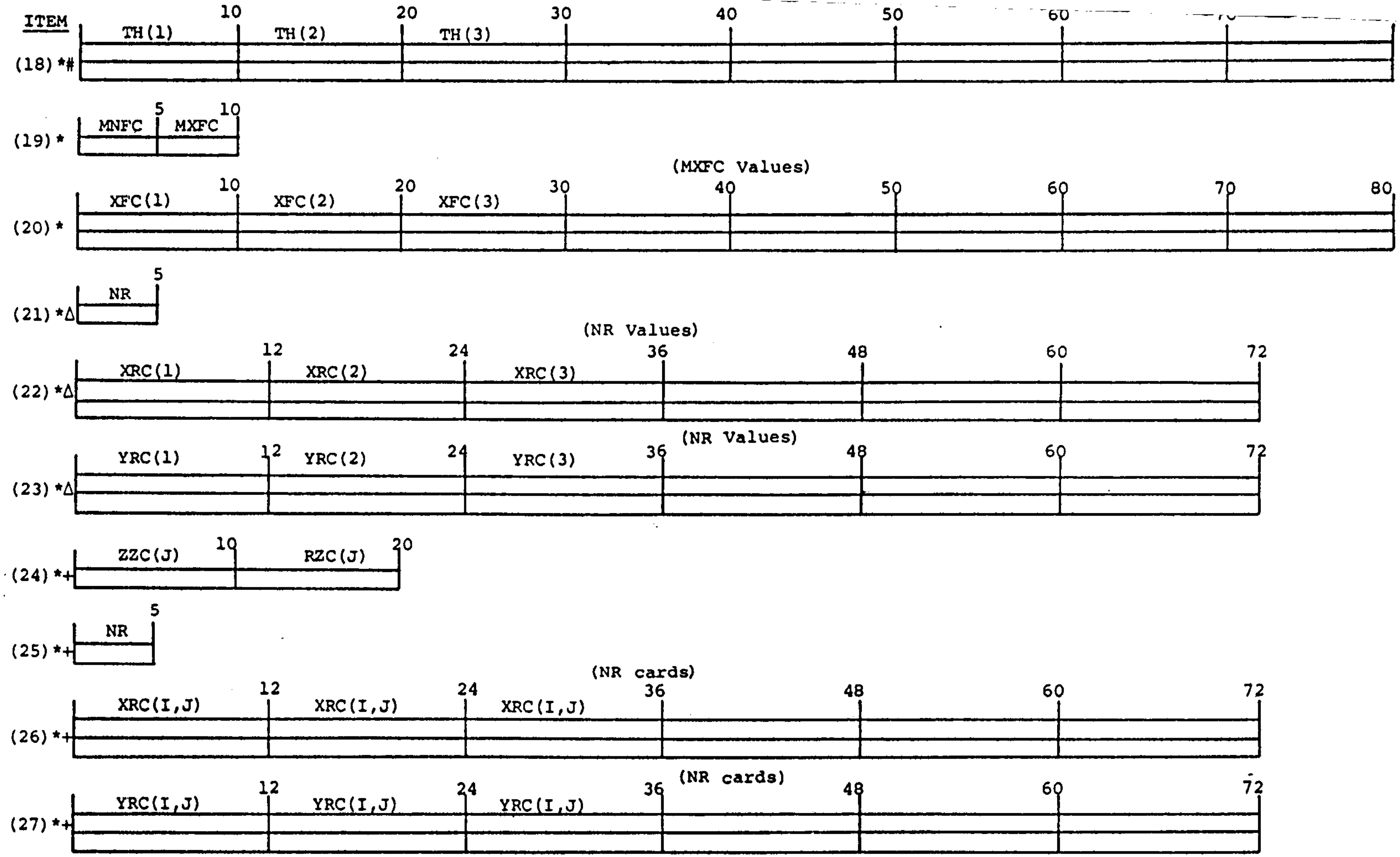

* Omit items (18) through (29) if NCIR < 2

Δ Omit items (21) through (23) if NCF ≠ 0

\+ Omit items (24) through (29) if NCF = 0

\# Omit item (18) if NTH = 0

(d) Page 4

Figure 8.- Continued.

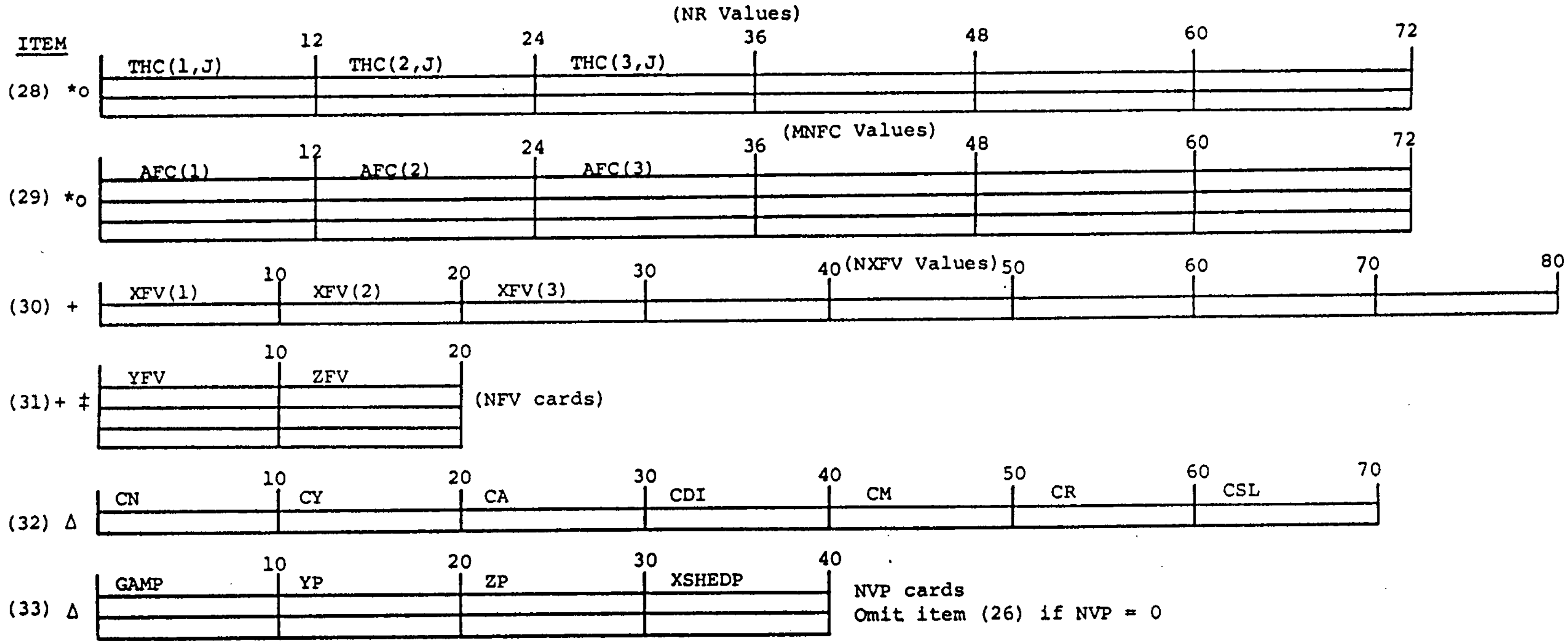

Δ Omit items (32) through (37) if NVP + NVR + NVM + NVA = 0

\+ Omit items (30), (31) if NXFV = 0

‡ Omit item (31) if NFV = 0

* Omit items (28), (29) if NCIR < 2

o Omit items (28), (29) if NCF = 0

(e) Page 5

Figure 8.- Continued.

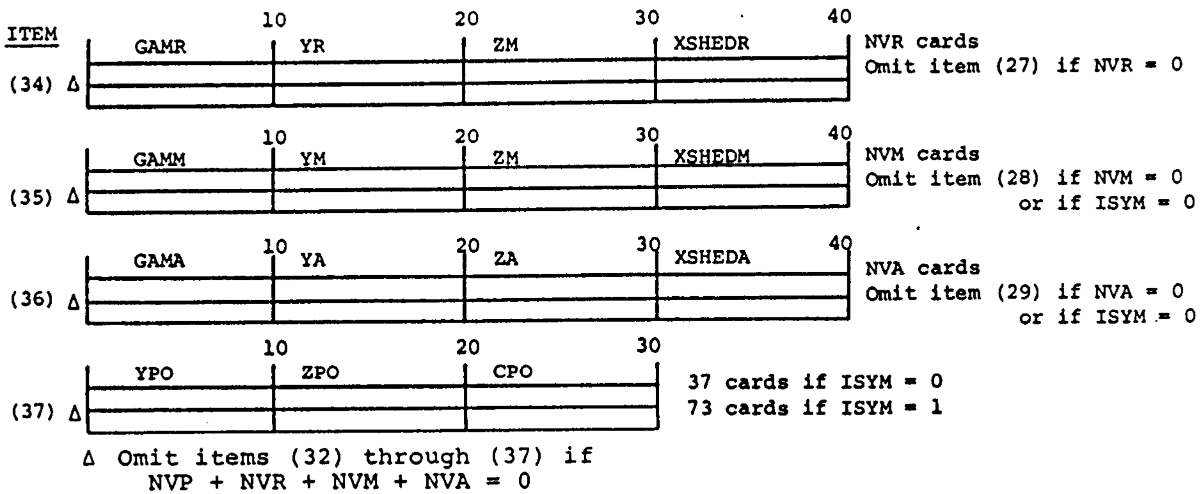

(f) Page 6

Figure 8.- Concluded.

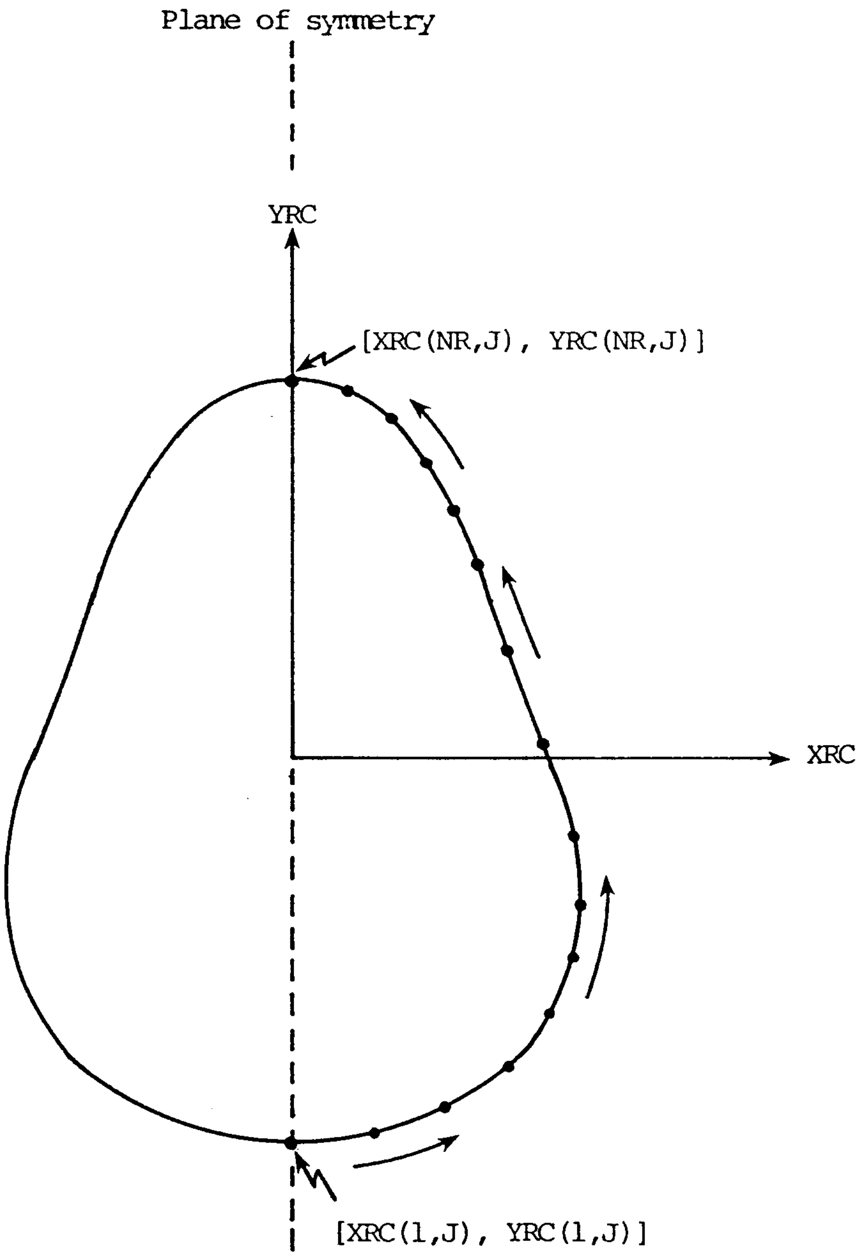

Figure 9.- Convention for ordering coordinates for a noncircular cross section at X = XFC(J).

```
Item
 (1)    0    0    0    1    0    1    1    0    7    0    0    0    0    0    0
 (2)    4    0    1    0    3    1    0    0    1    0
 (3)   SAMPLE CASE 1
       NIELSEN ENGINEERING & RESEARCH, INC.        PROGRAM VTXCLD
       3 CALIBER OGIVE-CYLINDER                    REF. NASA TN D-1297
       INITIAL FLOW CONDITIONS  ALPHAC = 15.00 DEGREES, PHI = 0 DEGREES
 (4)  17.34900   4.70000  14.10000  50.47800   4.70000
 (5)  15.00000   0.00000  440000.
 (7)   2.35000  47.000     2.35000   0.0       0.0       1.05      0.0        .6
 (8)    .04      0.0       0.0       0.0       0.0       0.0       0.0       0.0
 (9)   -1    2
 (12)  71
 (13)  0.00100   0.00119   0.00141   0.00168   0.00199   0.00237   0.00281   0.00334
       0.00396   0.00470   0.00558   0.00662   0.00786   0.00932   0.01104   0.01308
       0.01548   0.01831   0.02163   0.02554   0.03011   0.03545   0.04166   0.04888
       0.05721   0.06679   0.07775   0.09019   0.10424   0.11995   0.13737   0.15650
       0.17726   0.19953   0.22310   0.24769   0.27298   0.29857   0.52902   0.75946
       0.98991   1.01552   1.04105   1.06611   1.09032   1.11331   1.13480   1.15457
       1.17248   1.18849   1.20261   1.21492   1.22554   1.23462   1.24231   1.24878
       1.25419   1.25870   1.26243   1.26551   1.26804   1.27012   1.27183   1.27322
       1.27436   1.27529   1.27604   1.27666   1.27716   1.27757   1.27790
 (14)  0.00034   0.00041   0.00048   0.00057   0.00068   0.00081   0.00096   0.00114
       0.00135   0.00160   0.00189   0.00224   0.00265   0.00313   0.00370   0.00437
       0.00514   0.00605   0.00710   0.00831   0.00971   0.01130   0.01311   0.01515
       0.01742   0.01992   0.02263   0.02553   0.02857   0.03168   0.03478   0.03775
       0.04049   0.04285   0.04472   0.04597   0.04653   0.04655   0.04655   0.04655
       0.04655   0.04642   0.04558   0.04401   0.04181   0.03907   0.03594   0.03257
       0.02911   0.02568   0.02238   0.01931   0.01650   0.01398   0.01177   0.00984
       0.00819   0.00678   0.00560   0.00461   0.00378   0.00310   0.00253   0.00207
       0.00169   0.00137   0.00112   0.00091   0.00074   0.00060   0.00049
 (15)  0.34149   0.34123   0.34092   0.34056   0.34013   0.33962   0.33901   0.33829
       0.33743   0.33642   0.33523   0.33381   0.33213   0.33015   0.32782   0.32507
       0.32183   0.31803   0.31357   0.30837   0.30230   0.29525   0.28710   0.27770
       0.26693   0.25465   0.24074   0.22510   0.20763   0.18830   0.16711   0.14409
       0.11935   0.09305   0.06543   0.03676   0.00737   0.00000   0.00000   0.00000
       0.00000  -0.01802  -0.04771  -0.07699  -0.10545  -0.13272  -0.15847  -0.18243
      -0.20441  -0.22429  -0.24204  -0.25770  -0.27134  -0.28312  -0.29318  -0.30171
      -0.30890  -0.31491  -0.31991  -0.32406  -0.32748  -0.33030  -0.33261  -0.33451
      -0.33606  -0.33733  -0.33836  -0.33920  -0.33988  -0.34044  -0.34090
 (30)  2.35      4.70      9.40     21.150    28.20     35.25     47.00
```

(a) Sample Case 1

Figure 10.- Sample cases for program VTXCLD.

```
Item
 (1)    0    0    0    1    0    1    1    0    7    0    0    0    0    0    0
 (2)    4    0    1    0    3    1    0    0    1    0
 (3)    SAMPLE CASE 2
        NIELSEN ENGINEERING & RESEARCH, INC.        PROGRAM VTXCLD
        3 CALIBER OGIVE-CYLINDER                    REF. NASA TN D-1297
        INITIAL FLOW CONDITIONS  ALPHAC = 20.00 DEGREES, PHI = 0 DEGREES
 (4)   17.34900   4.70000  14.10000  50.47800   4.70000
 (5)   20.00000   0.00000   440000.
 (7)    2.35000  47.000     2.35000   0.0       0.0       1.05      0.0       .6
 (8)     .04      0.0       0.0       0.0       0.0       0.0       0.0       0.0
 (9)    61    2
 (10) 0.20000E-02 0.25126E-02 0.31565E-02 0.39648E-02 0.49785E-02 0.62473E-02
      0.78333E-02 0.98141E-02 0.12284E-01 0.15366E-01 0.19194E-01 0.23941E-01
      0.29802E-01 0.37014E-01 0.45830E-01 0.56547E-01 0.69476E-01 0.84914E-01
      0.10314E+00 0.12439E+00 0.14874E+00 0.17615E+00 0.20641E+00 0.23895E+00
      0.27310E+00 0.30800E+00 0.34291E+00 0.37782E+00 0.41273E+00 0.44765E+00
      0.48256E+00 0.51747E+00 0.55238E+00 0.58730E+00 0.62221E+00 0.65712E+00
      0.69203E+00 0.72695E+00 0.76186E+00 0.79677E+00 0.83168E+00 0.86660E+00
      0.90151E+00 0.93642E+00 0.97133E+00 0.10062E+01 0.10411E+01 0.10753E+01
      0.11077E+01 0.11375E+01 0.11641E+01 0.11871E+01 0.12066E+01 0.12226E+01
      0.12356E+01 0.12459E+01 0.12539E+01 0.12601E+01 0.12649E+01 0.12685E+01
      0.12712E+01
 (11) 0.81719E-07 0.26387E-07 0.11344E-06 0.13696E-06 0.24535E-06 0.36439E-06
      0.59532E-06 0.91349E-06 0.14535E-05 0.22591E-05 0.34840E-05 0.53899E-05
      0.81163E-05 0.12185E-04 0.17927E-04 0.25719E-04 0.35925E-04 0.48499E-04
      0.61993E-04 0.74917E-04 0.84224E-04 0.82314E-04 0.74762E-04 0.27384E-04
      0.13014E-05-0.35579E-04 0.29103E-04-0.32427E-04 0.30364E-04-0.31699E-04
      0.30799E-04-0.31411E-04 0.31004E-04-0.31254E-04 0.31134E-04-0.31135E-04
      0.31252E-04-0.31005E-04 0.31408E-04-0.30802E-04 0.31691E-04-0.30371E-04
      0.32373E-04-0.28832E-04 0.31665E-04 0.13720E-04-0.44716E-04-0.77072E-04
     -0.92338E-04-0.92578E-04-0.81301E-04-0.63716E-04-0.46689E-04-0.31532E-04
     -0.20487E-04-0.12619E-04-0.76726E-05-0.43306E-05-0.27866E-05-0.10763E-05
     -0.14198E-05
 (12)   71
 (13)   0.00100   0.00119   0.00141   0.00168   0.00199   0.00237   0.00281   0.00334
        0.00396   0.00470   0.00558   0.00662   0.00786   0.00932   0.01104   0.01308
        0.01548   0.01831   0.02163   0.02554   0.03011   0.03545   0.04166   0.04888
        0.05721   0.06679   0.07775   0.09019   0.10424   0.11995   0.13737   0.15650
        0.17726   0.19953   0.22310   0.24769   0.27298   0.29857   0.52902   0.75946
        0.98991   1.01552   1.04105   1.06611   1.09032   1.11331   1.13480   1.15457
        1.17248   1.18849   1.20261   1.21492   1.22554   1.23462   1.24231   1.24878
        1.25419   1.25870   1.26243   1.26551   1.26804   1.27012   1.27183   1.27322
        1.27436   1.27529   1.27604   1.27666   1.27716   1.27757   1.27790
 (14)   0.00034   0.00041   0.00048   0.00057   0.00068   0.00081   0.00096   0.00114
        0.00135   0.00160   0.00189   0.00224   0.00265   0.00313   0.00370   0.00437
        0.00514   0.00605   0.00710   0.00831   0.00971   0.01130   0.01311   0.01515
        0.01742   0.01992   0.02263   0.02553   0.02857   0.03168   0.03478   0.03775
        0.04049   0.04285   0.04472   0.04597   0.04653   0.04655   0.04655   0.04655
```

(b) Sample Case 2

Figure 10.- Continued.

	0.04655	0.04642	0.04558	0.04401	0.04181	0.03907	0.03594	0.03257
	0.02911	0.02568	0.02238	0.01931	0.01650	0.01398	0.01177	0.00984
	0.00819	0.00678	0.00560	0.00461	0.00378	0.00310	0.00253	0.00207
	0.00169	0.00137	0.00112	0.00091	0.00074	0.00060	0.00049	
(15)	0.34149	0.34123	0.34092	0.34056	0.34013	0.33962	0.33901	0.33829
	0.33743	0.33642	0.33523	0.33381	0.33213	0.33015	0.32782	0.32507
	0.32183	0.31803	0.31357	0.30837	0.30230	0.29525	0.28710	0.27770
	0.26693	0.25465	0.24074	0.22510	0.20763	0.18830	0.16711	0.14409
	0.11935	0.09305	0.06543	0.03676	0.00737	0.00000	0.00000	0.00000
	0.00000	-0.01802	-0.04771	-0.07699	-0.10545	-0.13272	-0.15847	-0.18243
	-0.20441	-0.22429	-0.24204	-0.25770	-0.27134	-0.28312	-0.29318	-0.30171
	-0.30890	-0.31491	-0.31991	-0.32406	-0.32748	-0.33030	-0.33261	-0.33451
	-0.33606	-0.33733	-0.33836	-0.33920	-0.33988	-0.34044	-0.34090	
(30)	2.35	4.70	9.40	21.150	28.20	35.25	47.00	

(b) Concluded

Figure 10.- Continued.

```
Item

(1)    1    0    0    1    0    1    1    0    8    0    0    0    0    0    0
(2)    5    0    1    0    3    1    0    0    1    0
(3)    SAMPLE CASE 3
       NIELSEN ENGINEERING & RESEARCH, INC.          PROGRAM VTXCLD
       3 CALIBER NOSE                                 REF. MIT AL 138
       2 : 1 ELLIPTIC CROSS SECTION
       INITIAL FLOW CONDITIONS  ALPHAC = 15.00 DEGREES, PHI = 0 DEGREES
(4)    4.4301    2.375     7.125     23.75      2.375
(5)    15.00000  0.00000   1348000.
(7)    1.1875    23.750    1.1875    0.0       0.0       1.05      0.0       .6
(8)    .04       0.0       0.0       0.0       0.0       0.0       0.0       0.0
(9)    -1  2
(12)   65
(13)   0.00000   0.00023   0.00092   0.00208   0.00369   0.00576   0.00829   0.01126
       0.01468   0.01854   0.02284   0.02756   0.03270   0.03825   0.04421   0.05056
       0.05729   0.06440   0.07188   0.07970   0.08787   0.09636   0.10517   0.11427
       0.12366   0.13333   0.14325   0.15341   0.16380   0.17440   0.18520   0.19617
       0.20730   0.21857   0.22997   0.24147   0.25307   0.26474   0.27646   0.28822
       0.30000   0.47500   0.65000   0.82500   1.00000   1.02354   1.04693   1.07003
       1.09271   1.11480   1.13620   1.15675   1.17634   1.19483   1.21213   1.22812
       1.24271   1.25579   1.26730   1.27716   1.28532   1.29171   1.29631   1.29908
       1.30000
(14)   0.00000   0.00008   0.00034   0.00076   0.00134   0.00208   0.00298   0.00402
       0.00521   0.00653   0.00798   0.00954   0.01121   0.01297   0.01481   0.01673
       0.01870   0.02072   0.02277   0.02485   0.02693   0.02901   0.03107   0.03309
       0.03508   0.03701   0.03888   0.04067   0.04237   0.04397   0.04547   0.04685
       0.04811   0.04923   0.05022   0.05107   0.05177   0.05232   0.05271   0.05295
       0.05303   0.05303   0.05303   0.05303   0.05303   0.05271   0.05177   0.05022
       0.04811   0.04547   0.04237   0.03888   0.03508   0.03107   0.02693   0.02277
       0.01870   0.01481   0.01121   0.00798   0.00521   0.00298   0.00134   0.00034
       0.00000
(15)   0.36495   0.36463   0.36367   0.36209   0.35987   0.35703   0.35358   0.34954
       0.34490   0.33969   0.33393   0.32762   0.32080   0.31347   0.30566   0.29739
       0.28868   0.27955   0.27003   0.26013   0.24987   0.23928   0.22838   0.21719
       0.20573   0.19402   0.18207   0.16992   0.15756   0.14503   0.13234   0.11950
       0.10654   0.09346   0.08029   0.06703   0.05371   0.04033   0.02691   0.01346
(16)   0.00000   0.00000   0.00000   0.00000   0.00000  -0.02691  -0.05371  -0.08029
      -0.10654  -0.13234  -0.15756  -0.18207  -0.20573  -0.22838  -0.24987  -0.27003
      -0.28868  -0.30566  -0.32080  -0.33393  -0.34490  -0.35358  -0.35987  -0.36367
      -0.36495
       0.00000   0.00011   0.00045   0.00101   0.00178   0.00277   0.00397   0.00536
       0.00695   0.00871   0.01064   0.01272   0.01494   0.01729   0.01975   0.02230
       0.02493   0.02763   0.03037   0.03313   0.03591   0.03868   0.04142   0.04413
       0.04677   0.04935   0.05184   0.05422   0.05649   0.05863   0.06062   0.06247
       0.06414   0.06565   0.06697   0.06810   0.06903   0.06976   0.07029   0.07060
       0.07071   0.07071   0.07071   0.07071   0.07071   0.07029   0.06903   0.06697
       0.06414   0.06062   0.05649   0.05184   0.04677   0.04142   0.03591   0.03037
       0.02493   0.01975   0.01494   0.01064   0.00695   0.00397   0.00178   0.00045
```

(c) Sample Case 3

Figure 10.- Continued.

	0.00000							
(17)	0.00000	0.00006	0.00022	0.00050	0.00089	0.00139	0.00199	0.00268
	0.00347	0.00435	0.00532	0.00636	0.00747	0.00864	0.00987	0.01115
	0.01247	0.01381	0.01518	0.01657	0.01795	0.01934	0.02071	0.02206
	0.02339	0.02467	0.02592	0.02711	0.02825	0.02931	0.03031	0.03123
	0.03207	0.03282	0.03348	0.03405	0.03451	0.03488	0.03514	0.03530
	0.03535	0.03535	0.03535	0.03535	0.03535	0.03514	0.03451	0.03348
	0.03207	0.03031	0.02825	0.02592	0.02339	0.02071	0.01795	0.01518
	0.01247	0.00987	0.00747	0.00532	0.00347	0.00199	0.00089	0.00022
	0.00000							
(30)	1.18750	2.37500	4.75000	7.12500	9.50000	14.25000	19.00000	23.75000

(c) Concluded

Figure 10.- Continued.

```
Item
(1)     2    0    0    1    0    1    1    0    8    0    0    0    0    0    0
(2)     5    0    1    0    3    1    0    0    1    1
(3)     SAMPLE CASE 4
        NIELSEN ENGINEERING & RESEARCH, INC.              PROGRAM VTXCLD
        SQUARE WITH ROUNDED CORNERS                       REF. SCHNEIDER
        NUMERICAL MAPPING
        INITIAL FLOW CONDITIONS  ALPHAC = 20.00 DEGREES, PHI = 0 DEGREES
(4)    12.5664    4.00000  12.00000  52.00000    4.0000
(5)    20.00000   0.00000   700000.
(6)     0.50000
(7)     2.00000  52.000     2.50000   0.0       0.0       1.05      0.0        .6
(8)      .05      0.0       0.0       0.0       0.0       0.0       0.0       0.0
(9)     -1    2
(12)    65
(13)    0.00000   0.00018   0.00071   0.00160   0.00284   0.00443   0.00638   0.00866
        0.01129   0.01426   0.01757   0.02120   0.02515   0.02942   0.03401   0.03889
        0.04407   0.04954   0.05529   0.06131   0.06759   0.07412   0.08090   0.08790
        0.09513   0.10256   0.11019   0.11801   0.12600   0.13416   0.14246   0.15090
        0.15946   0.16813   0.17690   0.18575   0.19467   0.20365   0.21266   0.22171
        0.23077   0.42308   0.61538   0.80769   1.00000   1.01811   1.03610   1.05387
        1.07131   1.08831   1.10477   1.12058   1.13564   1.14987   1.16318   1.17548
        1.18670   1.19676   1.20562   1.21320   1.21947   1.22439   1.22793   1.23006
        1.23077
(14)    0.00000   0.00006   0.00025   0.00055   0.00098   0.00152   0.00218   0.00295
        0.00383   0.00481   0.00589   0.00706   0.00831   0.00965   0.01106   0.01253
        0.01406   0.01564   0.01725   0.01889   0.02056   0.02223   0.02390   0.02556
        0.02721   0.02882   0.03039   0.03191   0.03337   0.03475   0.03606   0.03727
        0.03839   0.03940   0.04030   0.04107   0.04171   0.04222   0.04259   0.04281
        0.04288   0.04288   0.04288   0.04288   0.04288   0.04259   0.04171   0.04030
        0.03839   0.03606   0.03337   0.03039   0.02721   0.02390   0.02056   0.01725
        0.01406   0.01106   0.00831   0.00589   0.00383   0.00218   0.00098   0.00025
        0.00000
(15)    0.34584   0.34522   0.34460   0.34357   0.34213   0.34027   0.33800   0.33530
        0.33218   0.32864   0.32467   0.32026   0.31542   0.31014   0.30442   0.29825
        0.29162   0.28455   0.27701   0.26902   0.26056   0.25165   0.24227   0.23243
        0.22212   0.21136   0.20014   0.18847   0.17635   0.16379   0.15081   0.13740
        0.12357   0.10936   0.09475   0.07978   0.06445   0.04880   0.03283   0.01657
        0.00000   0.00000   0.00000   0.00000   0.00000  -0.03283  -0.06445  -0.09475
       -0.12357  -0.15081  -0.17635  -0.20014  -0.22212  -0.24227  -0.26056  -0.27701
       -0.29162  -0.30442  -0.31542  -0.32467  -0.33218  -0.33800  -0.34213  -0.34460
       -0.34584
(19)    20    1
(20)   26.00000
(21)    25
(22) 0.00000E+00 0.33333E+00 0.66667E+00 0.10000E+01 0.13333E+01 0.15885E+01
     0.18047E+01 0.19493E+01 0.20000E+01 0.20000E+01 0.20000E+01 0.20000E+01
     0.20000E+01 0.20000E+01 0.20000E+01 0.20000E+01 0.20000E+01 0.19494E+01
     0.18047E+01 0.15885E+01 0.13333E+01 0.10000E+01 0.66667E+00 0.33333E+00
```

(d) Sample Case 4

Figure 10.- Continued.

```
         0.00000E+00
(23)    -0.20000E+01-0.20000E+01-0.20000E+01-0.20000E+01-0.20000E+01-0.19493E+01
        -0.18047E+01-0.15885E+01-0.13333E+01-0.10000E+01-0.66667E+00-0.33333E+00
         0.00000E+00 0.33333E+00 0.66667E+00 0.10000E+01 0.13333E+01 0.15885E+01
         0.18047E+01 0.19493E+01 0.20000E+01 0.20000E+01 0.20000E+01 0.20000E+01
         0.20000E+01
(30)       2.00000    7.00000   12.00000   17.00000   22.00000   32.00000   42.00000   52.00000
```

(d) Concluded

Figure 10.- Continued.

Item

(1)	0	0	0	1	0	1	1	0	7	0	0	0	0	0	0
(2)	4	0	1	0	3	1	0	0	1	1					

```
(3)   SAMPLE CASE 5     COMPRESSIBILITY CORRECTION
      NIELSEN ENGINEERING & RESEARCH, INC.        PROGRAM VTXCLD
      3 CALIBER OGIVE-CYLINDER                    REF. NASA TN D-1297
      INITIAL FLOW CONDITIONS  ALPHAC = 15.00 DEGREES, PHI = 0 DEGREES
```

(4)	17.34900	4.70000	14.10000	50.47800	4.70000			
(5)	15.00000	0.00000	440000.					
(6)	0.800							
(7)	2.35000	47.000	2.35000	0.0	0.0	1.05	0.0	.6
(8)	.04	0.0	0.0	0.0	0.0	0.0	0.0	0.0
(9)	-1	2						
(12)	71							
(13)	0.00100	0.00119	0.00141	0.00168	0.00199	0.00237	0.00281	0.00334
	0.00396	0.00470	0.00558	0.00662	0.00786	0.00932	0.01104	0.01308
	0.01548	0.01831	0.02163	0.02554	0.03011	0.03545	0.04166	0.04888
	0.05721	0.06679	0.07775	0.09019	0.10424	0.11995	0.13737	0.15650
	0.17726	0.19953	0.22310	0.24769	0.27298	0.29857	0.52902	0.75946
	0.98991	1.01552	1.04105	1.06611	1.09032	1.11331	1.13480	1.15457
	1.17248	1.18849	1.20261	1.21492	1.22554	1.23462	1.24231	1.24878
	1.25419	1.25870	1.26243	1.26551	1.26804	1.27012	1.27183	1.27322
	1.27436	1.27529	1.27604	1.27666	1.27716	1.27757	1.27790	
(14)	0.00034	0.00041	0.00048	0.00057	0.00068	0.00081	0.00096	0.00114
	0.00135	0.00160	0.00189	0.00224	0.00265	0.00313	0.00370	0.00437
	0.00514	0.00605	0.00710	0.00831	0.00971	0.01130	0.01311	0.01515
	0.01742	0.01992	0.02263	0.02553	0.02857	0.03168	0.03478	0.03775
	0.04049	0.04285	0.04472	0.04597	0.04653	0.04655	0.04655	0.04655
	0.04655	0.04642	0.04558	0.04401	0.04181	0.03907	0.03594	0.03257
	0.02911	0.02568	0.02238	0.01931	0.01650	0.01398	0.01177	0.00984
	0.00819	0.00678	0.00560	0.00461	0.00378	0.00310	0.00253	0.00207
	0.00169	0.00137	0.00112	0.00091	0.00074	0.00060	0.00049	
(15)	0.34149	0.34123	0.34092	0.34056	0.34013	0.33962	0.33901	0.33829
	0.33743	0.33642	0.33523	0.33381	0.33213	0.33015	0.32782	0.32507
	0.32183	0.31803	0.31357	0.30837	0.30230	0.29525	0.28710	0.27770
	0.26693	0.25465	0.24074	0.22510	0.20763	0.18830	0.16711	0.14409
	0.11935	0.09305	0.06543	0.03676	0.00737	0.00000	0.00000	0.00000
	0.00000	-0.01802	-0.04771	-0.07699	-0.10545	-0.13272	-0.15847	-0.18243
	-0.20441	-0.22429	-0.24204	-0.25770	-0.27134	-0.28312	-0.29318	-0.30171
	-0.30890	-0.31491	-0.31991	-0.32406	-0.32748	-0.33030	-0.33261	-0.33451
	-0.33606	-0.33733	-0.33836	-0.33920	-0.33988	-0.34044	-0.34090	
(30)	2.35	4.70	9.40	21.150	28.20	35.25	47.00	

(e) Sample Case 5

Figure 10.- Continued.

```
Item
(1)     0    0    0    1    0    1    1    0    7    0    0    0    0    0    0
(2)     4    0    1    0    3    1    0    0    1    0
(3)     SAMPLE CASE 6     TRANSITION REGION
        NIELSEN ENGINEERING & RESEARCH, INC.         PROGRAM VTXCLD
        3 CALIBER OGIVE-CYLINDER                     REF. NASA TN D-1297
        INITIAL FLOW CONDITIONS  ALPHAC = 20.00 DEGREES, PHI = 0 DEGREES
(4)    17.34900   4.70000  14.10000  50.47800   4.70000
(5)    20.00000   0.00000   440000.
(7)     2.35000  47.000     2.35000   7.05      11.75      1.05       0.0        .6
(8)      .04      0.0       0.0       0.0       0.0        0.0        0.0        0.0
(9)     61    2
(10)  0.20000E-02 0.25126E-02 0.31565E-02 0.39648E-02 0.49785E-02 0.62473E-02
      0.78333E-02 0.98141E-02 0.12284E-01 0.15366E-01 0.19194E-01 0.23941E-01
      0.29802E-01 0.37014E-01 0.45830E-01 0.56547E-01 0.69476E-01 0.84914E-01
      0.10314E+00 0.12439E+00 0.14874E+00 0.17615E+00 0.20641E+00 0.23895E+00
      0.27310E+00 0.30800E+00 0.34291E+00 0.37782E+00 0.41273E+00 0.44765E+00
      0.48256E+00 0.51747E+00 0.55238E+00 0.58730E+00 0.62221E+00 0.65712E+00
      0.69203E+00 0.72695E+00 0.76186E+00 0.79677E+00 0.83168E+00 0.86660E+00
      0.90151E+00 0.93642E+00 0.97133E+00 0.10062E+01 0.10411E+01 0.10753E+01
      0.11077E+01 0.11375E+01 0.11641E+01 0.11871E+01 0.12066E+01 0.12226E+01
      0.12356E+01 0.12459E+01 0.12539E+01 0.12601E+01 0.12649E+01 0.12685E+01
      0.12712E+01
(11)  0.81719E-07 0.26387E-07 0.11344E-06 0.13696E-06 0.24535E-06 0.36439E-06
      0.59532E-06 0.91349E-06 0.14535E-05 0.22591E-05 0.34840E-05 0.53899E-05
      0.81163E-05 0.12185E-04 0.17927E-04 0.25719E-04 0.35925E-04 0.48499E-04
      0.61993E-04 0.74917E-04 0.84224E-04 0.82314E-04 0.74762E-04 0.27384E-04
      0.13014E-05-0.35579E-04 0.29103E-04-0.32427E-04 0.30364E-04-0.31699E-04
      0.30799E-04-0.31411E-04 0.31004E-04-0.31254E-04 0.31134E-04-0.31135E-04
      0.31252E-04-0.31005E-04 0.31408E-04-0.30802E-04 0.31691E-04-0.30371E-04
      0.32373E-04-0.28832E-04 0.31665E-04 0.13720E-04-0.44716E-04-0.77072E-04
     -0.92338E-04-0.92578E-04-0.81301E-04-0.63716E-04-0.46689E-04-0.31532E-04
     -0.20487E-04-0.12619E-04-0.76726E-05-0.43306E-05-0.27866E-05-0.10763E-05
     -0.14198E-05
(12)    71
(13)    0.00100   0.00119   0.00141   0.00168   0.00199   0.00237   0.00281   0.00334
        0.00396   0.00470   0.00558   0.00662   0.00786   0.00932   0.01104   0.01308
        0.01548   0.01831   0.02163   0.02554   0.03011   0.03545   0.04166   0.04888
        0.05721   0.06679   0.07775   0.09019   0.10424   0.11995   0.13737   0.15650
        0.17726   0.19953   0.22310   0.24769   0.27298   0.29857   0.52902   0.75946
        0.98991   1.01552   1.04105   1.06611   1.09032   1.11331   1.13480   1.15457
        1.17248   1.18849   1.20261   1.21492   1.22554   1.23462   1.24231   1.24878
        1.25419   1.25870   1.26243   1.26551   1.26804   1.27012   1.27183   1.27322
        1.27436   1.27529   1.27604   1.27666   1.27716   1.27757   1.27790
(14)    0.00034   0.00041   0.00048   0.00057   0.00068   0.00081   0.00096   0.00114
        0.00135   0.00160   0.00189   0.00224   0.00265   0.00313   0.00370   0.00437
        0.00514   0.00605   0.00710   0.00831   0.00971   0.01130   0.01311   0.01515
        0.01742   0.01992   0.02263   0.02553   0.02857   0.03168   0.03478   0.03775
        0.04049   0.04285   0.04472   0.04597   0.04653   0.04655   0.04655   0.04655
```

(f) Sample Case 6

Figure 10.- Continued.

	0.04655	0.04642	0.04558	0.04401	0.04181	0.03907	0.03594	0.03257
	0.02911	0.02568	0.02238	0.01931	0.01650	0.01398	0.01177	0.00984
	0.00819	0.00678	0.00560	0.00461	0.00378	0.00310	0.00253	0.00207
	0.00169	0.00137	0.00112	0.00091	0.00074	0.00060	0.00049	
(15)	0.34149	0.34123	0.34092	0.34056	0.34013	0.33962	0.33901	0.33829
	0.33743	0.33642	0.33523	0.33381	0.33213	0.33015	0.32782	0.32507
	0.32183	0.31803	0.31357	0.30837	0.30230	0.29525	0.28710	0.27770
	0.26693	0.25465	0.24074	0.22510	0.20763	0.18830	0.16711	0.14409
	0.11935	0.09305	0.06543	0.03676	0.00737	0.00000	0.00000	0.00000
	0.00000	-0.01802	-0.04771	-0.07699	-0.10545	-0.13272	-0.15847	-0.18243
	-0.20441	-0.22429	-0.24204	-0.25770	-0.27134	-0.28312	-0.29318	-0.30171
	-0.30890	-0.31491	-0.31991	-0.32406	-0.32748	-0.33030	-0.33261	-0.33451
	-0.33606	-0.33733	-0.33836	-0.33920	-0.33988	-0.34044	-0.34090	
(30)	2.35	4.70	9.40	21.150	28.20	35.25	47.00	

(f) Concluded

Figure 10.- Continued.

```
Item
(1)     0   0   1   1   0   1   1   0   7   57   0   0   0   0   1
(2)     5   1   1   1   3   1   0   0   0   0
(3)     SAMPLE CASE 7     ASYMMETRIC SEPARATION
        NIELSEN ENGINEERING & RESEARCH, INC.          PROGRAM VTXCLD
        3 CALIBER OGIVE-CYLINDER                      REF. NSWC TR82-384
        ASYMMETRIC SEPARATION CASE
        INITIAL FLOW CONDITIONS  ALPHAC = 45.0 DEGREES, PHI = 0 DEGREES
(4)     25.65207   5.71500   17.14500   72.00900   5.71500
(5)     45.00000   0.00000   106100.
(7)     0.85725    32.5755   0.85725    0.0        0.0        1.05       0.0        0.6
(8)     .04        0.0       0.0        5.145      2.00       0.0        0.0        0.0
(9)     -1   2
(12)    55
(13)    0.00000    0.00033   0.00130    0.00293    0.00520    0.00811    0.01165    0.01581
        0.02058    0.02595   0.03190    0.03841    0.04547    0.05306    0.06116    0.06974
        0.07878    0.08826   0.09815    0.10842    0.11905    0.13000    0.14125    0.15277
        0.16452    0.17647   0.18859    0.20085    0.21321    0.22563    0.23810    0.48810
        0.73810    0.98810   1.23810    1.25678    1.27534    1.29368    1.31167    1.32921
        1.34619    1.36250   1.37804    1.39273    1.40645    1.41914    1.43072    1.44110
        1.45024    1.45807   1.46454    1.46961    1.47326    1.47546    1.47619
(14)    0.00000    0.00011   0.00045    0.00100    0.00176    0.00273    0.00389    0.00522
        0.00672    0.00836   0.01013    0.01200    0.01396    0.01598    0.01804    0.02012
        0.02219    0.02423   0.02622    0.02814    0.02997    0.03168    0.03327    0.03471
        0.03599    0.03709   0.03801    0.03874    0.03926    0.03958    0.03968    0.03968
        0.03968    0.03968   0.03968    0.03944    0.03874    0.03758    0.03599    0.03401
        0.03168    0.02907   0.02622    0.02321    0.02012    0.01701    0.01396    0.01106
        0.00836    0.00595   0.00389    0.00222    0.00100    0.00025    0.00000
(15)    0.34286    0.34233   0.34076    0.33815    0.33452    0.32988    0.32426    0.31770
        0.31021    0.30185   0.29265    0.28266    0.27191    0.26046    0.24834    0.23561
        0.22231    0.20849   0.19419    0.17946    0.16434    0.14886    0.13308    0.11702
        0.10073    0.08424   0.06758    0.05080    0.03392    0.01698    0.00000    0.00000
        0.00000    0.00000   0.00000    -0.02545   -0.05080   -0.07593   -0.10073   -0.12508
        -0.14886   -0.17195  -0.19419   -0.21547   -0.23561   -0.25448   -0.27191   -0.28775
        -0.30185   -0.31407  -0.32426   -0.33232   -0.33815   -0.34168   -0.34286
(30)    7.4295     14.859    20.574     24.0030    26.8605    30.00375   32.5755
(31)    2.12159    2.12159
        1.92860    2.29842
        1.72094    2.45776
        1.50019    2.59840
        1.26801    2.71926
        1.02619    2.81943
        0.77655    2.89814
        0.52101    2.95479
        0.26150    2.98896
        0.00000    3.00038
        -0.26150   2.98896
        -0.52101   2.95479
        -0.77655   2.89814
```

(g) Sample Case 7

Figure 10.- Continued.

-1.02619	2.81943
-1.26801	2.71926
-1.50019	2.59840
-1.72094	2.45776
-1.92860	2.29842
-2.12158	2.12159
2.62672	2.62672
2.38780	2.84566
2.13069	3.04294
1.85738	3.21707
1.56992	3.36671
1.27052	3.49072
0.96145	3.58817
0.64506	3.65831
0.32376	3.70061
0.00000	3.71475
-0.32376	3.70061
-0.64506	3.65831
-0.96145	3.58817
-1.27052	3.49072
-1.56992	3.36671
-1.85737	3.21707
-2.13069	3.04295
-2.38779	2.84566
-2.62672	2.62673
3.13186	3.13186
2.84699	3.39291
2.54044	3.62813
2.21456	3.83573
1.87183	4.01415
1.51485	4.16202
1.14634	4.27821
0.76911	4.36184
0.38602	4.41227
0.00000	4.42912
-0.38602	4.41227
-0.76911	4.36184
-1.14634	4.27821
-1.51485	4.16202
-1.87183	4.01415
-2.21456	3.83574
-2.54044	3.62813
-2.84699	3.39291
-3.13186	3.13187

(g) Concluded

Figure 10.- Continued.

Item															
(1)	2	0	0	1	0	1	1	0	0	0	0	0	0	0	0
(2)	5	1	1	1	3	2	0	0	0	0					

```
(3)   SAMPLE CASE 8
      NIELSEN ENGINEERING & RESEARCH, INC.          PROGRAM VTXCLD
      LOBE BODY
      NUMERICAL MAPPING
      INITIAL FLOW CONDITIONS  ALPHAC = 15.00 DEGREES, PHI = 0 DEGREES
(4)   15.05941   4.37884   7.00000  14.00000   4.37884
(5)   15.00000   0.00000   729000.
(7)    2.00000  14.000     2.00000   0.0       0.0       1.05      0.0       1.0
(8)     .05      0.0       0.0       0.0       0.0       0.0       0.0       0.0
(9)    0    0
(12)   2
(13)   0.00000   1.00000
(14)   0.15639   0.15639
(15)   0.00000   0.00000
(19)   20   1
(20)   2.00000
(21)   28
(22)  0.00000E+00 0.01558E+00 0.03105E+00 0.04629E+00 0.06110E+00 0.07524E+00
      0.08840E+00 0.10026E+00 0.11049E+00 0.11882E+00 0.12508E+00 0.12926E+00
      0.13147E+00 0.13194E+00 0.13097E+00 0.12891E+00 0.12607E+00 0.11400E+00
      0.10000E+00 0.08365E+00 0.07847E+00 0.07212E+00 0.06431E+00 0.05476E+00
      0.04333E+00 0.03011E+00 0.01546E+00 0.00000E+00
(23) -0.17874E+00-0.17809E+00-0.17612E+00-0.17275E+00-0.16786E+00-0.16134E+00
     -0.15312E+00-0.14319E+00-0.13168E+00-0.11882E+00-0.10496E+00-0.09051E+00
     -0.07590E+00-0.06152E+00-0.04767E+00-0.03454E+00-0.02223E+00 0.01900E+00
      0.05800E+00 0.09970E+00 0.11206E+00 0.12492E+00 0.13791E+00 0.15044E+00
      0.16171E+00 0.17077E+00 0.17668E+00 0.17874E+00
```

(h) Sample Case 8

Figure 10.- Continued.

```
Item

(1)     0    0    0    1    0    1    1    0    4    0    9    0    9    0    0
(2)     5    0    1    0    3    1    0    0    1    0
(3)     SAMPLE CASE 9
        NIELSEN ENGINEERING & RESEARCH, INC.        PROGRAM VTXCLD
        3 CALIBER OGIVE-CYLINDER                    REF. NASA TN D-1297
        RESTART CALCULATION
        INITIAL FLOW CONDITIONS  ALPHAC = 20.00 DEGREES, PHI = 0 DEGREES
(4)    17.34900   4.70000  14.10000  50.47800   4.70000
(5)    20.00000   0.00000   440000.
(7)    21.15000  47.000     2.35000   0.0       0.0       1.05      0.0       .6
(8)      .04      0.0       0.0       0.0       0.0       0.0       0.0      0.0
(9)     61    2
(10)   0.20000E-02 0.25126E-02 0.31565E-02 0.39648E-02 0.49785E-02 0.62473E-02
       0.78333E-02 0.98141E-02 0.12284E-01 0.15366E-01 0.19194E-01 0.23941E-01
       0.29802E-01 0.37014E-01 0.45830E-01 0.56547E-01 0.69476E-01 0.84914E-01
       0.10314E+00 0.12439E+00 0.14874E+00 0.17615E+00 0.20641E+00 0.23895E+00
       0.27310E+00 0.30800E+00 0.34291E+00 0.37782E+00 0.41273E+00 0.44765E+00
       0.48256E+00 0.51747E+00 0.55238E+00 0.58730E+00 0.62221E+00 0.65712E+00
       0.69203E+00 0.72695E+00 0.76186E+00 0.79677E+00 0.83168E+00 0.86660E+00
       0.90151E+00 0.93642E+00 0.97133E+00 0.10062E+01 0.10411E+01 0.10753E+01
       0.11077E+01 0.11375E+01 0.11641E+01 0.11871E+01 0.12066E+01 0.12226E+01
       0.12356E+01 0.12459E+01 0.12539E+01 0.12601E+01 0.12649E+01 0.12685E+01
       0.12712E+01
(11)   0.81719E-07 0.26387E-07 0.11344E-06 0.13696E-06 0.24535E-06 0.36439E-06
       0.59532E-06 0.91349E-06 0.14535E-05 0.22591E-05 0.34840E-05 0.53899E-05
       0.81163E-05 0.12185E-04 0.17927E-04 0.25719E-04 0.35925E-04 0.48499E-04
       0.61993E-04 0.74917E-04 0.84224E-04 0.82314E-04 0.74762E-04 0.27384E-04
       0.13014E-05-0.35579E-04 0.29103E-04-0.32427E-04 0.30364E-04-0.31699E-04
       0.30799E-04-0.31411E-04 0.31004E-04-0.31254E-04 0.31134E-04-0.31135E-04
       0.31252E-04-0.31005E-04 0.31408E-04-0.30802E-04 0.31691E-04-0.30371E-04
       0.32373E-04-0.28832E-04 0.31665E-04 0.13720E-04-0.44716E-04-0.77072E-04
      -0.92338E-04-0.92578E-04-0.81301E-04-0.63716E-04-0.46689E-04-0.31532E-04
      -0.20487E-04-0.12619E-04-0.76726E-05-0.43306E-05-0.27866E-05-0.10763E-05
      -0.14198E-05
(12)    71
(13)    0.00100   0.00119   0.00141   0.00168   0.00199   0.00237   0.00281   0.00334
        0.00396   0.00470   0.00558   0.00662   0.00786   0.00932   0.01104   0.01308
        0.01548   0.01831   0.02163   0.02554   0.03011   0.03545   0.04166   0.04888
        0.05721   0.06679   0.07775   0.09019   0.10424   0.11995   0.13737   0.15650
        0.17726   0.19953   0.22310   0.24769   0.27298   0.29857   0.52902   0.75946
        0.98991   1.01552   1.04105   1.06611   1.09032   1.11331   1.13480   1.15457
        1.17248   1.18849   1.20261   1.21492   1.22554   1.23462   1.24231   1.24878
        1.25419   1.25870   1.26243   1.26551   1.26804   1.27012   1.27183   1.27322
        1.27436   1.27529   1.27604   1.27666   1.27716   1.27757   1.27790
(14)    0.00034   0.00041   0.00048   0.00057   0.00068   0.00081   0.00096   0.00114
        0.00135   0.00160   0.00189   0.00224   0.00265   0.00313   0.00370   0.00437
        0.00514   0.00605   0.00710   0.00831   0.00971   0.01130   0.01311   0.01515
        0.01742   0.01992   0.02263   0.02553   0.02857   0.03168   0.03478   0.03775
```

(i) Sample Case 9

Figure 10.- Concluded.

	0.04049	0.04285	0.04472	0.04597	0.04653	0.04655	0.04655	0.04655
	0.04655	0.04642	0.04558	0.04401	0.04181	0.03907	0.03594	0.03257
	0.02911	0.02568	0.02238	0.01931	0.01650	0.01398	0.01177	0.00984
	0.00819	0.00678	0.00560	0.00461	0.00378	0.00310	0.00253	0.00207
	0.00169	0.00137	0.00112	0.00091	0.00074	0.00060	0.00049	
(15)	0.34149	0.34123	0.34092	0.34056	0.34013	0.33962	0.33901	0.33829
	0.33743	0.33642	0.33523	0.33381	0.33213	0.33015	0.32782	0.32507
	0.32183	0.31803	0.31357	0.30837	0.30230	0.29525	0.28710	0.27770
	0.26693	0.25465	0.24074	0.22510	0.20763	0.18830	0.16711	0.14409
	0.11935	0.09305	0.06543	0.03676	0.00737	0.00000	0.00000	0.00000
	0.00000	-0.01802	-0.04771	-0.07699	-0.10545	-0.13272	-0.15847	-0.18243
	-0.20441	-0.22429	-0.24204	-0.25770	-0.27134	-0.28312	-0.29318	-0.30171
	-0.30890	-0.31491	-0.31991	-0.32406	-0.32748	-0.33030	-0.33261	-0.33451
	-0.33606	-0.33733	-0.33836	-0.33920	-0.33988	-0.34044	-0.34090	
(30)	23.500	28.20	35.25	47.00				
(32)	0.7971	0.0000	-0.0882	0.0420	0.9279	0.0000	0.0000	
(33)	0.20616	1.06070	3.01228	2.35000				
	0.24437	0.96040	2.50698	4.70000				
	0.26560	0.41861	2.93954	7.05000				
	0.28099	0.55608	3.56029	9.40000				
	0.29309	1.17566	3.55488	11.75000				
	0.30194	1.71703	2.75480	14.10000				
	0.29493	2.01224	2.07150	16.45000				
	0.28698	2.26274	1.29529	18.80000				
	0.28005	2.48200	0.30224	21.15000				
(37)	0.00000	-2.34975	0.10546					
	0.20479	-2.34081	0.10200					
	0.40803	-2.31405	0.09174					
	0.60816	-2.26968	0.07500					
	0.80366	-2.20804	0.05231					
	0.99305	-2.12960	0.02440					
	1.17488	-2.03494	-0.00784					
	1.34776	-1.92480	-0.04337					
	1.51039	-1.80001	-0.08103					
	1.66152	-1.66152	-0.11960					
	1.80001	-1.51039	-0.15778					
	1.92480	-1.34776	-0.19427					
	2.03494	-1.17488	-0.22781					
	2.12960	-0.99305	-0.25715					
	2.20804	-0.80366	-0.28114					
	2.26968	-0.60816	-0.29872					
	2.31405	-0.40803	-0.30890					
	2.34081	-0.20479	-0.31077					
	2.34975	0.00000	-0.30344					
	2.34081	0.20479	-0.28592					
	2.31405	0.40803	-0.25687					
	2.26969	0.60816	-0.21437					
	2.20804	0.80366	-0.15752					

(i) Continued

Figure 10.- Concluded.

2.12960	0.99305	-0.11272
2.03494	1.17488	-0.18283
1.92480	1.34776	-0.14507
1.80001	1.51039	-0.09519
1.66153	1.66152	-0.08168
1.51039	1.80001	-0.08009
1.34776	1.92480	-0.07103
1.17488	2.03494	-0.06786
0.99305	2.12960	-0.09245
0.80366	2.20804	-0.13819
0.60816	2.26968	-0.12903
0.40803	2.31405	-0.10701
0.20480	2.34081	-0.07569
0.00000	2.34975	-0.05908

(i) Concluded

Figure 10.- Concluded.

```
SAMPLE CASE 1
NIELSEN ENGINEERING & RESEARCH, INC.          PROGRAM VTXCLD
3 CALIBER OGIVE-CYLINDER                      REF. NASA TN D-1297
INITIAL FLOW CONDITIONS  ALPHAC = 15.00 DEGREES, PHI = 0 DEGREES


       REFERENCE QUANTITIES
         REF. AREA ........  17.35
         REF. LENGTH ......   4.70
         X(MOMENT CENTER) .  14.10
         BODY LENGTH (L)...  50.48
         BASE DIAMETER (D).   4.70
         STRATFORD (LAM)...  0.087
         STRATFORD (TURB)..  0.350


       FLOW CONDITIONS
         ALPHA C (DEG.) ...  15.00
         PHI (DEG.) .......   0.00
         MACH NUMBER ......   0.00
         REYNOLDS NO. (D)..   4.400E+05
         VORTEX FACTOR ....   0.60

         ALPHA (DEG.) .....  15.00
         BETA (DEG.) ......   0.00
         U/VO .............  0.966
         VO*DT ............  2.433
         RE/D .............   9.362E+04
         RE/D SIN(ALPHA) ..   2.423E+04


       INITIAL CONDITIONS      XI        XF        DX       XTR1      XTR2       TOL       EMKF      RGAM     RCORE/D
                             2.350    47.000     2.350    51.700    56.400   0.04000     1.050     0.000     0.025


       OPTIONS...

    NCIR   NCF  ISYM NBLSEP NSEPR NDFUS NDPHI   INP  NXFV   NFV   NVP   NVR   NVM   NVA NASYM
      0     0     0     1     0     1     1     0     7     0     0     0     0     0     0


  NPRNTP NPRNTS NPRNTV NPLOTV NPLOTA  NTH NCORE NSKIN NCOMP
      0     1     0     3     1     0     0     1     0


DEFINITIONS OF OUTPUT QUANTITIES ...
    CA(X)      (DCA/DX)/(Q*D) , POSITIVE AFT
    CN(X)      (DCN/DX)/(Q*D) , POSITIVE UP
    CY(X)      (DCY/DX)/(Q*D) , POSITIVE RIGHT
    CA         FX/(Q*REFS) , POSITIVE AFT
    CN         FZ/(Q*REFS) , POSITIVE UP
    CY         FY/(Q*REFS) , POSITIVE RIGHT
    CM         M/(Q*REFS*REFL) , POSITIVE NOSE UP
    CR         R/(Q*REFS*REFL) , POSITIVE NOSE RIGHT
    CLL        L/(Q*REFS*REFL) , POSITIVE COUNTERCLOCKWISE
```

(a) Page 1

Figure 11.- Output for sample case 1.

INPUT GEOMETRY CHARACTERISTICS
NXR = 71

X/L	R/L	DR/DX	X	R
0.0010	0.0003	0.3415	0.0505	0.0172
0.0012	0.0004	0.3412	0.0601	0.0207
0.0014	0.0005	0.3409	0.0712	0.0242
0.0017	0.0006	0.3406	0.0848	0.0288
0.0020	0.0007	0.3401	0.1005	0.0343
0.0024	0.0008	0.3396	0.1196	0.0409
0.0028	0.0010	0.3390	0.1418	0.0485
0.0033	0.0011	0.3383	0.1686	0.0575
0.0040	0.0014	0.3374	0.1999	0.0681
0.0047	0.0016	0.3364	0.2372	0.0808
0.0056	0.0019	0.3352	0.2817	0.0954
0.0066	0.0022	0.3338	0.3342	0.1131
0.0079	0.0026	0.3321	0.3968	0.1338
0.0093	0.0031	0.3302	0.4705	0.1580
0.0110	0.0037	0.3278	0.5573	0.1868
0.0131	0.0044	0.3251	0.6603	0.2206
0.0155	0.0051	0.3218	0.7814	0.2595
0.0183	0.0060	0.3180	0.9243	0.3054
0.0216	0.0071	0.3136	1.0918	0.3584
0.0255	0.0083	0.3084	1.2892	0.4195
0.0301	0.0097	0.3023	1.5199	0.4901
0.0355	0.0113	0.2952	1.7894	0.5704
0.0417	0.0131	0.2871	2.1029	0.6618
0.0489	0.0152	0.2777	2.4674	0.7647
0.0572	0.0174	0.2669	2.8878	0.8793
0.0668	0.0199	0.2546	3.3714	1.0055
0.0777	0.0226	0.2407	3.9247	1.1423
0.0902	0.0255	0.2251	4.5526	1.2887
0.1042	0.0286	0.2076	5.2618	1.4422
0.1199	0.0317	0.1883	6.0548	1.5991
0.1374	0.0348	0.1671	6.9342	1.7556
0.1565	0.0377	0.1441	7.8998	1.9055
0.1773	0.0405	0.1194	8.9477	2.0439
0.1995	0.0428	0.0931	10.0719	2.1630
0.2231	0.0447	0.0654	11.2616	2.2574
0.2477	0.0460	0.0368	12.5029	2.3205
0.2730	0.0465	0.0074	13.7795	2.3487
0.2986	0.0465	0.0000	15.0712	2.3498
0.5290	0.0465	0.0000	26.7039	2.3498
0.7595	0.0465	0.0000	38.3360	2.3498
0.9899	0.0465	0.0000	49.9687	2.3498
1.0155	0.0464	-0.0180	51.2614	2.3432
1.0410	0.0456	-0.0477	52.5501	2.3008
1.0661	0.0440	-0.0770	53.8151	2.2215
1.0903	0.0418	-0.1054	55.0372	2.1105
1.1133	0.0391	-0.1327	56.1977	1.9722
1.1348	0.0359	-0.1585	57.2824	1.8142
1.1546	0.0326	-0.1824	58.2804	1.6441
1.1725	0.0291	-0.2044	59.1844	1.4694
1.1885	0.0257	-0.2243	59.9926	1.2963
1.2026	0.0224	-0.2420	60.7053	1.1297
1.2149	0.0193	-0.2577	61.3267	0.9747
1.2255	0.0165	-0.2713	61.8628	0.8329
1.2346	0.0140	-0.2831	62.3211	0.7057
1.2423	0.0118	-0.2932	62.7093	0.5941
1.2488	0.0098	-0.3017	63.0359	0.4967

(b) Page 2

Figure 11.- Continued.

1.2542	0.0082	-0.3089	63.3090	0.4134
1.2587	0.0068	-0.3149	63.5367	0.3422
1.2624	0.0056	-0.3199	63.7249	0.2827
1.2655	0.0046	-0.3241	63.8804	0.2327
1.2680	0.0038	-0.3275	64.0081	0.1908
1.2701	0.0031	-0.3303	64.1131	0.1565
1.2718	0.0025	-0.3326	64.1994	0.1277
1.2732	0.0021	-0.3345	64.2696	0.1045
1.2744	0.0017	-0.3361	64.3271	0.0853
1.2753	0.0014	-0.3373	64.3741	0.0692
1.2760	0.0011	-0.3384	64.4119	0.0565
1.2767	0.0009	-0.3392	64.4432	0.0459
1.2772	0.0007	-0.3399	64.4685	0.0374
1.2776	0.0006	-0.3404	64.4892	0.0303
1.2779	0.0005	-0.3409	64.5058	0.0247

(c) Page 3

Figure 11.- Continued.

SOURCE LOCATIONS AND BODY RADIUS AND SURFACE SLOPE AT THESE LOCATIONS

SOURCE SPACING IS 0.75000 TIMES LOCAL RADIUS

X/L	0.00200	0.00251	0.00316	0.00396	0.00498	0.00625	0.00783
R/L	0.00068	0.00086	0.00108	0.00135	0.00169	0.00211	0.00264
DR/DX	0.34012	0.33942	0.33854	0.33742	0.33604	0.33432	0.33217
X/L	0.00981	0.01228	0.01537	0.01919	0.02394	0.02980	0.03701
R/L	0.00329	0.00411	0.00510	0.00633	0.00782	0.00962	0.01176
DR/DX	0.32948	0.32614	0.32198	0.31684	0.31050	0.30271	0.29320
X/L	0.04583	0.05655	0.06948	0.08491	0.10314	0.12439	0.14874
R/L	0.01429	0.01724	0.02058	0.02430	0.02833	0.03247	0.03655
DR/DX	0.28167	0.26779	0.25124	0.23173	0.20900	0.18290	0.15343
X/L	0.17615	0.20641	0.23895	0.27310	0.30800	0.34291	0.37782
R/L	0.04034	0.04340	0.04553	0.04653	0.04655	0.04655	0.04655
DR/DX	0.12067	0.08499	0.04695	0.00734	0.00000	0.00000	0.00000
X/L	0.41273	0.44765	0.48256	0.51747	0.55238	0.58730	0.62221
R/L	0.04655	0.04655	0.04655	0.04655	0.04655	0.04655	0.04655
DR/DX	0.00000	0.00000	0.00000	0.00000	0.00000	0.00000	0.00000
X/L	0.65712	0.69203	0.72695	0.76186	0.79677	0.83168	0.86660
R/L	0.04655	0.04655	0.04655	0.04655	0.04655	0.04655	0.04655
DR/DX	0.00000	0.00000	0.00000	0.00000	0.00000	0.00000	0.00000
X/L	0.90151	0.93642	0.97133	1.00625	1.04110	1.07528	1.10766
R/L	0.04655	0.04655	0.04655	0.04647	0.04558	0.04318	0.03974
DR/DX	0.00000	0.00000	0.00000	-0.01149	-0.04776	-0.08777	-0.12602
X/L	1.13747	1.16408	1.18713	1.20661	1.22265	1.23560	1.24587
R/L	0.03548	0.03073	0.02597	0.02138	0.01727	0.01370	0.01071
DR/DX	-0.16171	-0.19410	-0.22260	-0.24713	-0.26762	-0.28440	-0.29787
X/L	1.25390	1.26011	1.26486	1.26847	1.27120		
R/L	0.00828	0.00633	0.00482	0.00364	0.00274		
DR/DX	-0.30852	-0.31680	-0.32318	-0.32807	-0.33176		

X(ST)	XS(1)	X(RM)	R(MAX)	XS(L)	X(ST)
0.00166	0.00200	0.29857	0.04655	1.27290	1.27257

(d) Page 4

Figure 11.- Continued.

FOR THIS CASE THERE ARE 61 SOURCES

X/L	2. 0000E-03	2. 5126E-03	3. 1565E-03	3. 9648E-03	4. 9785E-03	6. 2473E-03
Q	8. 1719E-08	2. 6387E-08	1. 1344E-07	1. 3696E-07	2. 4535E-07	3. 6439E-07
X/L	7. 8333E-03	9. 8141E-03	1. 2284E-02	1. 5366E-02	1. 9194E-02	2. 3941E-02
Q	5. 9532E-07	9. 1349E-07	1. 4535E-06	2. 2591E-06	3. 4840E-06	5. 3899E-06
X/L	2. 9802E-02	3. 7014E-02	4. 5830E-02	5. 6547E-02	6. 9476E-02	8. 4914E-02
Q	8. 1163E-06	1. 2185E-05	1. 7927E-05	2. 5719E-05	3. 5925E-05	4. 8499E-05
X/L	1. 0314E-01	1. 2439E-01	1. 4874E-01	1. 7615E-01	2. 0641E-01	2. 3895E-01
Q	6. 1993E-05	7. 4917E-05	8. 4224E-05	8. 2314E-05	7. 4762E-05	2. 7384E-05
X/L	2. 7310E-01	3. 0800E-01	3. 4291E-01	3. 7782E-01	4. 1273E-01	4. 4765E-01
Q	1. 3014E-06	-3. 5579E-05	2. 9103E-05	-3. 2427E-05	3. 0364E-05	-3. 1699E-05
X/L	4. 8256E-01	5. 1747E-01	5. 5238E-01	5. 8730E-01	6. 2221E-01	6. 5712E-01
Q	3. 0799E-05	-3. 1411E-05	3. 1004E-05	-3. 1254E-05	3. 1134E-05	-3. 1135E-05
X/L	6. 9203E-01	7. 2695E-01	7. 6186E-01	7. 9677E-01	8. 3168E-01	8. 6660E-01
Q	3. 1252E-05	-3. 1005E-05	3. 1408E-05	-3. 0802E-05	3. 1691E-05	-3. 0371E-05
X/L	9. 0151E-01	9. 3642E-01	9. 7133E-01	1. 0062E+00	1. 0411E+00	1. 0753E+00
Q	3. 2373E-05	-2. 8832E-05	3. 1665E-05	1. 3720E-05	-4. 4716E-05	-7. 7072E-05
X/L	1. 1077E+00	1. 1375E+00	1. 1641E+00	1. 1871E+00	1. 2066E+00	1. 2226E+00
Q	-9. 2338E-05	-9. 2578E-05	-8. 1301E-05	-6. 3716E-05	-4. 6689E-05	-3. 1532E-05
X/L	1. 2356E+00	1. 2459E+00	1. 2539E+00	1. 2601E+00	1. 2649E+00	1. 2685E+00
Q	-2. 0487E-05	-1. 2619E-05	-7. 6726E-06	-4. 3306E-06	-2. 7866E-06	-1. 0763E-06
X/L	1. 2712E+00					
Q	-1. 4198E-06					

(e) Page 5

Figure 11.- Continued.

SHAPE CALCULATED FROM SOURCE DISTRIBUTION

X/L	0.01000	0.02000	0.03000	0.04000	0.05000	0.06000	0.07000
R/L(S.D.)	0.00333	0.00657	0.00966	0.01262	0.01545	0.01815	0.02072
R/L(INPT)	0.00336	0.00658	0.00968	0.01263	0.01546	0.01815	0.02071
M-INDEX	2	1	1	1	1	1	1
X/L	0.08000	0.09000	0.10000	0.11000	0.12000	0.13000	0.14000
R/L(S.D.)	0.02316	0.02548	0.02767	0.02973	0.03168	0.03350	0.03520
R/L(INPT)	0.02315	0.02549	0.02765	0.02971	0.03169	0.03347	0.03519
M-INDEX	1	1	2	2	2	2	2
X/L	0.15000	0.16000	0.17000	0.18000	0.19000	0.20000	0.21000
R/L(S.D.)	0.03678	0.03824	0.03958	0.04080	0.04190	0.04289	0.04375
R/L(INPT)	0.03674	0.03821	0.03953	0.04078	0.04184	0.04289	0.04368
M-INDEX	2	2	2	2	2	1	2
X/L	0.22000	0.23000	0.24000	0.25000	0.26000	0.27000	0.28000
R/L(S.D.)	0.04448	0.04508	0.04557	0.04595	0.04623	0.04643	0.04655
R/L(INPT)	0.04447	0.04507	0.04558	0.04602	0.04624	0.04646	0.04654
M-INDEX	1	1	1	2	1	2	2
X/L	0.29000	0.30000	0.31000	0.32000	0.33000	0.34000	0.35000
R/L(S.D.)	0.04660	0.04661	0.04658	0.04656	0.04656	0.04658	0.04661
R/L(INPT)	0.04654	0.04655	0.04655	0.04655	0.04655	0.04655	0.04655
M-INDEX	2	2	2	1	1	2	2
X/L	0.36000	0.37000	0.38000	0.39000	0.40000	0.41000	0.42000
R/L(S.D.)	0.04663	0.04661	0.04658	0.04656	0.04656	0.04658	0.04661
R/L(INPT)	0.04655	0.04655	0.04655	0.04655	0.04655	0.04655	0.04655
M-INDEX	2	2	2	1	1	2	2
X/L	0.43000	0.44000	0.45000	0.46000	0.47000	0.48000	0.49000
R/L(S.D.)	0.04663	0.04661	0.04658	0.04656	0.04656	0.04658	0.04661
R/L(INPT)	0.04655	0.04655	0.04655	0.04655	0.04655	0.04655	0.04655
M-INDEX	2	2	2	1	1	2	2
X/L	0.50000	0.51000	0.52000	0.53000	0.54000	0.55000	0.56000
R/L(S.D.)	0.04663	0.04661	0.04658	0.04656	0.04656	0.04658	0.04661
R/L(INPT)	0.04655	0.04655	0.04655	0.04655	0.04655	0.04655	0.04655
M-INDEX	2	2	2	1	1	2	2
X/L	0.57000	0.58000	0.59000	0.60000	0.61000	0.62000	0.63000
R/L(S.D.)	0.04663	0.04661	0.04658	0.04656	0.04656	0.04658	0.04661
R/L(INPT)	0.04655	0.04655	0.04655	0.04655	0.04655	0.04655	0.04655
M-INDEX	2	2	2	1	1	2	2
X/L	0.64000	0.65000	0.66000	0.67000	0.68000	0.69000	0.70000
R/L(S.D.)	0.04663	0.04661	0.04658	0.04656	0.04656	0.04658	0.04661
R/L(INPT)	0.04655	0.04655	0.04655	0.04655	0.04655	0.04655	0.04655
M-INDEX	2	2	2	1	1	2	2
X/L	0.71000	0.72000	0.73000	0.74000	0.75000	0.76000	0.77000
R/L(S.D.)	0.04663	0.04661	0.04658	0.04656	0.04656	0.04658	0.04661
R/L(INPT)	0.04655	0.04655	0.04655	0.04655	0.04655	0.04655	0.04655
M-INDEX	2	2	2	1	1	2	2
X/L	0.78000	0.79000	0.80000	0.81000	0.82000	0.83000	0.84000

(f) Page 6

Figure 11.- Continued.

R/L(S.D.)	0.04663	0.04661	0.04658	0.04656	0.04656	0.04658	0.04661
R/L(INPT)	0.04655	0.04655	0.04655	0.04655	0.04655	0.04655	0.04655
M-INDEX	2	2	2	1	1	2	2
X/L	0.85000	0.86000	0.87000	0.88000	0.89000	0.90000	0.91000
R/L(S.D.)	0.04663	0.04661	0.04658	0.04656	0.04656	0.04659	0.04661
R/L(INPT)	0.04655	0.04655	0.04655	0.04655	0.04655	0.04655	0.04655
M-INDEX	2	2	2	1	1	2	2
X/L	0.92000	0.93000	0.94000	0.95000	0.96000	0.97000	0.98000
R/L(S.D.)	0.04663	0.04661	0.04658	0.04656	0.04656	0.04659	0.04662
R/L(INPT)	0.04655	0.04655	0.04655	0.04655	0.04655	0.04655	0.04655
M-INDEX	2	2	2	1	1	2	2
X/L	0.99000	1.00000	1.01000	1.02000	1.03000	1.04000	1.05000
R/L(S.D.)	0.04663	0.04660	0.04650	0.04632	0.04603	0.04562	0.04510
R/L(INPT)	0.04655	0.04650	0.04645	0.04627	0.04594	0.04561	0.04502
M-INDEX	2	2	2	2	2	1	2
X/L	1.06000	1.07000	1.08000	1.09000	1.10000	1.11000	1.12000
R/L(S.D.)	0.04446	0.04370	0.04283	0.04183	0.04072	0.03949	0.03813
R/L(INPT)	0.04439	0.04366	0.04275	0.04184	0.04066	0.03946	0.03810
M-INDEX	2	2	2	1	2	2	2
X/L	1.13000	1.14000	1.15000	1.16000	1.17000	1.18000	1.19000
R/L(S.D.)	0.03667	0.03508	0.03336	0.03153	0.02957	0.02749	0.02529
R/L(INPT)	0.03664	0.03505	0.03335	0.03152	0.02959	0.02750	0.02533
M-INDEX	2	2	1	1	2	1	2
X/L	1.20000	1.21000	1.22000	1.23000	1.24000	1.25000	1.26000
R/L(S.D.)	0.02295	0.02049	0.01790	0.01518	0.01232	0.00931	0.00613
R/L(INPT)	0.02299	0.02054	0.01797	0.01526	0.01243	0.00947	0.00637
M-INDEX	2	2	2	2	2	2	2
X/L	1.27000						
R/L(S.D.)	0.00261						
R/L(INPT)	0.00314						
M-INDEX	3						

(g) Page 7

Figure 11.- Continued.

VELOCITIES ON THE BODY SURFACE

		------------ VELOCITIES	------------		
		AXIAL	RADIAL	TANGEN	NORMAL
X/L	R/L	VA/VO	VR/VO	VT/VO	VN/VO
0.00166	0.00056	-0.36995	0.20695	-0.28348	0.31518
0.01000	0.00336	-0.21290	0.25881	-0.12128	0.31241
0.02000	0.00658	-0.17241	0.26097	-0.08583	0.30078
0.03000	0.00968	-0.14372	0.25854	-0.06272	0.28907
0.04000	0.01263	-0.12127	0.25403	-0.04590	0.27772
0.05000	0.01546	-0.10158	0.24796	-0.03188	0.26606
0.06000	0.01815	-0.08411	0.24088	-0.01999	0.25436
0.07000	0.02071	-0.06836	0.23350	-0.00956	0.24311
0.08000	0.02315	-0.05460	0.22528	-0.00098	0.23180
0.09000	0.02549	-0.04138	0.21565	0.00704	0.21947
0.10000	0.02765	-0.02970	0.20686	0.01402	0.20851
0.11000	0.02971	-0.01892	0.19656	0.02010	0.19645
0.12000	0.03169	-0.00917	0.18670	0.02552	0.18518
0.13000	0.03347	0.00019	0.17622	0.03075	0.17352
0.14000	0.03519	0.00817	0.16559	0.03485	0.16208
0.15000	0.03674	0.01622	0.15482	0.03929	0.15063
0.16000	0.03821	0.02289	0.14304	0.04249	0.13849
0.17000	0.03953	0.02877	0.13198	0.04529	0.12726
0.18000	0.04078	0.03447	0.12030	0.04812	0.11552
0.19000	0.04184	0.03921	0.10841	0.05025	0.10376
0.20000	0.04289	0.04331	0.09628	0.05200	0.09188
0.21000	0.04368	0.04709	0.08368	0.05367	0.07962
0.22000	0.04447	0.04906	0.07003	0.05376	0.06648
0.23000	0.04507	0.04918	0.05708	0.05237	0.05417
0.24000	0.04558	0.04804	0.04524	0.05006	0.04300
0.25000	0.04602	0.04598	0.03442	0.04713	0.03283
0.26000	0.04624	0.04320	0.02473	0.04374	0.02375
0.27000	0.04646	0.03964	0.01620	0.03982	0.01577
0.28000	0.04654	0.03555	0.00882	0.03560	0.00863
0.29000	0.04654	0.03067	0.00267	0.03068	0.00259
0.30000	0.04655	0.02488	-0.00156	0.02488	-0.00156
0.31000	0.04655	0.01885	-0.00295	0.01885	-0.00295
0.32000	0.04655	0.01415	-0.00149	0.01415	-0.00149
0.33000	0.04655	0.01205	0.00128	0.01205	0.00128
0.34000	0.04655	0.01239	0.00311	0.01239	0.00311
0.35000	0.04655	0.01361	0.00259	0.01361	0.00259
0.36000	0.04655	0.01374	0.00011	0.01374	0.00011
0.37000	0.04655	0.01185	-0.00247	0.01185	-0.00247
0.38000	0.04655	0.00865	-0.00318	0.00865	-0.00318
0.39000	0.04655	0.00598	-0.00148	0.00598	-0.00148
0.40000	0.04655	0.00536	0.00133	0.00536	0.00133
0.41000	0.04655	0.00680	0.00314	0.00680	0.00314
0.42000	0.04655	0.00884	0.00256	0.00884	0.00256
0.43000	0.04655	0.00959	0.00006	0.00959	0.00006
0.44000	0.04655	0.00820	-0.00250	0.00820	-0.00250
0.45000	0.04655	0.00543	-0.00316	0.00543	-0.00316
0.46000	0.04655	0.00317	-0.00143	0.00317	-0.00143
0.47000	0.04655	0.00291	0.00138	0.00291	0.00138
0.48000	0.04655	0.00465	0.00315	0.00465	0.00315
0.49000	0.04655	0.00693	0.00253	0.00693	0.00253
0.50000	0.04655	0.00785	0.00000	0.00785	0.00000
0.51000	0.04655	0.00661	-0.00253	0.00661	-0.00253
0.52000	0.04655	0.00400	-0.00315	0.00400	-0.00315
0.53000	0.04655	0.00191	-0.00139	0.00191	-0.00139
0.54000	0.04655	0.00182	0.00142	0.00182	0.00142
0.55000	0.04655	0.00371	0.00316	0.00371	0.00316

(h) Page 8

Figure 11.- Continued.

0.56000	0.04655	0.00609	0.00250	0.00609	0.00250
0.57000	0.04655	0.00708	-0.00005	0.00708	-0.00005
0.58000	0.04655	0.00589	-0.00256	0.00589	-0.00256
0.59000	0.04655	0.00336	-0.00314	0.00336	-0.00314
0.60000	0.04655	0.00138	-0.00134	0.00138	-0.00134
0.61000	0.04655	0.00140	0.00147	0.00140	0.00147
0.62000	0.04655	0.00339	0.00317	0.00339	0.00317
0.63000	0.04655	0.00583	0.00247	0.00583	0.00247
0.64000	0.04655	0.00685	-0.00010	0.00685	-0.00010
0.65000	0.04655	0.00569	-0.00259	0.00569	-0.00259
0.66000	0.04655	0.00322	-0.00313	0.00322	-0.00313
0.67000	0.04655	0.00133	-0.00129	0.00133	-0.00129
0.68000	0.04655	0.00146	0.00151	0.00146	0.00151
0.69000	0.04655	0.00353	0.00318	0.00353	0.00318
0.70000	0.04655	0.00602	0.00244	0.00602	0.00244
0.71000	0.04655	0.00708	-0.00015	0.00708	-0.00015
0.72000	0.04655	0.00595	-0.00262	0.00595	-0.00262
0.73000	0.04655	0.00354	-0.00311	0.00354	-0.00311
0.74000	0.04655	0.00175	-0.00125	0.00175	-0.00125
0.75000	0.04655	0.00199	0.00156	0.00199	0.00156
0.76000	0.04655	0.00417	0.00319	0.00417	0.00319
0.77000	0.04655	0.00674	0.00240	0.00674	0.00240
0.78000	0.04655	0.00785	-0.00020	0.00785	-0.00020
0.79000	0.04655	0.00679	-0.00265	0.00679	-0.00265
0.80000	0.04655	0.00448	-0.00310	0.00448	-0.00310
0.81000	0.04655	0.00284	-0.00120	0.00284	-0.00120
0.82000	0.04655	0.00325	0.00160	0.00325	0.00160
0.83000	0.04655	0.00560	0.00320	0.00560	0.00320
0.84000	0.04655	0.00832	0.00237	0.00832	0.00237
0.85000	0.04655	0.00958	-0.00025	0.00958	-0.00025
0.86000	0.04655	0.00869	-0.00268	0.00869	-0.00268
0.87000	0.04655	0.00662	-0.00308	0.00662	-0.00308
0.88000	0.04655	0.00527	-0.00115	0.00527	-0.00115
0.89000	0.04655	0.00604	0.00165	0.00604	0.00165
0.90000	0.04655	0.00879	0.00321	0.00879	0.00321
0.91000	0.04655	0.01193	0.00234	0.01193	0.00234
0.92000	0.04655	0.01368	-0.00030	0.01368	-0.00030
0.93000	0.04655	0.01339	-0.00272	0.01339	-0.00272
0.94000	0.04655	0.01207	-0.00310	0.01207	-0.00310
0.95000	0.04655	0.01166	-0.00113	0.01166	-0.00113
0.96000	0.04655	0.01364	0.00179	0.01364	0.00179
0.97000	0.04655	0.01816	0.00359	0.01816	0.00359
0.98000	0.04655	0.02416	0.00287	0.02416	0.00287
1.27257	0.00228	-0.31678	-0.21911	-0.23115	-0.30810

(i) Page 9

Figure 11.- Continued.

```
SOURCE DISTRIBUTION REPRESENTING CIRCULAR BODY
  NSOR = 61  NPRT =  2

X/L LOCATIONS
     0.20000E-02 0.25126E-02 0.31565E-02 0.39648E-02 0.49785E-02 0.62473E-02
     0.78333E-02 0.98141E-02 0.12284E-01 0.15366E-01 0.19194E-01 0.23941E-01
     0.29802E-01 0.37014E-01 0.45830E-01 0.56547E-01 0.69476E-01 0.84914E-01
     0.10314E+00 0.12439E+00 0.14874E+00 0.17615E+00 0.20641E+00 0.23895E+00
     0.27310E+00 0.30800E+00 0.34291E+00 0.37782E+00 0.41273E+00 0.44765E+00
     0.48256E+00 0.51747E+00 0.55238E+00 0.58730E+00 0.62221E+00 0.65712E+00
     0.69203E+00 0.72695E+00 0.76186E+00 0.79677E+00 0.83168E+00 0.86660E+00
     0.90151E+00 0.93642E+00 0.97133E+00 0.10062E+01 0.10411E+01 0.10753E+01
     0.11077E+01 0.11375E+01 0.11641E+01 0.11871E+01 0.12066E+01 0.12226E+01
     0.12356E+01 0.12459E+01 0.12539E+01 0.12601E+01 0.12649E+01 0.12685E+01
     0.12712E+01

SOURCE STRENGTHS  QS=Q/(4*PI*L*L*U)
     0.81719E-07 0.26387E-07 0.11344E-06 0.13696E-06 0.24535E-06 0.36439E-06
     0.59532E-06 0.91349E-06 0.14535E-05 0.22591E-05 0.34840E-05 0.53899E-05
     0.81163E-05 0.12185E-04 0.17927E-04 0.25719E-04 0.35925E-04 0.48499E-04
     0.61993E-04 0.74917E-04 0.84224E-04 0.82314E-04 0.74762E-04 0.27384E-04
     0.13014E-05-0.35579E-04 0.29103E-04-0.32427E-04 0.30364E-04-0.31699E-04
     0.30799E-04-0.31411E-04 0.31004E-04-0.31254E-04 0.31134E-04-0.31135E-04
     0.31252E-04-0.31005E-04 0.31408E-04-0.30802E-04 0.31691E-04-0.30371E-04
     0.32373E-04-0.28832E-04 0.31665E-04 0.13720E-04-0.44716E-04-0.77072E-04
    -0.92338E-04-0.92578E-04-0.81301E-04-0.63716E-04-0.46689E-04-0.31532E-04
    -0.20487E-04-0.12619E-04-0.76726E-05-0.43306E-05-0.27866E-05-0.10763E-05
    -0.14198E-05

ADDITIONAL OUTPUT PRINTED AT THE FOLLOWING AXIAL STATIONS

XFV =        2.35    4.70    9.40   21.15   28.20   35.25   47.00
```

(j) Page 10

Figure 11.- Continued.

X	R	DR/DX	X/L	RETR
2.3500	0.7316	0.2807	0.0466	0.569E+05

BODY SURFACE PRESSURE DISTRIBUTION

J	Y	Z	BETA	U/VO	V/VO	W/VO	VT/VO	CP	DPHI/DT
1	0.0000	-0.7316	0.000	0.8619	0.0000	-0.2418	0.2418	0.4793	-0.2807
2	0.0638	-0.7288	5.000	0.8619	0.0660	-0.2370	0.2460	0.4762	-0.2797
3	0.1270	-0.7205	10.000	0.8619	0.1305	-0.2226	0.2580	0.4670	-0.2765
4	0.1893	-0.7067	15.000	0.8619	0.1920	-0.1989	0.2765	0.4518	-0.2712
5	0.2502	-0.6875	20.000	0.8619	0.2491	-0.1667	0.2997	0.4310	-0.2638
6	0.3092	-0.6630	25.000	0.8619	0.3005	-0.1267	0.3261	0.4051	-0.2544
7	0.3658	-0.6336	30.000	0.8619	0.3451	-0.0800	0.3542	0.3747	-0.2431
8	0.4196	-0.5993	35.000	0.8619	0.3819	-0.0278	0.3829	0.3404	-0.2300
9	0.4703	-0.5604	40.000	0.8619	0.4103	0.0286	0.4113	0.3029	-0.2150
10	0.5173	-0.5173	45.000	0.8619	0.4298	0.0878	0.4387	0.2631	-0.1985
11	0.5604	-0.4703	50.000	0.8619	0.4401	0.1483	0.4645	0.2218	-0.1804
12	0.5993	-0.4196	55.000	0.8619	0.4413	0.2086	0.4881	0.1798	-0.1610
13	0.6336	-0.3658	60.000	0.8619	0.4336	0.2673	0.5094	0.1380	-0.1404
14	0.6630	-0.3092	65.000	0.8619	0.4174	0.3230	0.5278	0.0971	-0.1186
15	0.6875	-0.2502	70.000	0.8619	0.3936	0.3744	0.5432	0.0580	-0.0960
16	0.7067	-0.1893	75.000	0.8619	0.3630	0.4204	0.5554	0.0212	-0.0727
17	0.7205	-0.1270	80.000	0.8619	0.3267	0.4600	0.5642	-0.0125	-0.0487
18	0.7288	-0.0638	85.000	0.8619	0.2859	0.4926	0.5696	-0.0429	-0.0245
19	0.7316	0.0000	90.000	0.8619	0.2418	0.5176	0.5713	-0.0694	0.0000
20	0.7288	0.0638	95.000	0.8619	0.1960	0.5348	0.5696	-0.0918	0.0245
21	0.7205	0.1270	100.000	0.8619	0.1496	0.5440	0.5642	-0.1100	0.0487
22	0.7067	0.1893	105.000	0.8619	0.1042	0.5456	0.5554	-0.1241	0.0727
23	0.6875	0.2502	110.000	0.8619	0.0609	0.5398	0.5432	-0.1340	0.0960
24	0.6630	0.3092	115.000	0.8619	0.0209	0.5274	0.5278	-0.1402	0.1186
25	0.6336	0.3658	120.000	0.8619	-0.0147	0.5091	0.5094	-0.1428	0.1404
26	0.5993	0.4196	125.000	0.8619	-0.0451	0.4861	0.4881	-0.1422	0.1610
27	0.5604	0.4703	130.000	0.8619	-0.0696	0.4592	0.4645	-0.1391	0.1804
28	0.5173	0.5173	135.000	0.8619	-0.0878	0.4298	0.4387	-0.1339	0.1985
29	0.4703	0.5604	140.000	0.8619	-0.0994	0.3991	0.4113	-0.1272	0.2150
30	0.4196	0.5993	145.000	0.8619	-0.1045	0.3684	0.3829	-0.1195	0.2300
31	0.3658	0.6336	150.000	0.8619	-0.1032	0.3388	0.3542	-0.1115	0.2431
32	0.3092	0.6630	155.000	0.8619	-0.0961	0.3116	0.3261	-0.1037	0.2544
33	0.2502	0.6875	160.000	0.8619	-0.0837	0.2878	0.2997	-0.0966	0.2638
34	0.1893	0.7067	165.000	0.8619	-0.0668	0.2683	0.2765	-0.0905	0.2712
35	0.1270	0.7205	170.000	0.8619	-0.0465	0.2538	0.2580	-0.0860	0.2765
36	0.0638	0.7288	175.000	0.8619	-0.0239	0.2448	0.2460	-0.0831	0.2797
37	0.0000	0.7316	180.000	0.8619	0.0000	0.2418	0.2418	-0.0822	0.2807

FORCE AND MOMENT COEFFICIENTS - PRESSURE INTEGRATION

X	CN(X)	CY(X)	CA(X)	CN	CY	CA	CM	CR	CSL	XCPN	XCPY
1.175	4.593E-02	4.054E-09	5.681E-02	2.924E-02	2.581E-09	3.617E-02	8.699E-02	7.988E-09	0.000E+00	0.117	-0.446

AXIAL SKIN FRICTION FORCE (ESTIMATE) - NOSE TO X 1.387E-03

TOTAL AXIAL FORCE - NOSE TO X 3.755E-02

(k) Page 11

Figure 11.- Continued.

STRATFORD SEPARATION CRITERION (LAMINAR) F(S) =0.02252

SUMMARY OF PRESSURE DISTRIBUTION AND SEPARATION POINTS ON BODY ... X = 2.35

+Y SIDE:		Y	Z	BETA	ARC	CP	CP'	DCP'/DX
	STAGNATION PT.	0.000	-0.732	0.000	0.199	0.479		
	MIN. PRESSURE	0.634	0.366	120.000	1.532	-0.143	0.000	0.000
	SEPARATION	0.000	0.000	0.000	0.000	0.000	0.000	0.000

-Y SIDE:		Y	Z	BETA	ARC	CP	CP'	DCP'/DX
	STAGNATION PT.	0.000	0.732	180.000	0.199	-0.082		
	MIN. PRESSURE	0.000	0.000	0.000	0.000	0.000	0.000	0.000
	SEPARATION	0.000	0.000	0.000	0.000	0.000	0.000	0.000

SEPARATION NOT FOUND AT X = 2.350

(1) Page 12

Figure 11.- Continued.

X	R	DR/DX	X/L	RETR
4.7000	1.3206	0.2215	0.0931	0.114E+06

BODY SURFACE PRESSURE DISTRIBUTION

J	Y	Z	BETA	U/VO	V/VO	W/VO	VT/VO	CP	DPHI/DT
1	0.0000	-1.3206	0.000	0.9294	0.0000	-0.2057	0.2057	0.3154	-0.2215
2	0.1151	-1.3156	5.000	0.9294	0.0629	-0.2010	0.2106	0.3126	-0.2206
3	0.2293	-1.3005	10.000	0.9294	0.1242	-0.1870	0.2245	0.3040	-0.2181
4	0.3418	-1.2756	15.000	0.9294	0.1827	-0.1640	0.2455	0.2899	-0.2139
5	0.4517	-1.2410	20.000	0.9294	0.2367	-0.1328	0.2714	0.2707	-0.2081
6	0.5581	-1.1969	25.000	0.9294	0.2852	-0.0940	0.3003	0.2468	-0.2007
7	0.6603	-1.1437	30.000	0.9294	0.3270	-0.0488	0.3306	0.2188	-0.1918
8	0.7575	-1.0818	35.000	0.9294	0.3612	0.0018	0.3612	0.1872	-0.1814
9	0.8489	-1.0116	40.000	0.9294	0.3871	0.0563	0.3912	0.1529	-0.1697
10	0.9338	-0.9338	45.000	0.9294	0.4043	0.1133	0.4199	0.1166	-0.1566
11	1.0116	-0.8489	50.000	0.9294	0.4125	0.1715	0.4467	0.0791	-0.1424
12	1.0818	-0.7575	55.000	0.9294	0.4117	0.2293	0.4713	0.0412	-0.1270
13	1.1437	-0.6603	60.000	0.9294	0.4023	0.2854	0.4932	0.0037	-0.1107
14	1.1969	-0.5581	65.000	0.9294	0.3847	0.3382	0.5123	-0.0325	-0.0936
15	1.2410	-0.4517	70.000	0.9294	0.3597	0.3867	0.5281	-0.0669	-0.0757
16	1.2756	-0.3418	75.000	0.9294	0.3281	0.4297	0.5407	-0.0987	-0.0573
17	1.3005	-0.2293	80.000	0.9294	0.2911	0.4663	0.5497	-0.1274	-0.0385
18	1.3156	-0.1151	85.000	0.9294	0.2499	0.4958	0.5552	-0.1526	-0.0193
19	1.3206	0.0000	90.000	0.9294	0.2057	0.5176	0.5570	-0.1740	0.0000
20	1.3156	0.1151	95.000	0.9294	0.1600	0.5316	0.5552	-0.1912	0.0193
21	1.3005	0.2293	100.000	0.9294	0.1141	0.5378	0.5497	-0.2044	0.0385
22	1.2756	0.3418	105.000	0.9294	0.0693	0.5362	0.5407	-0.2133	0.0573
23	1.2410	0.4517	110.000	0.9294	0.0270	0.5274	0.5281	-0.2184	0.0757
24	1.1969	0.5581	115.000	0.9294	-0.0118	0.5121	0.5123	-0.2197	0.0936
25	1.1437	0.6603	120.000	0.9294	-0.0460	0.4911	0.4932	-0.2177	0.1107
26	1.0818	0.7575	125.000	0.9294	-0.0747	0.4653	0.4713	-0.2129	0.1270
27	1.0116	0.8489	130.000	0.9294	-0.0973	0.4360	0.4467	-0.2056	0.1424
28	0.9338	0.9338	135.000	0.9294	-0.1133	0.4043	0.4199	-0.1966	0.1566
29	0.8489	1.0116	140.000	0.9294	-0.1226	0.3715	0.3912	-0.1864	0.1697
30	0.7575	1.0818	145.000	0.9294	-0.1252	0.3388	0.3612	-0.1756	0.1814
31	0.6603	1.1437	150.000	0.9294	-0.1213	0.3076	0.3306	-0.1648	0.1918
32	0.5581	1.1969	155.000	0.9294	-0.1113	0.2789	0.3003	-0.1546	0.2007
33	0.4517	1.2410	160.000	0.9294	-0.0960	0.2539	0.2714	-0.1455	0.2081
34	0.3418	1.2756	165.000	0.9294	-0.0762	0.2334	0.2455	-0.1379	0.2139
35	0.2293	1.3005	170.000	0.9294	-0.0528	0.2182	0.2245	-0.1322	0.2181
36	0.1151	1.3156	175.000	0.9294	-0.0270	0.2089	0.2106	-0.1287	0.2206
37	0.0000	1.3206	180.000	0.9294	0.0000	0.2057	0.2057	-0.1275	0.2215

FORCE AND MOMENT COEFFICIENTS - PRESSURE INTEGRATION

X	CN(X)	CY(X)	CA(X)	CN	CY	CA	CM	CR	CSL	XCPN	XCPY
3.525	1.720E-01	-9.779E-09	4.227E-03	1.387E-01	-3.644E-09	3.886E-02	3.334E-01	-6.019E-09	3.548E-11	2.807	21.862

AXIAL SKIN FRICTION FORCE (ESTIMATE) - NOSE TO X 4.954E-03

TOTAL AXIAL FORCE - NOSE TO X 4.381E-02

(m) Page 13

Figure 11.- Continued.

STRATFORD SEPARATION CRITERION (LAMINAR) F(S) =0.02252

SUMMARY OF PRESSURE DISTRIBUTION AND SEPARATION POINTS ON BODY ... X = 4.70

+Y SIDE:	Y	Z	BETA	ARC	CP	CP'	DCP'/DX
STAGNATION PT.	0.000	-1.321	0.000	0.094	0.315		
MIN. PRESSURE	1.197	0.558	115.000	2.650	-0.220	0.000	0.000
SEPARATION	0.672	1.136	149.376	3.442	-0.166	0.044	0.075

-Y SIDE:	Y	Z	BETA	ARC	CP	CP'	DCP'/DX
STAGNATION PT.	0.000	1.321	180.000	0.094	-0.127		
MIN. PRESSURE	-1.197	0.558	245.000	2.650	-0.220	0.000	0.000
SEPARATION	-0.672	1.136	210.624	3.442	-0.166	0.044	0.075

INITIAL POSITIONS AND STRENGTHS OF SHED VORTICITY AT X = 4.700

	NV	GAM/V	M(K)	Y	Z	BETA	VT/V	YC	ZC	RG/R
+Y SIDE:	1	0.0816	0.0801	0.7135	1.2053	149.3760	0.3344	0.7135	1.2053	1.0606
-Y SIDE:	2	-0.0816	0.0801	-0.7135	1.2053	210.6240	0.3344	-0.7135	1.2053	1.0606

(n) Page 14

Figure 11.- Continued.

FORCE AND MOMENT COEFFICIENTS - PRESSURE INTEGRATION

X	CN(X)	CY(X)	CA(X)	CN	CY	CA	CM	CR	CSL	XCPN	XCPY
5.875	1.986E-01	-2.253E-08	-2.917E-02	2.652E-01	-1.799E-08	2.029E-02	5.547E-01	-3.112E-08	6.505E-10	4.270	22.231

AXIAL SKIN FRICTION FORCE (ESTIMATE) - NOSE TO X   9.833E-03

TOTAL AXIAL FORCE - NOSE TO X   3.012E-02

STRATFORD SEPARATION CRITERION (LAMINAR)   F(S) =0.02252

SUMMARY OF PRESSURE DISTRIBUTION AND SEPARATION POINTS ON BODY ...   X =   7.05

		Y	Z	BETA	ARC	CP	CP'	DCP'/DX
+Y SIDE:	STAGNATION PT.	0.000	-1.774	0.000	0.027	0.191		
	MIN. PRESSURE	1.667	0.607	110.000	3.404	-0.265	0.000	0.000
	SEPARATION	1.249	1.259	135.225	4.185	-0.220	0.036	0.072

		Y	Z	BETA	ARC	CP	CP'	DCP'/DX
-Y SIDE:	STAGNATION PT.	0.000	1.774	180.000	0.027	-0.148		
	MIN. PRESSURE	-1.667	0.607	250.000	3.404	-0.265	0.000	0.000
	SEPARATION	-1.249	1.259	224.775	4.185	-0.220	0.036	0.072

INITIAL POSITIONS AND STRENGTHS OF SHED VORTICITY AT X =   7.050

	NV	GAM/V	M(K)	Y	Z	BETA	VT/V	YC	ZC	RC/R
+Y SIDE:	3	0.1137	0.0941	1.3155	1.3259	135.2251	0.3947	1.3155	1.3259	1.0531
-Y SIDE:	4	-0.1137	0.0941	-1.3155	1.3259	224.7749	0.3947	-1.3155	1.3259	1.0531

(o) Page 15

Figure 11.- Continued.

SUMMARY OF VORTEX FIELD AT X = 9.400 H = 4.70000

	NV	GAM/V	Y	Z	XSHED	BETA	YC	ZC	RG	RG/R
1	1	0.08163	0.53365	2.18837	4.70000	166.296	0.53365	2.18837	2.25250	1.07683
2	2	0.11370	1.14212	1.90860	7.05000	149.103	1.14212	1.90860	2.22423	1.06332
1	3	-0.08163	-0.53365	2.18837	4.70000	193.704	-0.53365	2.18837	2.25250	1.07683
2	4	-0.11370	-1.14212	1.90860	7.05000	210.897	-1.14212	1.90860	2.22423	1.06332

CENTROID OF VORTICITY

	GAM/V	Y	Z
+Y BODY:	0.19533	0.88784	2.02552
-Y BODY:	-0.19533	-0.88784	2.02552

(p) Page 16

Figure 11.- Continued.

X	R	DR/DX	X/L	RETR
9.4000	2.0918	0.1088	0.1862	0.228E+06

BODY SURFACE PRESSURE DISTRIBUTION

J	Y	Z	BETA	U/VO	V/VO	W/VO	VT/VO	CP	DPHI/DT
1	0.0000	-2.0918	0.000	1.0022	0.0000	-0.1091	0.1091	0.0928	-0.1091
2	0.1823	-2.0838	5.000	1.0022	0.0544	-0.1047	0.1180	0.0904	-0.1087
3	0.3632	-2.0600	10.000	1.0022	0.1074	-0.0918	0.1413	0.0831	-0.1075
4	0.5414	-2.0205	15.000	1.0022	0.1576	-0.0707	0.1727	0.0712	-0.1054
5	0.7154	-1.9656	20.000	1.0022	0.2036	-0.0420	0.2079	0.0550	-0.1026
6	0.8840	-1.8958	25.000	1.0022	0.2443	-0.0065	0.2444	0.0348	-0.0990
7	1.0459	-1.8115	30.000	1.0022	0.2786	0.0349	0.2808	0.0114	-0.0946
8	1.1998	-1.7135	35.000	1.0022	0.3057	0.0808	0.3162	-0.0149	-0.0895
9	1.3446	-1.6024	40.000	1.0022	0.3249	0.1302	0.3500	-0.0432	-0.0837
10	1.4791	-1.4791	45.000	1.0022	0.3358	0.1815	0.3817	-0.0728	-0.0773
11	1.6024	-1.3446	50.000	1.0022	0.3383	0.2334	0.4110	-0.1030	-0.0704
12	1.7135	-1.1998	55.000	1.0022	0.3324	0.2845	0.4375	-0.1330	-0.0628
13	1.8115	-1.0459	60.000	1.0022	0.3184	0.3334	0.4610	-0.1621	-0.0549
14	1.8958	-0.8840	65.000	1.0022	0.2970	0.3787	0.4813	-0.1895	-0.0465
15	1.9656	-0.7154	70.000	1.0022	0.2687	0.4193	0.4980	-0.2147	-0.0377
16	2.0205	-0.5414	75.000	1.0022	0.2346	0.4542	0.5112	-0.2370	-0.0287
17	2.0600	-0.3632	80.000	1.0022	0.1958	0.4824	0.5207	-0.2560	-0.0195
18	2.0838	-0.1823	85.000	1.0022	0.1536	0.5034	0.5263	-0.2713	-0.0101
19	2.0918	0.0000	90.000	1.0022	0.1091	0.5167	0.5281	-0.2825	-0.0007
20	2.0838	0.1823	95.000	1.0022	0.0638	0.5220	0.5259	-0.2897	0.0087
21	2.0600	0.3632	100.000	1.0022	0.0192	0.5195	0.5199	-0.2927	0.0181
22	2.0205	0.5414	105.000	1.0022	-0.0236	0.5094	0.5099	-0.2917	0.0272
23	1.9656	0.7154	110.000	1.0022	-0.0630	0.4921	0.4961	-0.2868	0.0362
24	1.8958	0.8840	115.000	1.0022	-0.0980	0.4684	0.4785	-0.2783	0.0449
25	1.8115	1.0459	120.000	1.0022	-0.1274	0.4389	0.4570	-0.2665	0.0532
26	1.7135	1.1998	125.000	1.0022	-0.1501	0.4046	0.4315	-0.2518	0.0612
27	1.6024	1.3446	130.000	1.0022	-0.1647	0.3661	0.4014	-0.2344	0.0689
28	1.4791	1.4791	135.000	1.0022	-0.1689	0.3232	0.3647	-0.2142	0.0768
29	1.3446	1.6024	140.000	1.0022	-0.1548	0.2723	0.3132	-0.1897	0.0872
30	1.1998	1.7135	145.000	1.0022	-0.0801	0.1893	0.2056	-0.1636	0.1170
31	1.0459	1.8115	150.000	1.0022	0.0398	0.1030	0.1104	-0.1126	0.0960
32	0.8840	1.8958	155.000	1.0022	-0.0692	0.1526	0.1676	-0.1726	0.1401
33	0.7154	1.9656	160.000	1.0022	-0.0586	0.1374	0.1494	-0.1528	0.1261
34	0.5414	2.0205	165.000	1.0022	0.0489	0.0998	-0.1112	-0.1555	0.1388
35	0.3632	2.0600	170.000	1.0022	0.0241	0.1065	-0.1092	-0.1565	0.1401
36	0.1823	2.0838	175.000	1.0022	-0.0091	0.1103	0.1107	-0.1477	0.1311
37	0.0000	2.0918	180.000	1.0022	0.0000	0.1091	0.1091	-0.1453	0.1290

FORCE AND MOMENT COEFFICIENTS - PRESSURE INTEGRATION

X	CN(X)	CY(X)	CA(X)	CN	CY	CA	CM	CR	CSL	XCPN	XCPY
8.225	1.743E-01	-1.575E-08	-4.443E-02	3.761E-01	-2.801E-08	-7.996E-03	6.933E-01	-4.365E-08	3.114E-10	5.436	21.424

AXIAL SKIN FRICTION FORCE (ESTIMATE) - NOSE TO X 1.554E-02

TOTAL AXIAL FORCE - NOSE TO X 7.541E-03

(q) Page 17

Figure 11.- Continued.

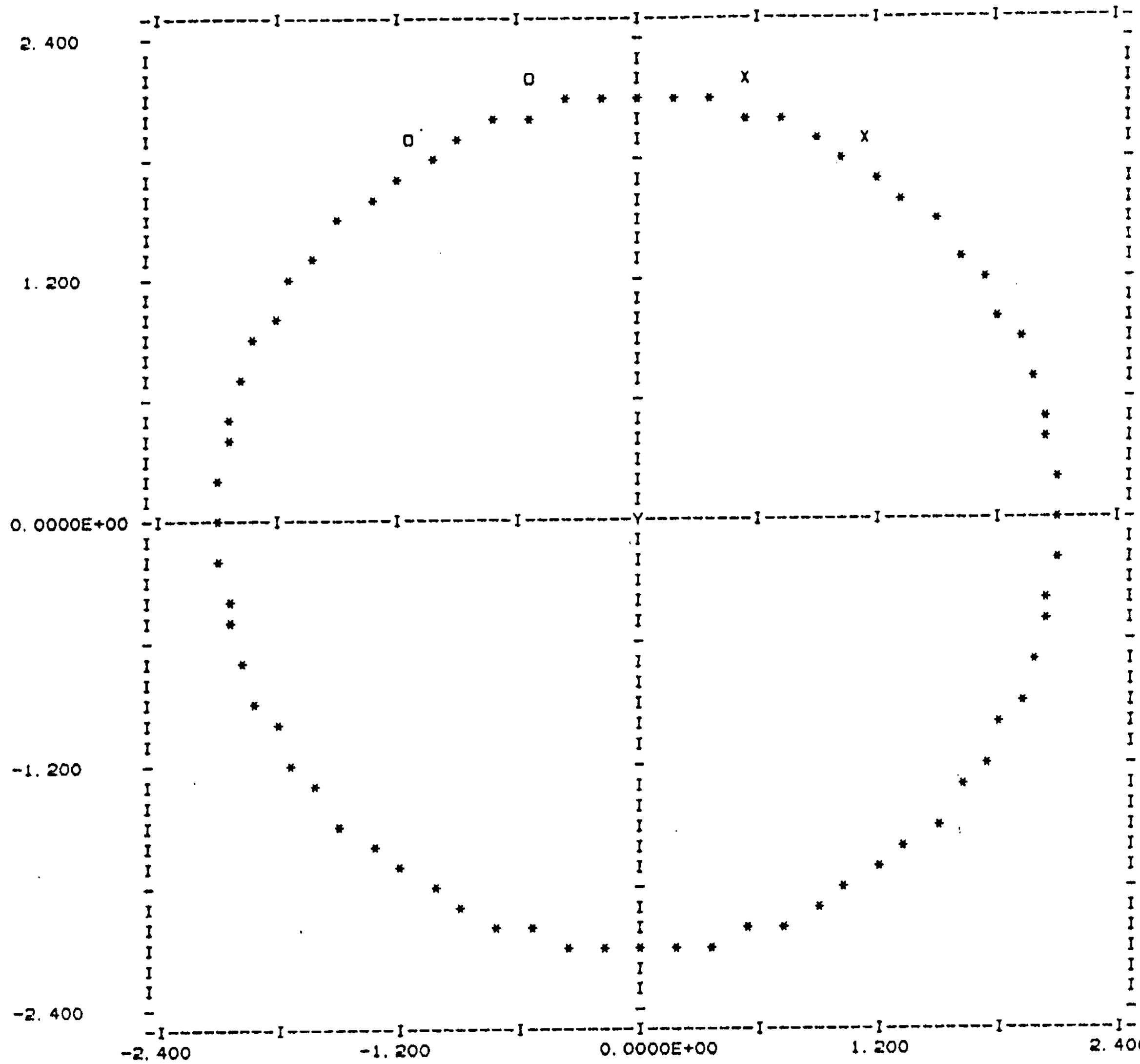

X	R	ALPHA	BETA	X/L
9. 400	2. 092	15. 000	0. 000	0. 186

(r) Page 18

Figure 11.- Continued.

STRATFORD SEPARATION CRITERION (LAMINAR) F(S) =0.02252

SUMMARY OF PRESSURE DISTRIBUTION AND SEPARATION POINTS ON BODY ... X = 9.40

		Y	Z	BETA	ARC	CP	CP'	DCP'/DX
+Y SIDE:	STAGNATION PT.	0.000	-2.092	0.000	-0.016	0.093		
	MIN. PRESSURE	2.060	0.363	100.000	3.650	-0.293	0.000	0.000
	SEPARATION	1.722	1.187	124.571	4.546	-0.253	0.031	0.067
-Y SIDE:		Y	Z	BETA	ARC	CP	CP'	DCP'/DX
	STAGNATION PT.	0.000	2.092	180.000	-0.016	-0.145		
	MIN. PRESSURE	-2.060	0.363	260.000	3.650	-0.293	0.000	0.000
	SEPARATION	-1.722	1.187	235.429	4.546	-0.253	0.031	0.067

INITIAL POSITIONS AND STRENGTHS OF SHED VORTICITY AT X = 9.400

	NV	GAM/V	M(K)	Y	Z	BETA	VT/V	YC	ZC	RG/R
+Y SIDE:	5	0.1372	0.1032	1.8086	1.2463	124.5706	0.4336	1.8086	1.2463	1.0500
-Y SIDE:	6	-0.1372	0.1032	-1.8086	1.2463	235.4294	0.4336	-1.8086	1.2463	1.0500

(s) Page 19

Figure 11.- Continued.

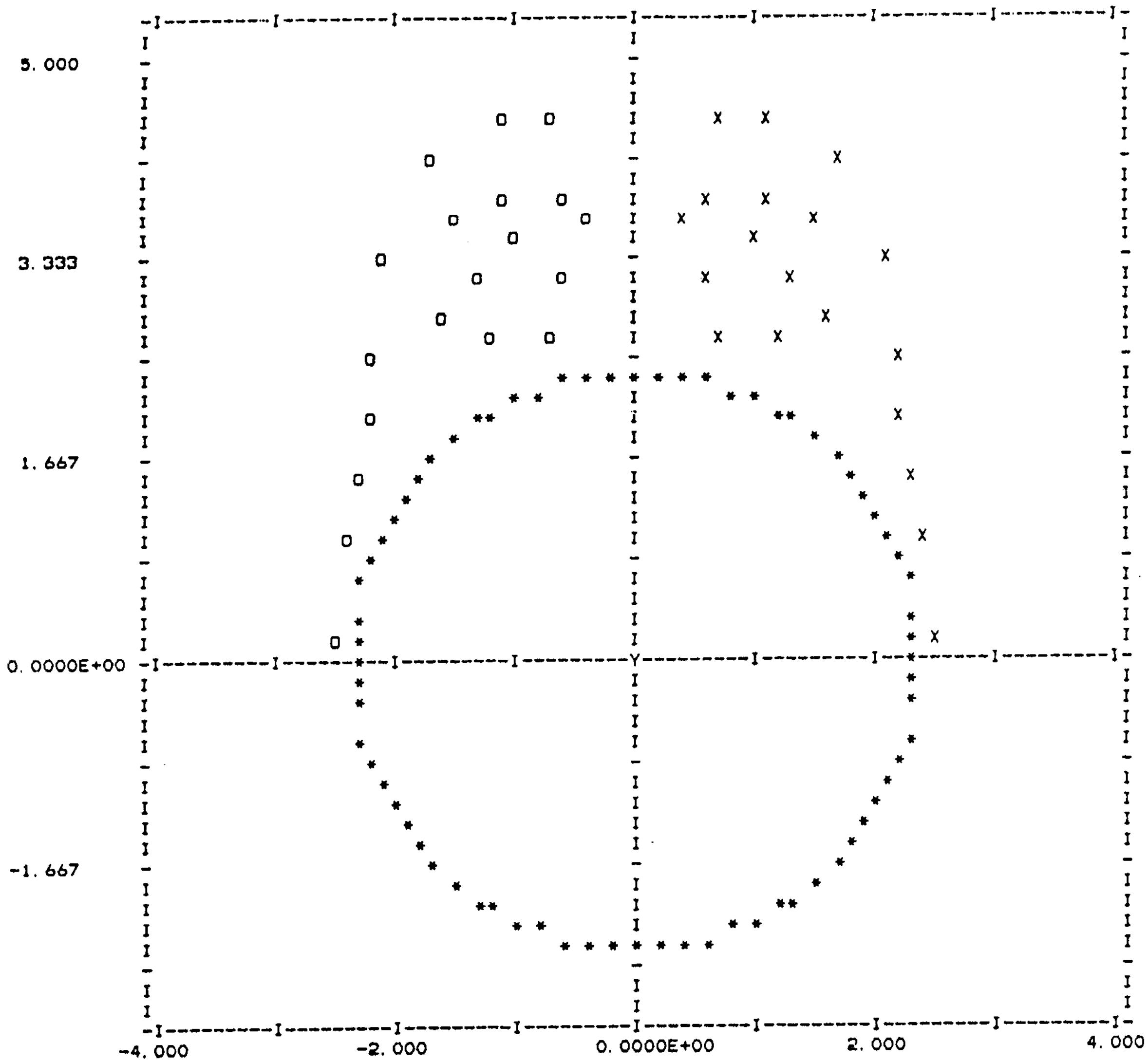

TOTAL FORCE AND MOMENT SUMMARY

X	ALPHA	BETA	CN	CY	CA	CDI	CM	CR	CSL
47.00	15.0000	0.0000	0.7952	0.0000	-0.0395	0.1036	-0.4574	0.0000	0.0000

(t) Page 50

Figure 11.- Continued.

SUMMARY OF VORTEX FIELD AT X = 47.000 H = 2.35000

	NV	GAM/V	Y	Z	XSHED	BETA	RG	RG/R
1	1	0.08163	0.97262	3.46246	4.70000	164.310	3.59647	1.53058
2	2	0.11370	1.29059	3.10862	7.05000	157.453	3.36588	1.43244
3	3	0.13724	0.62804	3.10403	9.40000	168.562	3.16692	1.34777
4	4	0.15271	0.59808	3.86885	11.75000	171.212	3.91480	1.66605
5	5	0.16561	1.13383	3.76197	14.10000	163.228	3.92912	1.67214
6	6	0.16479	1.52257	3.73054	16.45000	157.798	4.02929	1.71477
7	7	0.16463	1.60284	2.78042	18.80000	150.038	3.20934	1.36582
8	8	0.16235	1.19167	2.65328	21.15000	155.814	2.90860	1.23783
9	9	0.16009	0.66864	2.74533	23.50000	166.312	2.82558	1.20250
10	10	0.15709	0.38274	3.61303	25.85000	173.953	3.63325	1.54623
11	11	0.15421	0.65717	4.55521	28.20000	171.791	4.60237	1.95866
12	12	0.15164	1.14863	4.57774	30.55000	165.914	4.71964	2.00857
13	13	0.14840	1.69398	4.13687	32.90000	157.732	4.47026	1.90244
14	14	0.14551	2.10704	3.35555	35.25000	147.874	3.96224	1.68624
15	15	0.14551	2.18234	2.55449	37.60000	139.492	3.35976	1.42984
16	16	0.14263	2.23022	1.98161	39.95000	131.622	2.98340	1.26967
17	17	0.14011	2.27983	1.47818	42.30000	122.958	2.71710	1.15634
18	18	0.13832	2.37041	0.92689	44.64999	111.357	2.54518	1.08317
19	19	0.13568	2.45783	0.21525	46.99999	95.005	2.46724	1.05000
1	20	-0.08163	-0.97262	3.46246	4.70000	195.690	3.59647	1.53058
2	21	-0.11370	-1.29059	3.10862	7.05000	202.547	3.36588	1.43244
3	22	-0.13724	-0.62804	3.10403	9.40000	191.438	3.16692	1.34777
4	23	-0.15271	-0.59808	3.86885	11.75000	188.788	3.91480	1.66605
5	24	-0.16561	-1.13383	3.76197	14.10000	196.772	3.92912	1.67214
6	25	-0.16479	-1.52257	3.73054	16.45000	202.202	4.02929	1.71477
7	26	-0.16463	-1.60284	2.78042	18.80000	209.962	3.20934	1.36582
8	27	-0.16235	-1.19167	2.65328	21.15000	204.186	2.90860	1.23783
9	28	-0.16009	-0.66864	2.74533	23.50000	193.688	2.82558	1.20250
10	29	-0.15709	-0.38274	3.61303	25.85000	186.047	3.63325	1.54623
11	30	-0.15421	-0.65717	4.55521	28.20000	188.209	4.60237	1.95866
12	31	-0.15164	-1.14863	4.57774	30.55000	194.086	4.71964	2.00857
13	32	-0.14840	-1.69398	4.13687	32.90000	202.268	4.47026	1.90244
14	33	-0.14551	-2.10704	3.35555	35.25000	212.126	3.96224	1.68624
15	34	-0.14551	-2.18234	2.55449	37.60000	220.508	3.35976	1.42984
16	35	-0.14263	-2.23022	1.98161	39.95000	228.378	2.98340	1.26967
17	36	-0.14011	-2.27983	1.47818	42.30000	237.042	2.71710	1.15634
18	37	-0.13832	-2.37041	0.92689	44.64999	248.643	2.54518	1.08317
19	38	-0.13568	-2.45783	0.21525	46.99999	264.995	2.46724	1.05000

(u) Page 51

Figure 11.- Continued.

PRESSURE DISTRIBUTION AT FINAL X STATION

Y	Z	CP
0.00000	-2.34975	0.04431
0.20479	-2.34081	0.04238
0.40803	-2.31405	0.03666
0.60816	-2.26968	0.02734
0.80366	-2.20804	0.01472
0.99305	-2.12960	-0.00077
1.17488	-2.03494	-0.01862
1.34776	-1.92480	-0.03822
1.51039	-1.80001	-0.05889
1.66152	-1.66152	-0.07992
1.80001	-1.51039	-0.10055
1.92480	-1.34776	-0.12002
2.03494	-1.17488	-0.13755
2.12960	-0.99305	-0.15242
2.20804	-0.80366	-0.16390
2.26968	-0.60816	-0.17133
2.31405	-0.40803	-0.17406
2.34081	-0.20479	-0.17141
2.34975	0.00000	-0.16266
2.34081	0.20479	-0.14679
2.31405	0.40803	-0.12223
2.26969	0.60816	-0.08877
2.20804	0.80366	-0.09143
2.12960	0.99305	-0.08903
2.03494	1.17488	-0.06244
1.92480	1.34776	-0.06081
1.80001	1.51039	-0.05454
1.66153	1.66152	-0.05005
1.51039	1.80001	-0.05107
1.34776	1.92480	-0.06114
1.17488	2.03494	-0.08390
0.99305	2.12960	-0.11359
0.80366	2.20804	-0.13112
0.60816	2.26968	-0.11941
0.40803	2.31405	-0.07683
0.20480	2.34081	-0.03942
0.00000	2.34975	-0.02683

(v) Page 52

Figure 11.- Concluded.

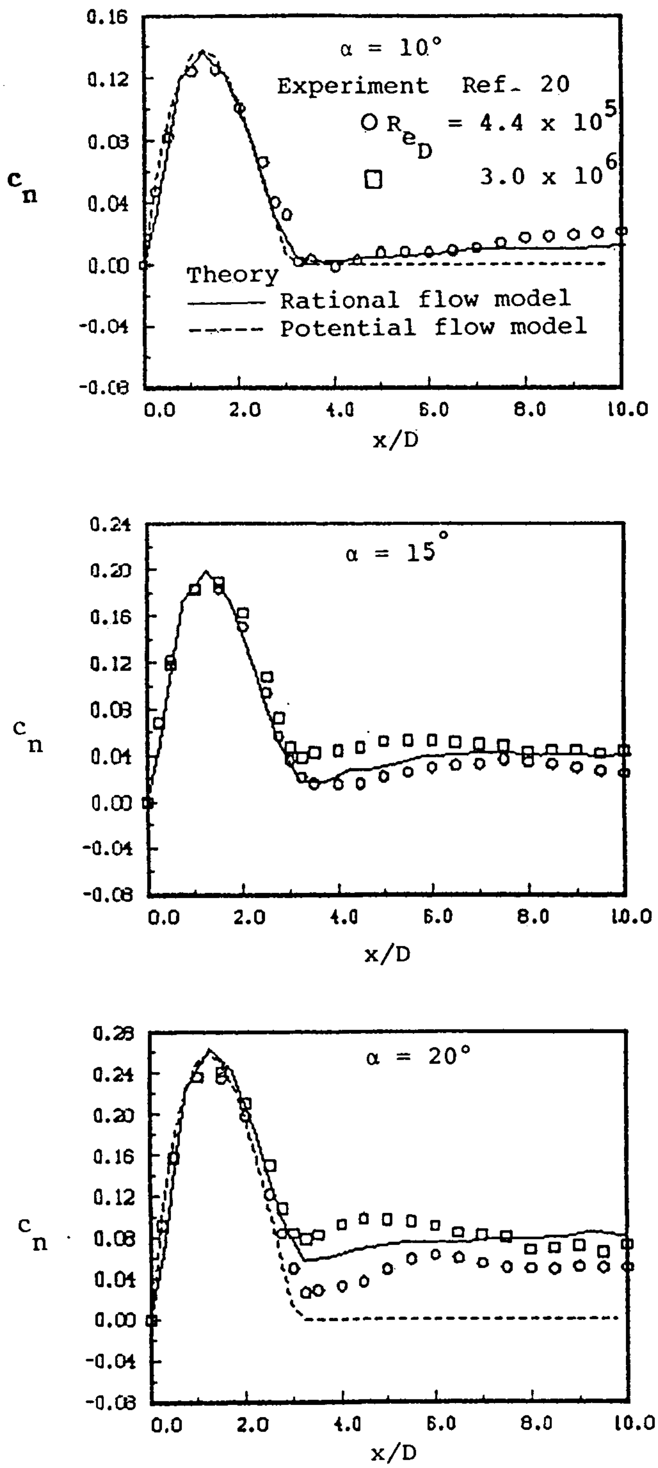

Figure 12.- Measured and predicted normal force distribution on an ogive-cylinder model.

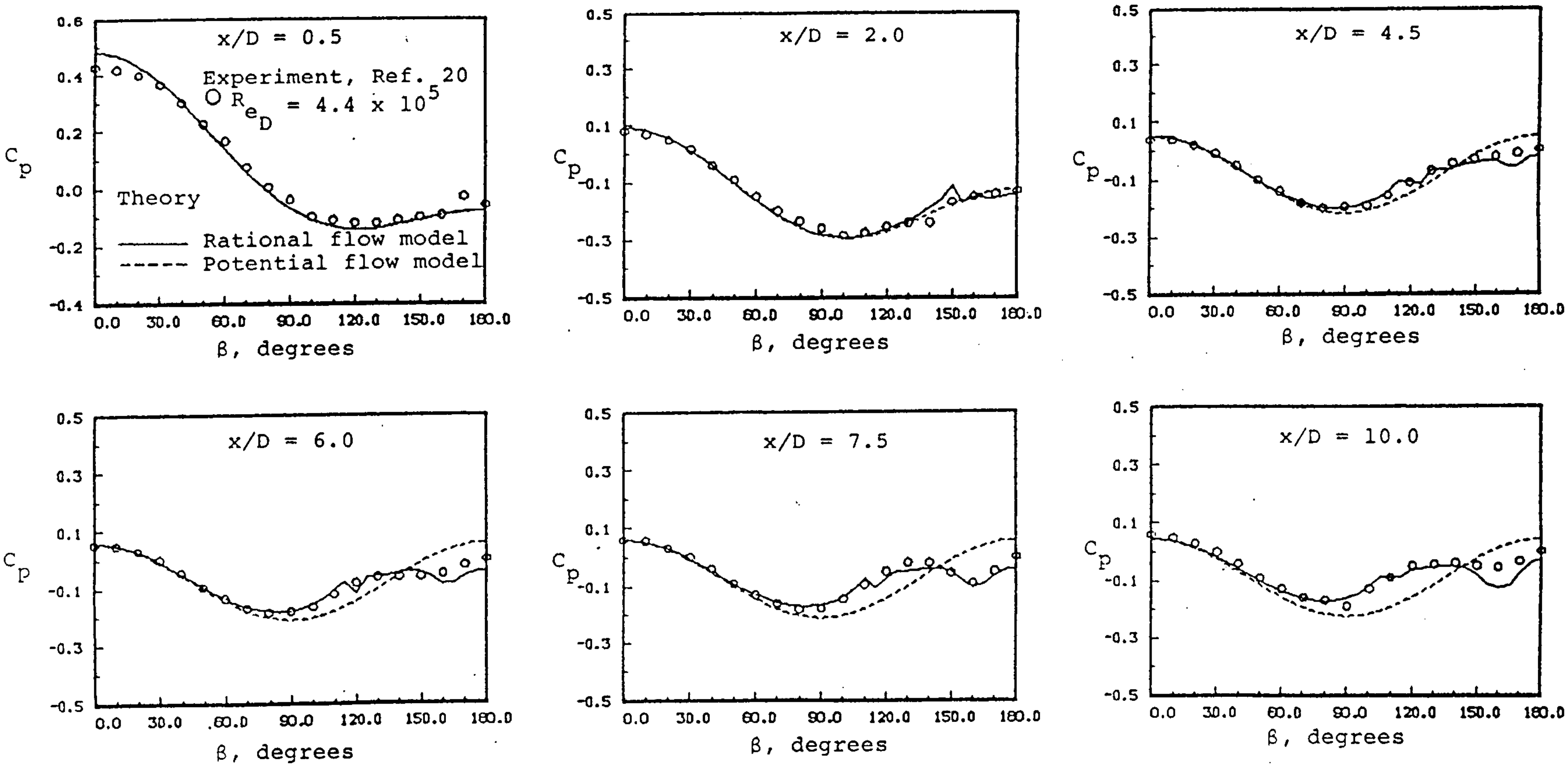

(a) $\alpha = 15°$

Figure 13.- Measured and predicted pressure distribution on an ogive-cylinder model.

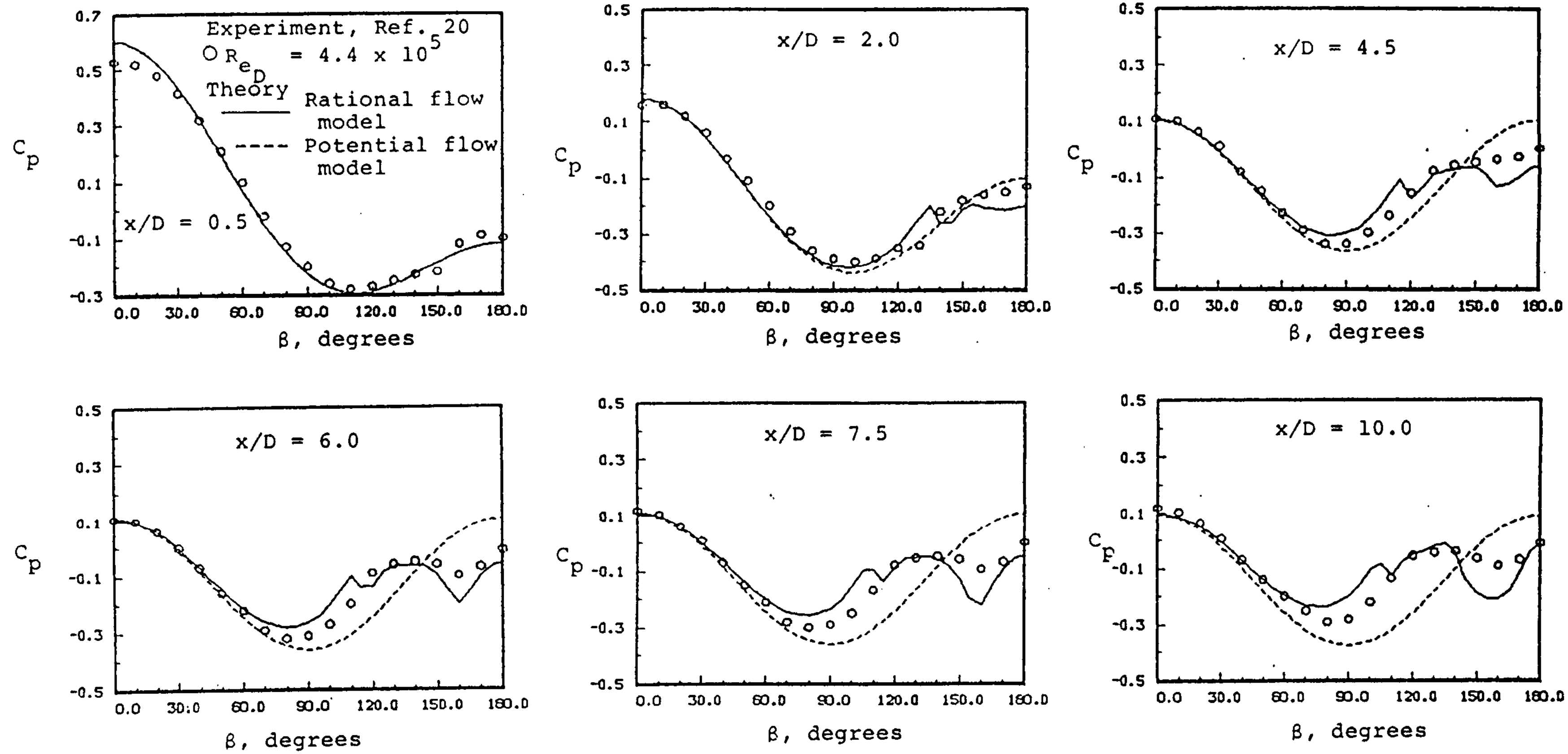

(b) α = 20°

Figure 13.- Concluded.

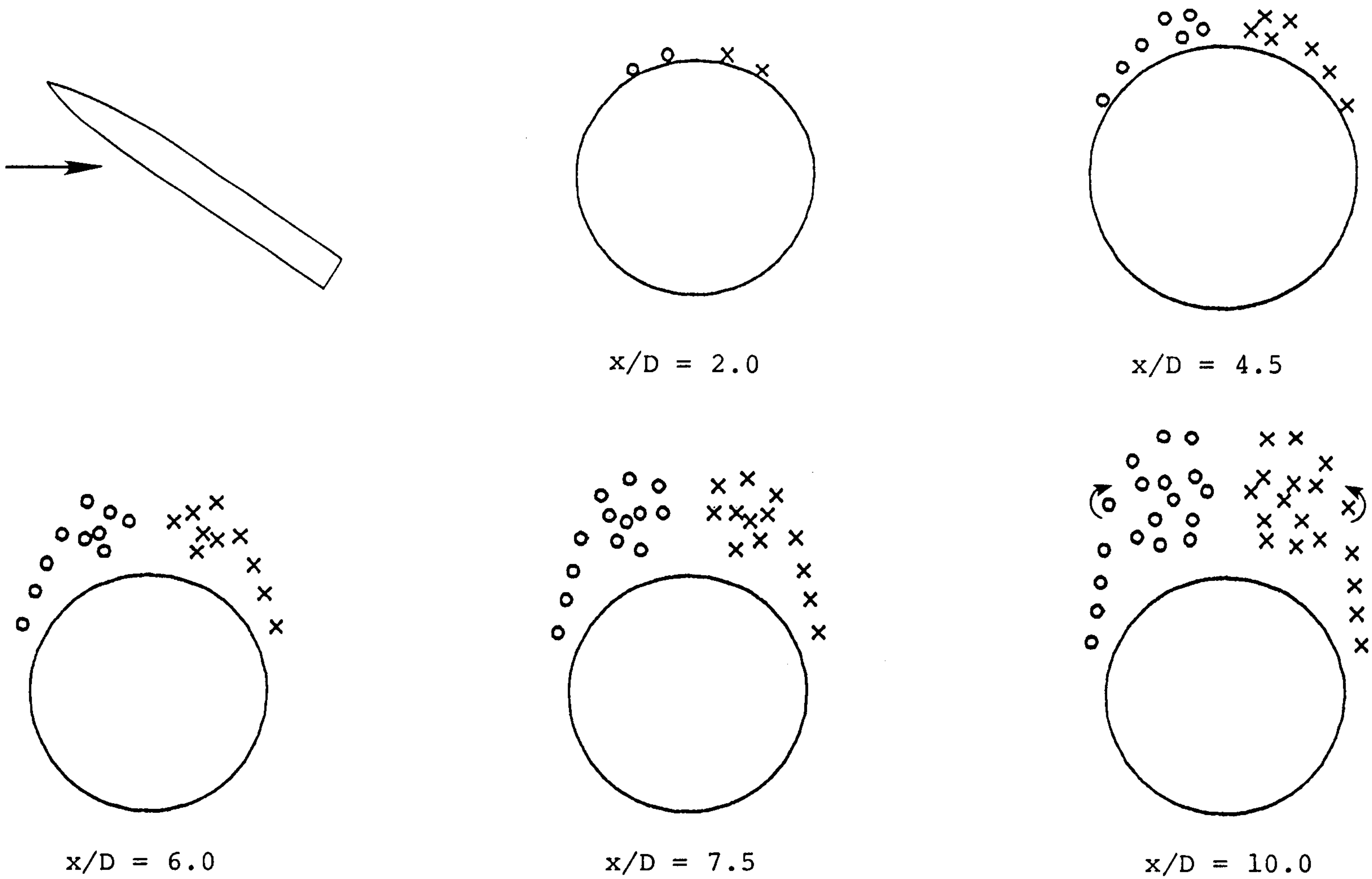

Figure 14.- Predicted vortex wake on an ogive-cylinder model at $\alpha = 15^\circ$.

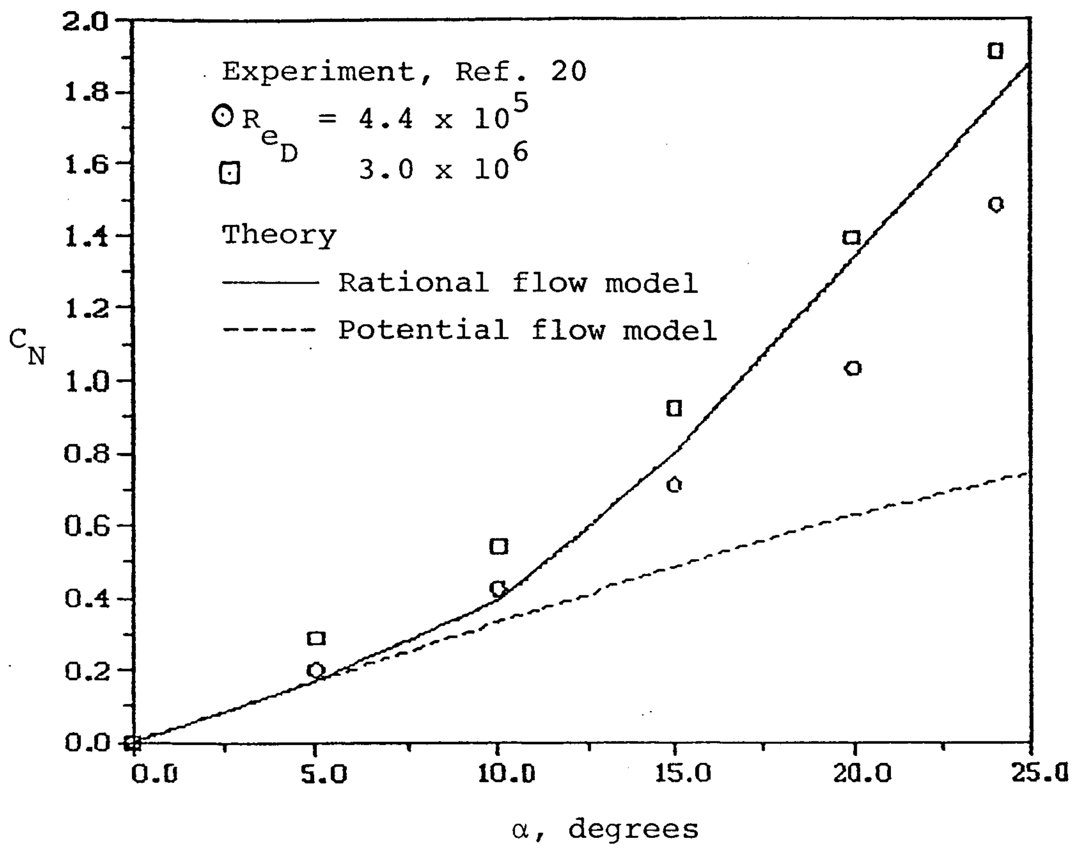

Figure 15.- Measured and predicted normal-force coefficient on an ogive-cylinder model.

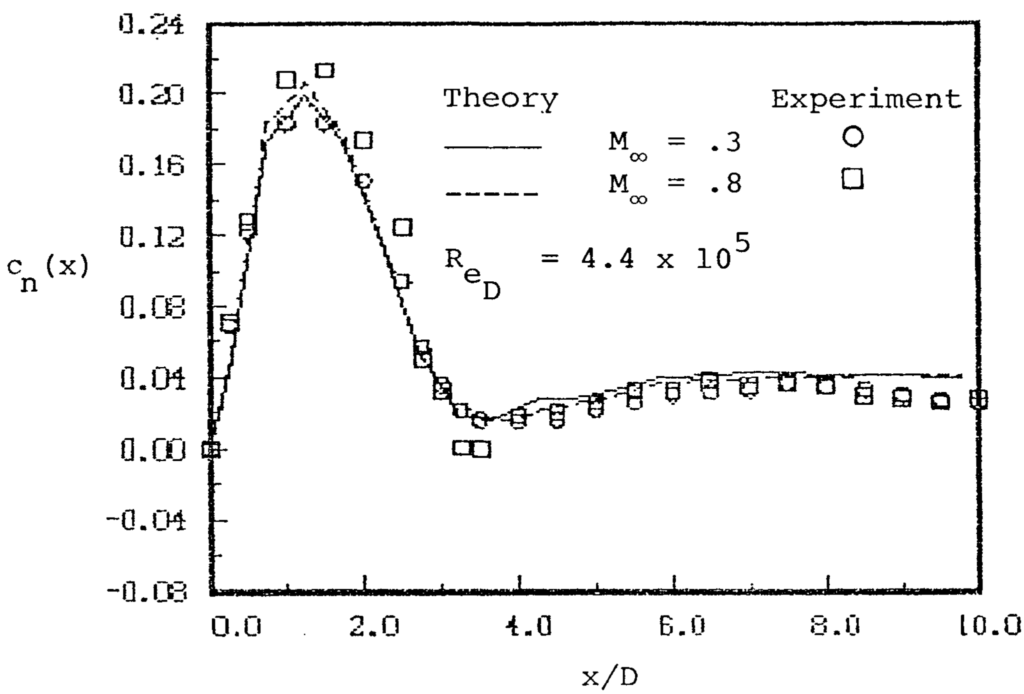

Figure 16.- Compressibility effects on comparison of measured and predicted normal force distribution on an ogive-cylinder model, $\alpha = 15°$.

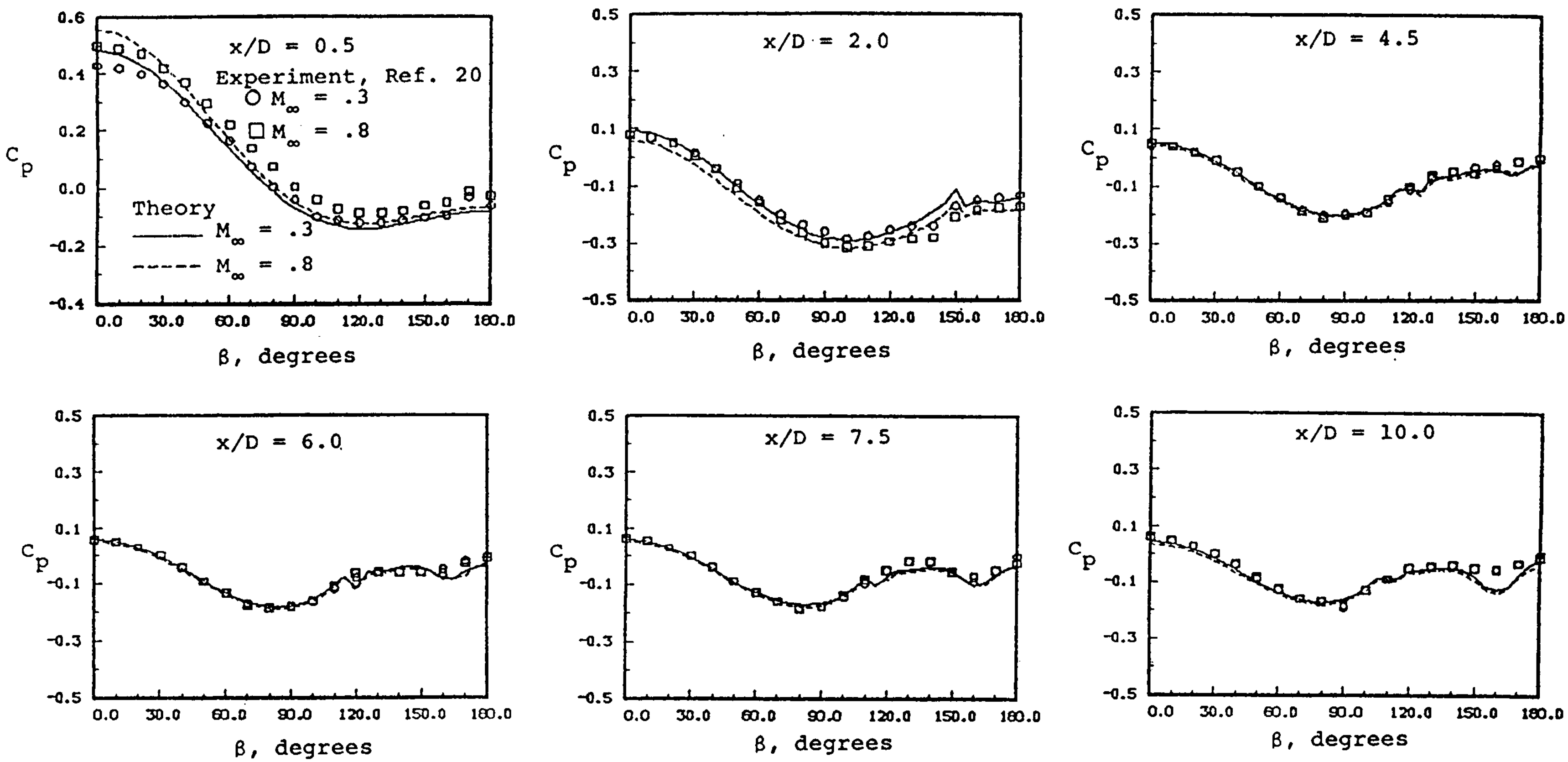

Figure 17.- Compressibility effects on measured and predicted pressure distributions on an ogive-cylinder model at $\alpha = 15°$.

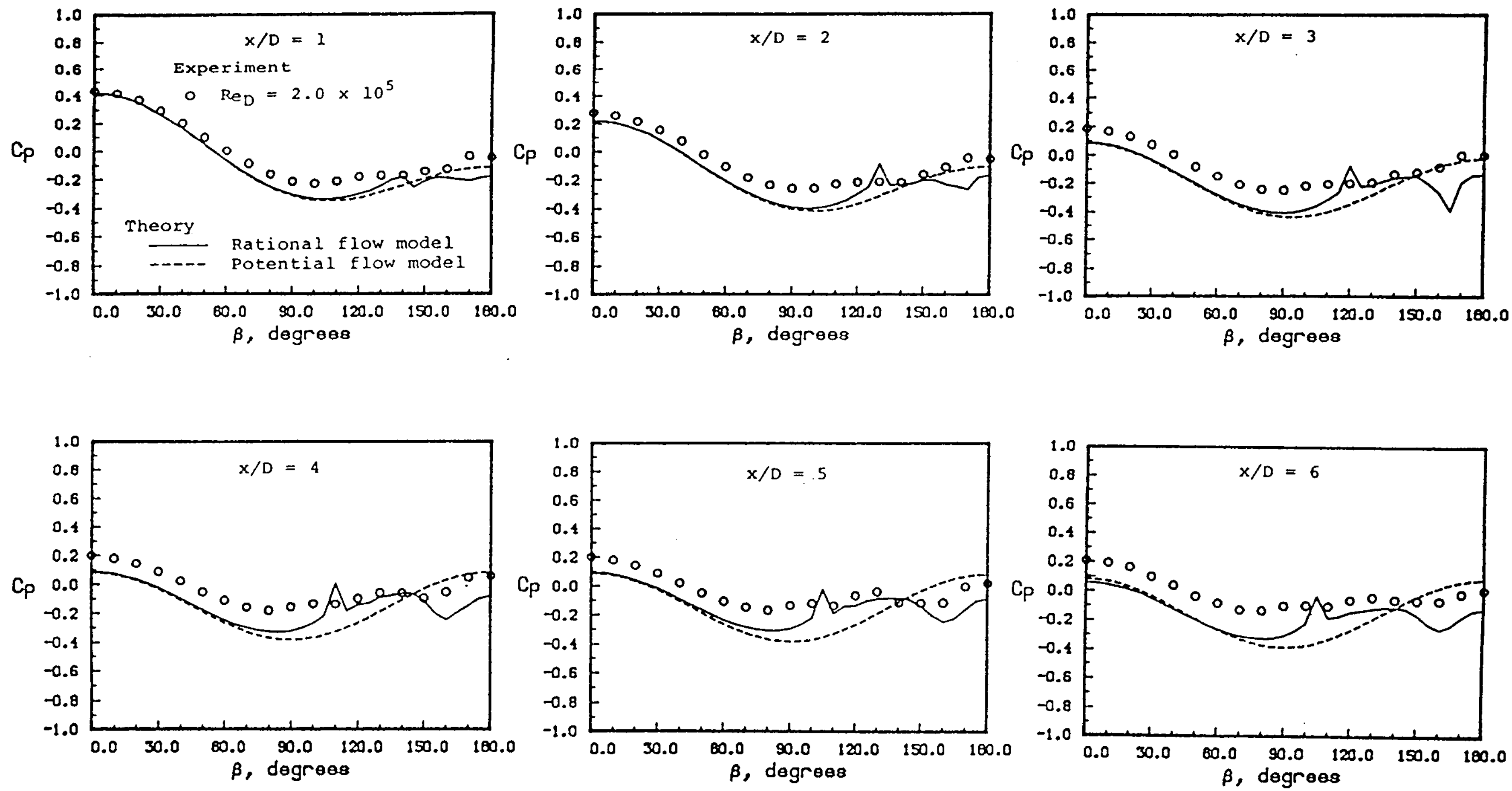

Figure 18.- Measured and predicted pressure distributions on a 3.5D ogive-cylinder model at $\alpha = 20°$.

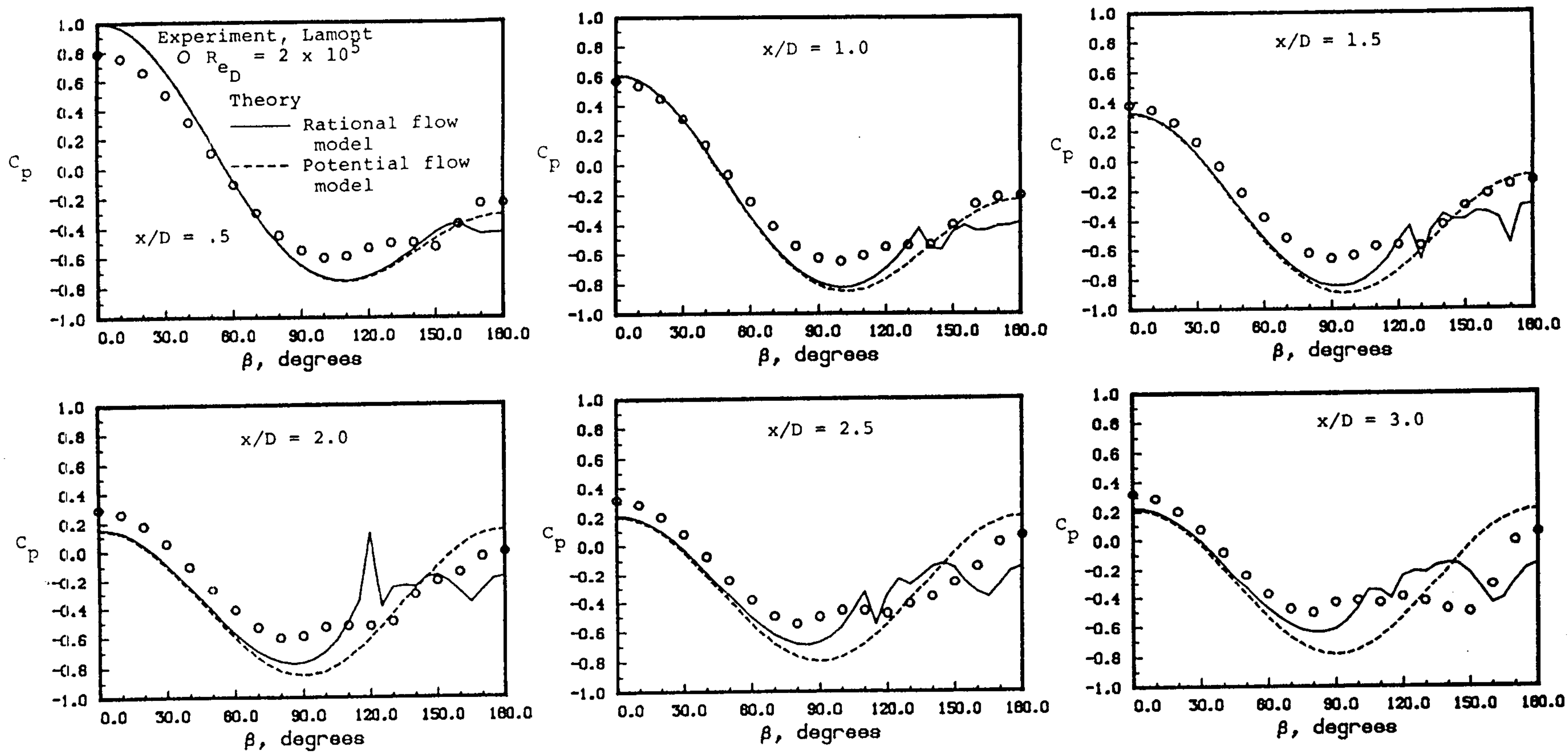

Figure 19.- Measured and predicted pressure distributions on a 2D ogive-cylinder model at $\alpha = 30^{\circ}$.

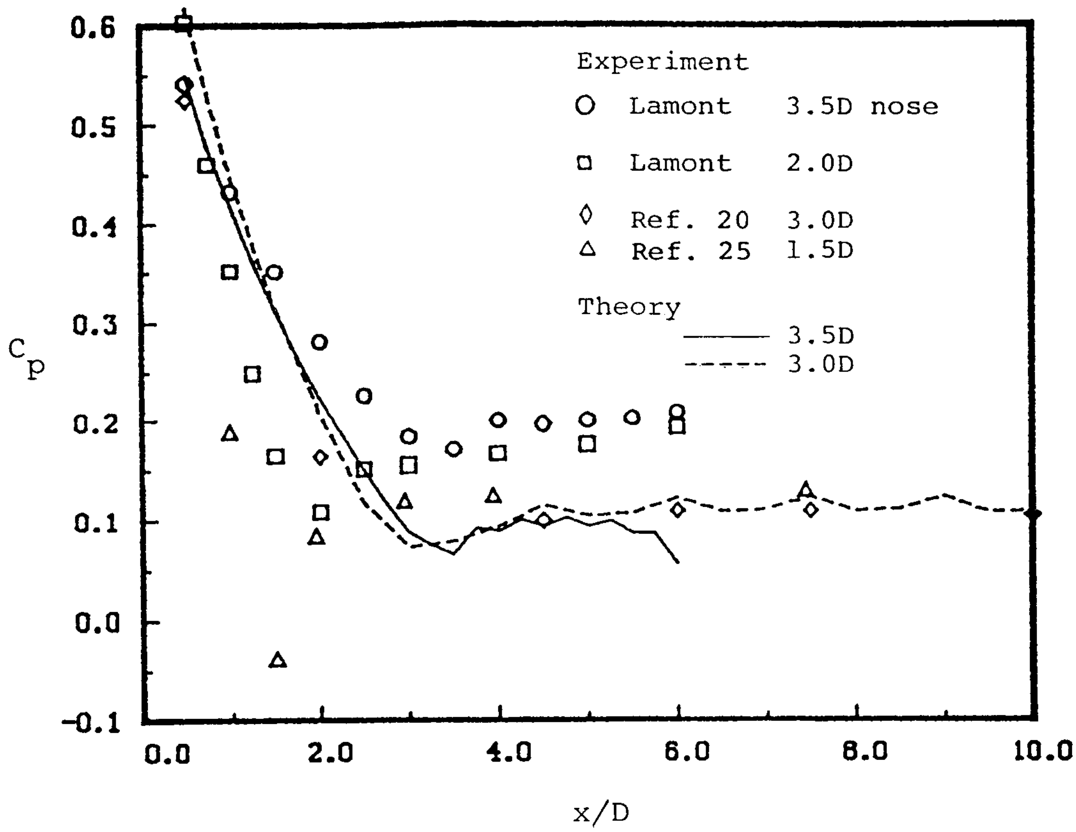

Figure 20.- Measured and predicted pressure distribution on the windward meridian of several ogive-cylinder models at $\alpha = 20°$.

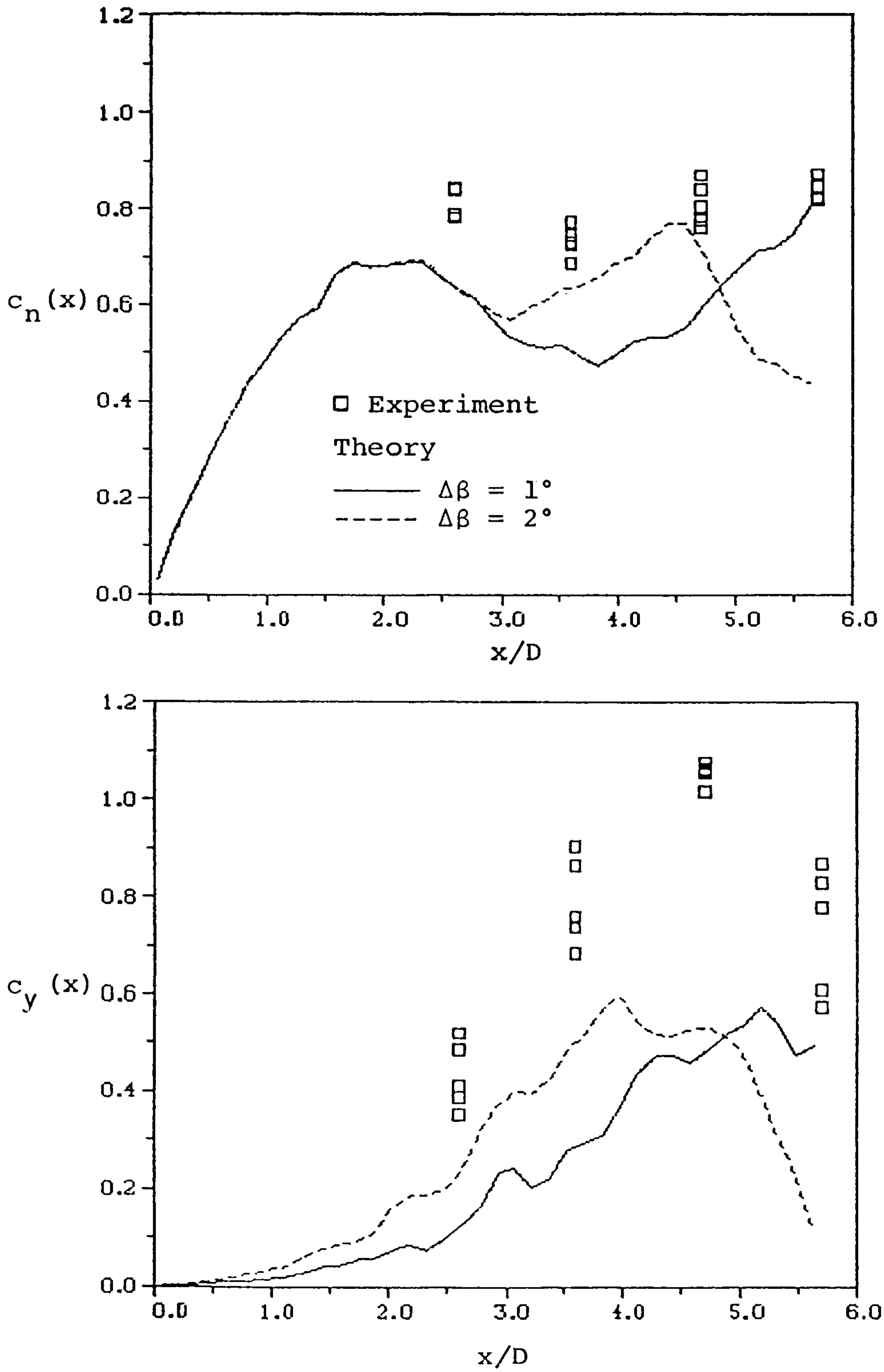

Figure 21.- Comparison of measured and predicted distributions of normal force and side force on an ogive-cylinder model at α = 45°.

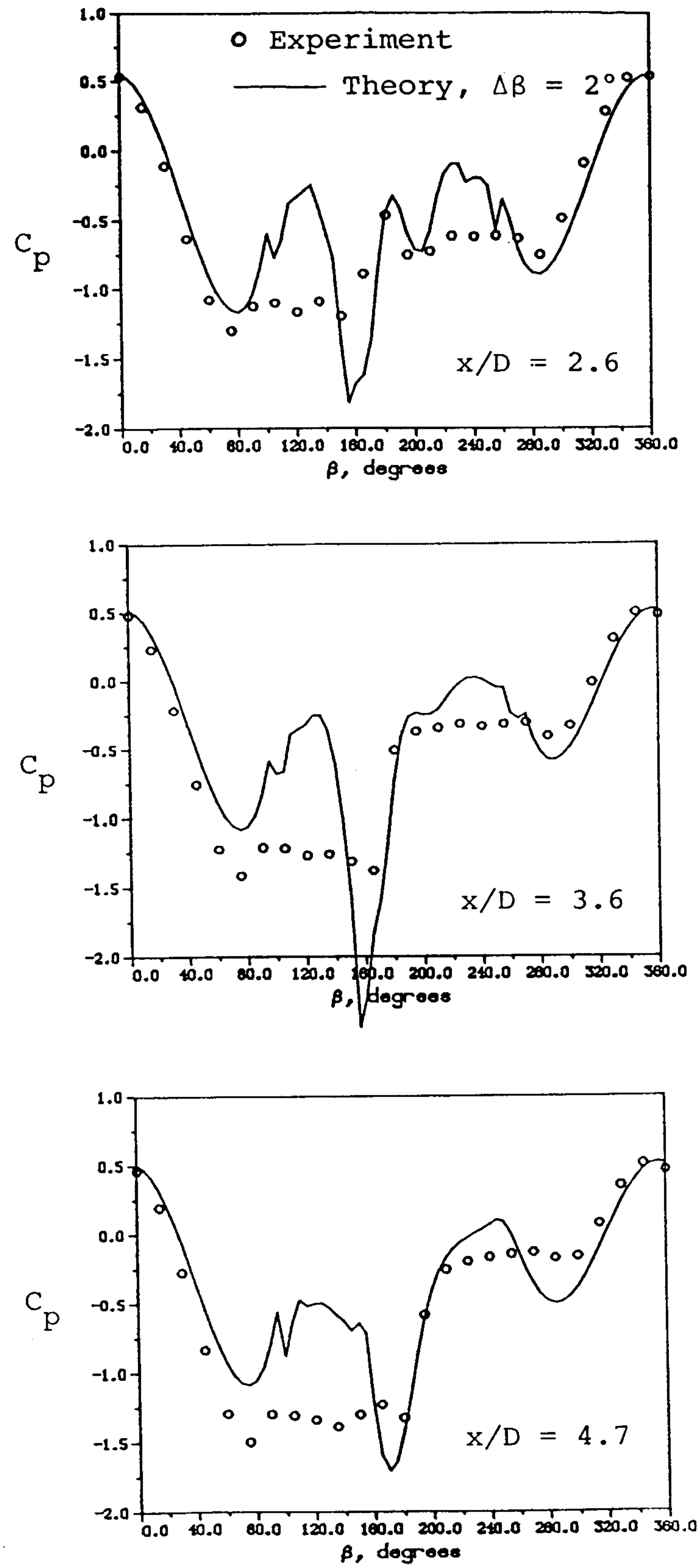

Figure 22.- Measured and predicted pressure distribution on an ogive-cylinder model at $\alpha = 45°$.

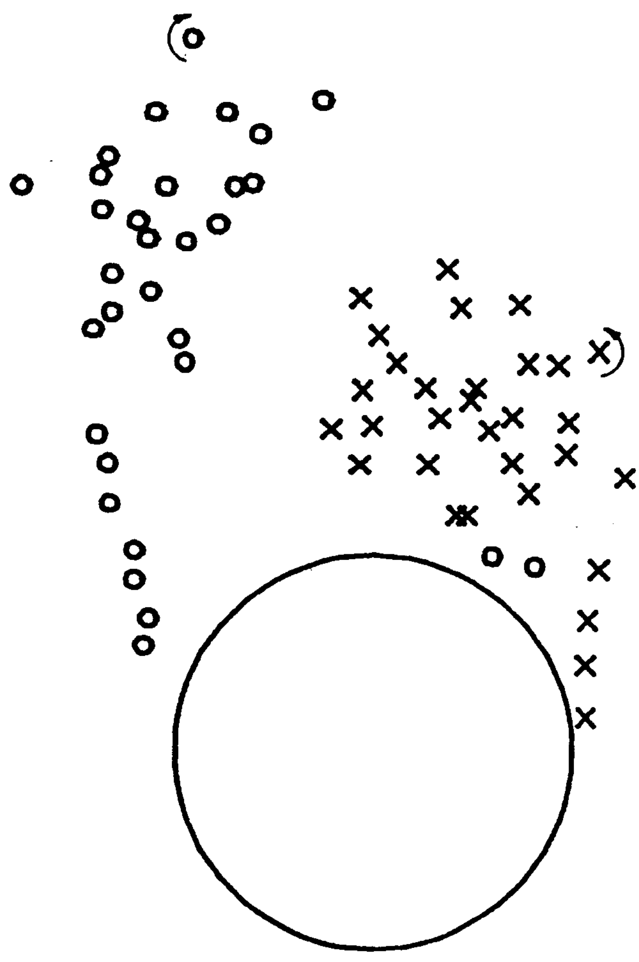

Figure 23.- Predicted asymmetric wake at $x/D = 4.7$ on an ogive-cylinder model at $\alpha = 45°$.

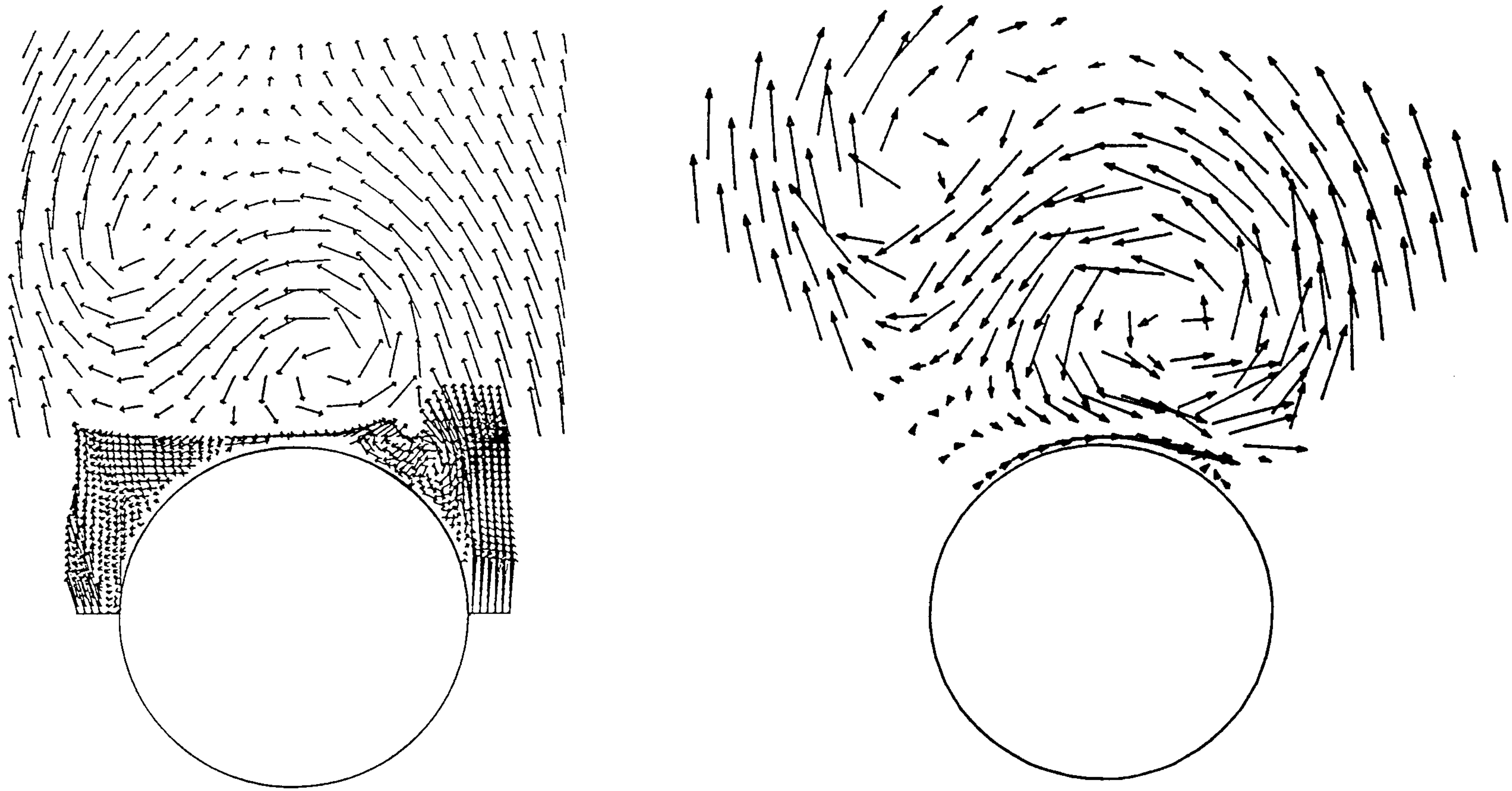

(a) Measured velocity field (Ref. 26)

(b) Predicted velocity field

Figure 24.- Measured and predicted velocity field at x/D = 4.7 on an ogive-cylinder model at α = 45°.

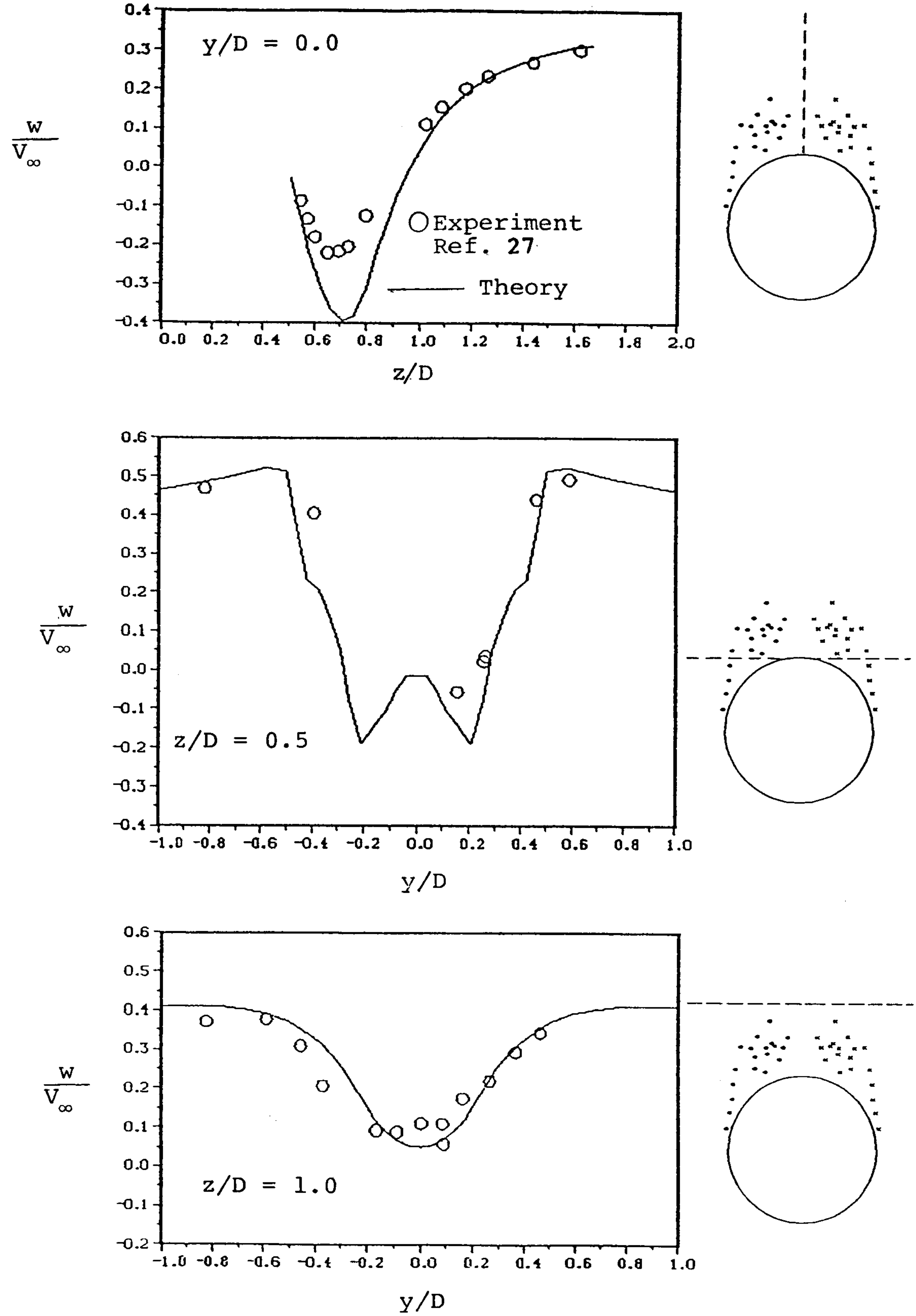

Figure 25 .- Measured and predicted velocity field at x/D = 4.9 on the lee side of an ogive-cylinder at α = 22.4°

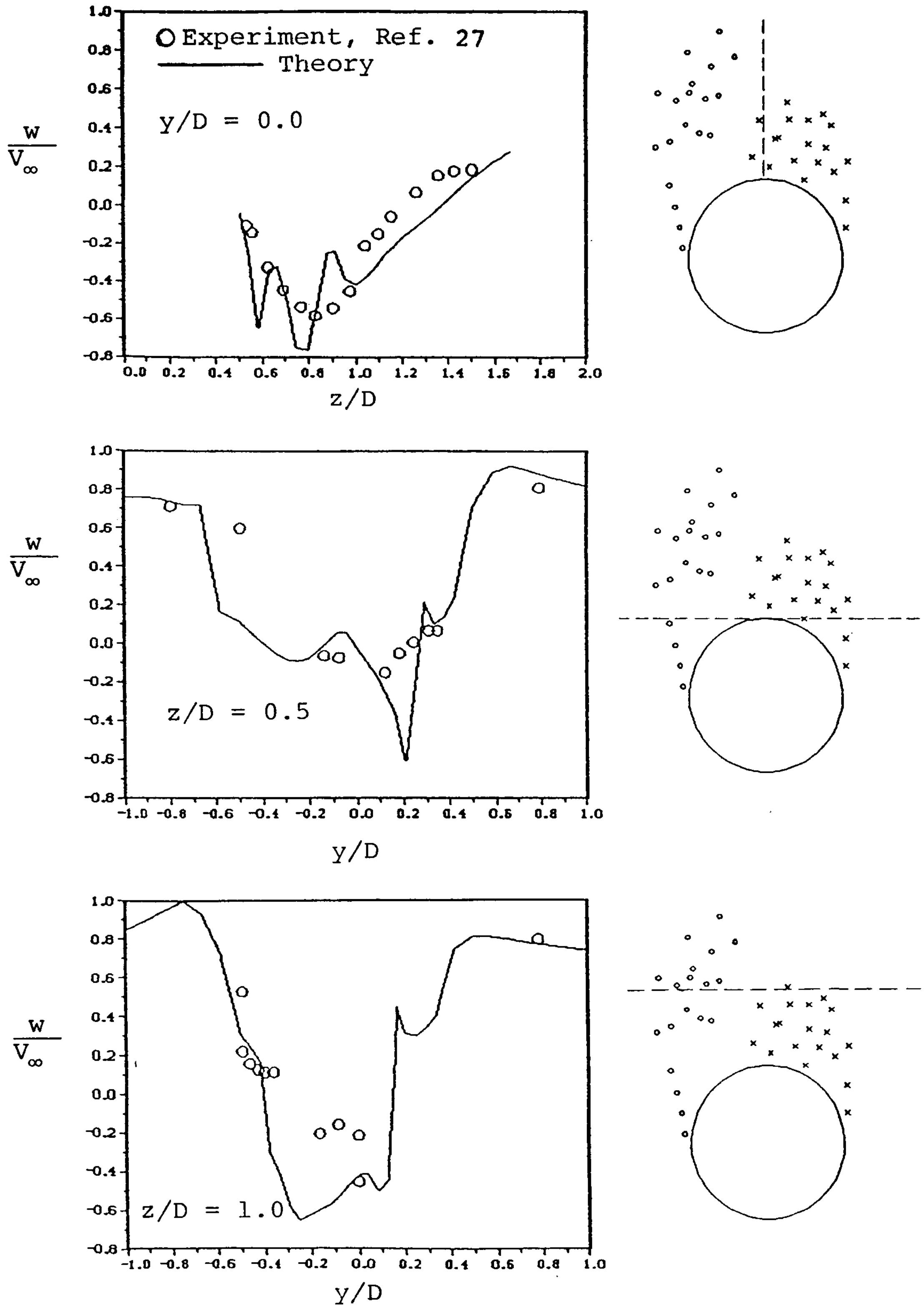

Figure 26.- Measured and predicted velocity field at x/D = 4.9 on the lee side of an ogive-cylinder at α = 37.5°.

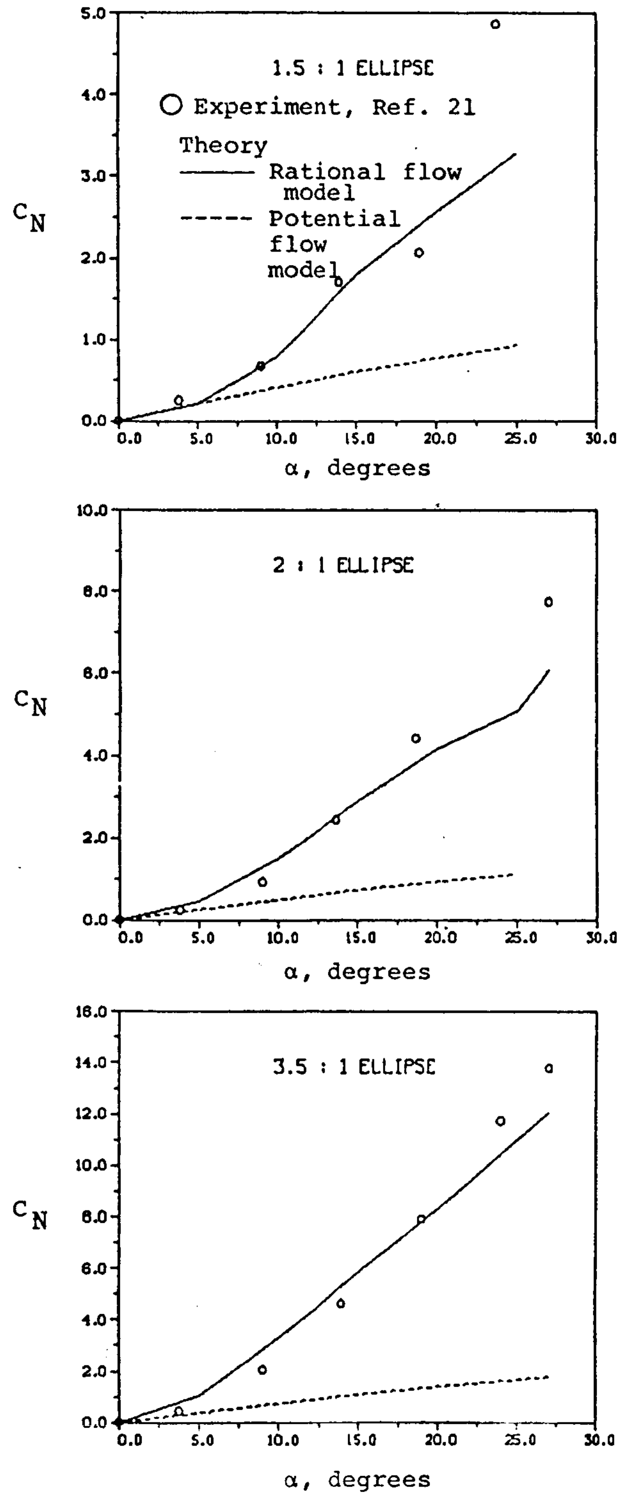

Figure 27.- Measured and predicted normal-force coefficients on a series of elliptic cross section bodies.

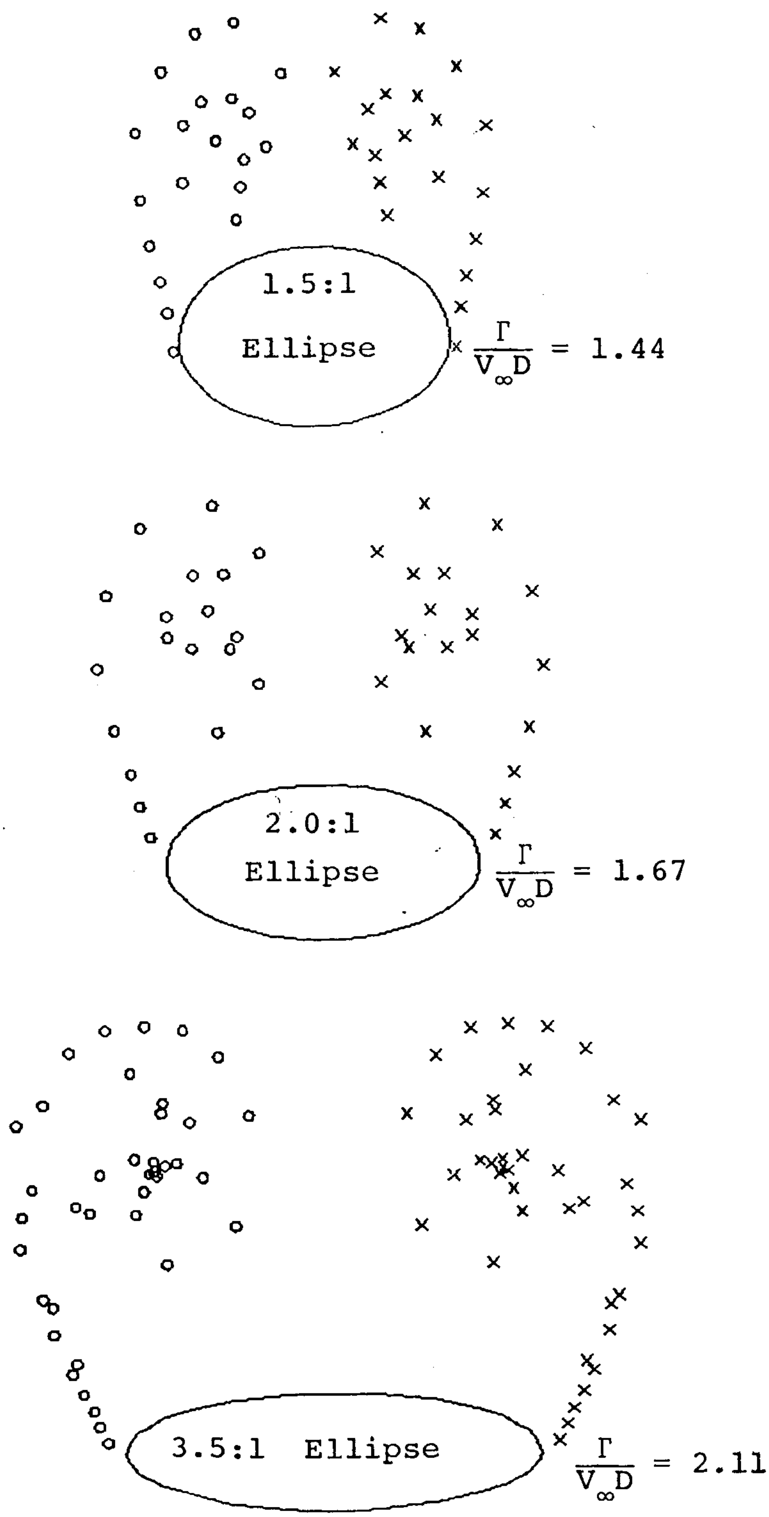

Figure 28.- Predicted vortex cloud wakes on a series of elliptic cross section bodies at $x/D = 10$, $\alpha = 20°$.

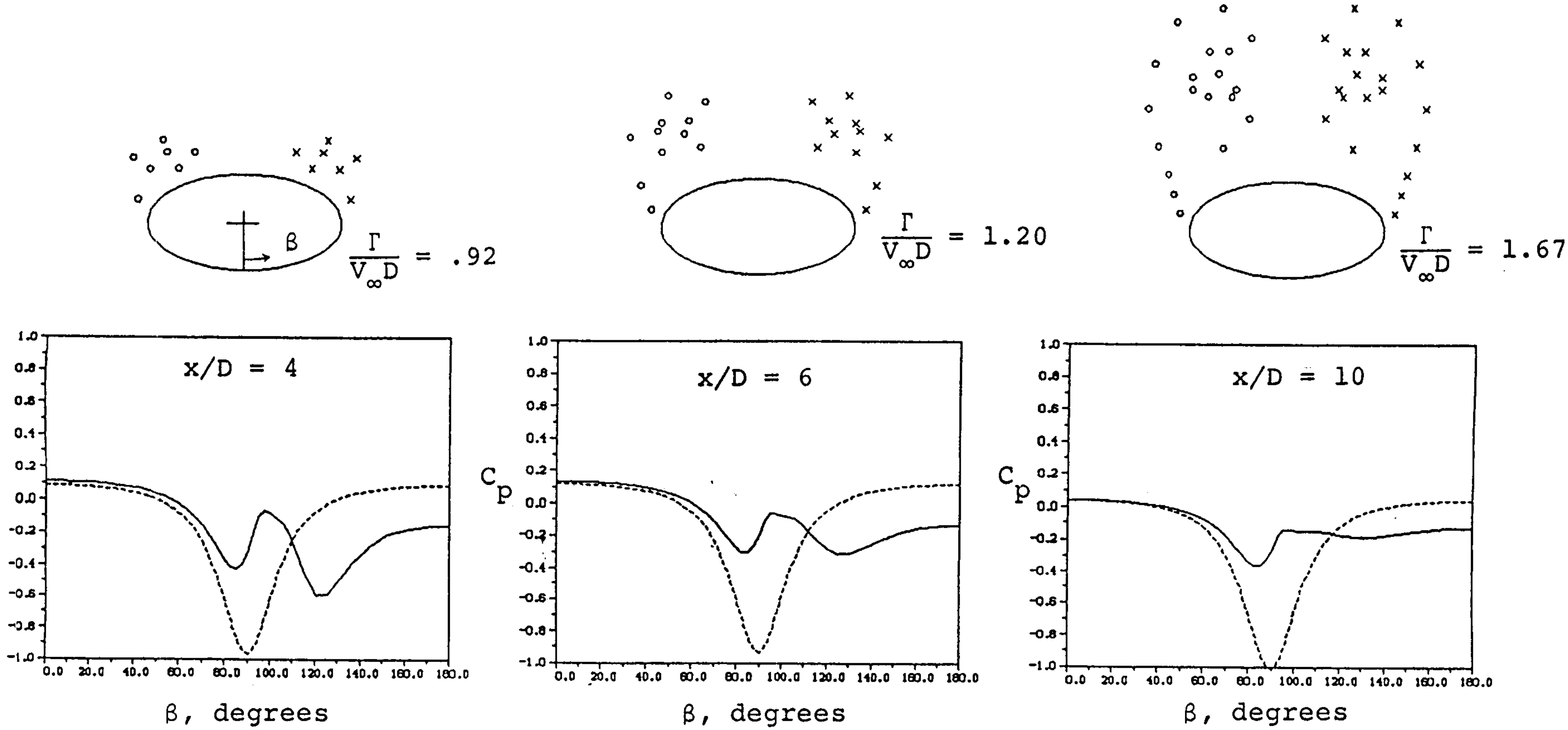

Figure 29.- Predicted circumferential pressure distribution on a 2:1 elliptic cross section body at $\alpha = 20°$.

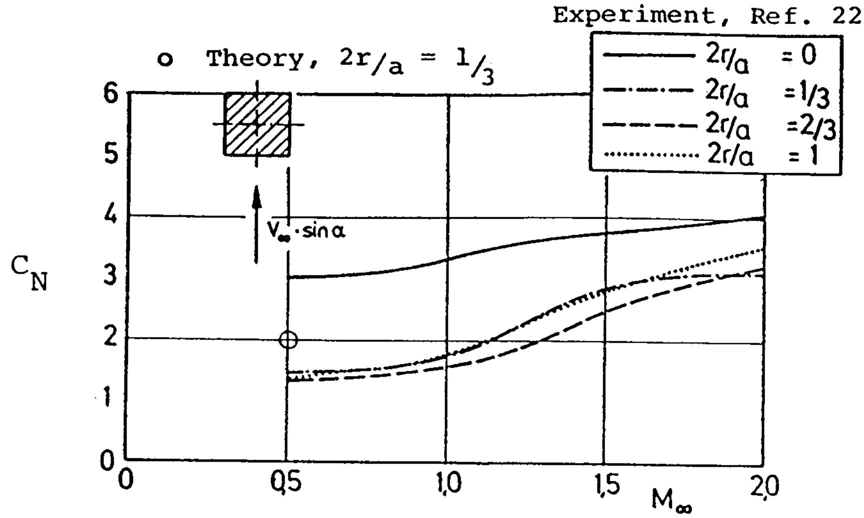

(a) $\phi = 0^{\circ}$

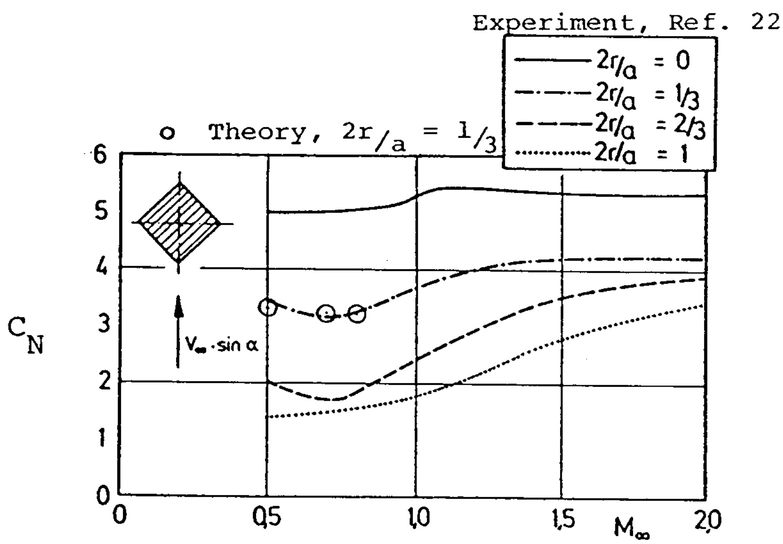

(b) $\phi = 45^{\circ}$

Figure 30.- Measured and predicted normal-force coefficient on a square cross section body at $\alpha = 20^{\circ}$.

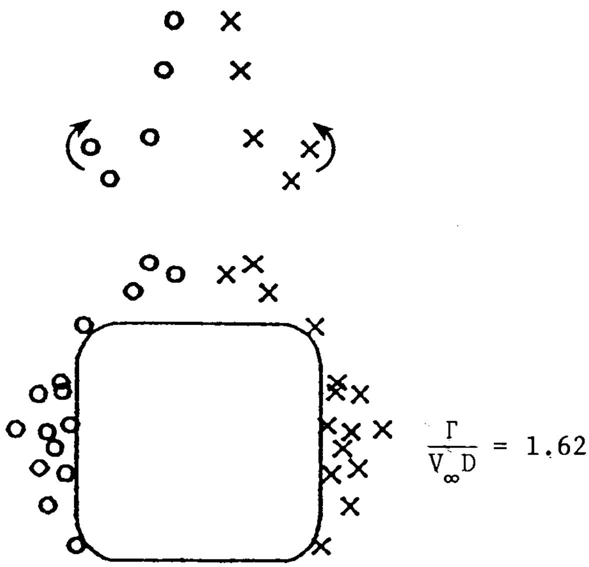

(a) ϕ = 0°

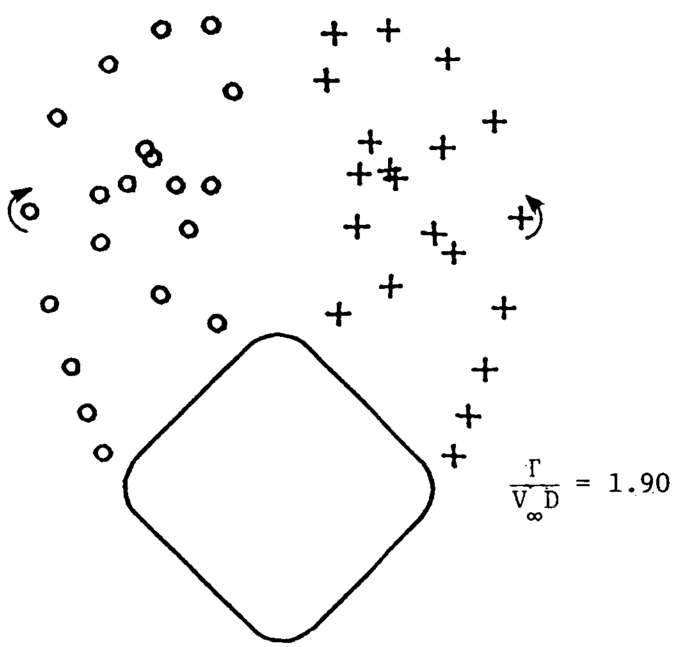

(b) ϕ = 45°

Figure 31.- Predicted vortex wake at x/D = 13 on a square cross section model at α = 20°, M_∞ = .5.

1. Report No.	2. Government Accession No.	3. Recipient's Catalog No.
NASA CR-4037		

4. Title and Subtitle	5. Report Date
Prediction of Vortex Shedding From Circular and Noncircular Bodies in Subsonic Flow	January 1987
	6. Performing Organization Code: 2021/C
7. Author(s): Michael R. Mendenhall and Daniel J. Lesieutre	8. Performing Organization Report No.: NEAR TR 354
9. Performing Organization Name and Address: Nielsen Engineering and Research, Inc., 510 Clyde Avenue, Mountain View, CA 94043	10. Work Unit No.
	11. Contract or Grant No.: NAS1-17962
12. Sponsoring Agency Name and Address: National Aeronautics and Space Administration, Washington, DC 20546	13. Type of Report and Period Covered: Contractor Report
	14. Sponsoring Agency Code: 533-02-01-04

15. Supplementary Notes

NASA Langley Research Center
Technical Monitor: Robert M. Hall

16. Abstract

An engineering prediction method and associated computer code VTXCLD are presented which predict nose vortex shedding from circular and noncircular bodies in subsonic flow at angles of attack and roll. The axisymmetric body is represented by point sources and doublets, and noncircular cross sections are transformed to a circle by either analytical or numerical conformal transformations. The leeward vortices are modeled by discrete vortices in crossflow planes along the body; thus, the three-dimensional steady flow problem is reduced to a two-dimensional, unsteady, separated flow problem for solution. Comparison of measured and predicted surface pressure distributions, flowfield surveys, and aerodynamic characteristics are presented for bodies with circular and noncircular cross sectional shapes.

17. Key Words (Suggested by Author(s))	18. Distribution Statement
Vortex shedding Circular bodies Noncircular bodies Discrete vortices	Unclassified - Unlimited Subject Category 34

19. Security Classif. (of this report)	20. Security Classif. (of this page)	21. No. of Pages	22. Price
Unclassified	Unclassified	168	A08

N-305 For sale by the National Technical Information Service, Springfield, Virginia 22161